Finite Element Modeling of Occupant Injury Risk and Crash Performance of W-Beam Guardrail Barriers in Roadside Crashes

Qian Wang

Thesis submitted to the faculty of the Virginia Polytechnic Institute and State University in partial fulfillment of the requirements for the degree of

Master of Science
In
Biomedical Engineering

Hampton C. Gabler, Chair
Stefan M. Duma
Warren N. Hardy

April 9, 2009
Blacksburg, Virginia

Keywords: Guardrail Barrier, Finite Element, Pendulum Test

Finite Element Modeling of Occupant Injury Risk and Crash Performance of W-Beam Guardrail Barriers in Roadside Crashes

Qian Wang

Abstract

This thesis presents the results of a research effort aimed at investigating the crash performance of w-beam guardrail barriers in vehicle-roadside crashes using the finite element method. The developed roadside barrier models can be used to assess the occupant injury risk, vehicle performance, and damage to guardrail barriers during a roadside accident. The finite element models of w-beam guardrail barriers may also help evaluate the crash performance of the w-beam barriers with minor damage in vehicle-barrier crashes. Thus, the results can be used to develop repair guidelines to assist highway personnel in identifying levels of minor barrier damage and deterioration.

Finite element models of the weak post w-beam guardrail barriers were developed and simulated using LS-DYNA. The simulation results were validated against full scale crash tests of pickup trucks and passenger cars impacting w-beam guardrail barriers. The maximum dynamic deflection of the guardrail, exit velocity and angle of the vehicle, and occupant injury risk were calculated and compared to the tests. Kinematics of the vehicle and guardrail were assessed qualitatively as well as quantitatively. The analysis showed that simulation results were in good agreement with test data. Additionally, the models were validated against pendulum tests conducted the Federal Outdoor Impact Laboratory (FOIL). Simulation results of pendulum tests showed that the test section taken from the current full scale models performed very similarly to that in the real pendulum tests.

The developed finite element models were subsequently used to examine the crash performance of weak post w-beam guardrail barriers with minor damage under vehicle impacts. Only rail/post deflection based minor damage to weak post w-beam guardrail barriers was considered in this study. Simulations were completed to obtain the damaged profiles of the guardrail systems; the damaged weak post guardrail barriers were impacted by the pickup model at mid-span for the second time. The impacting vehicle remained stable in all of these simulations. No conclusions could be drawn however whether these second impacts could have resulted in rail tearing or rupture.

Acknowledgments

I would like to acknowledge my advisor, Dr. Clay Gabler for his guidance. I would also like to acknowledge my committee members for their time and comments.

I would also like to thank our sponsor – the Transportation Research Board of the National Academics of Science under project NCHRP 22-23.

TABLE OF CONTENTS

LIST OF FIGURES

LIST OF TABLES

1. BACKGROUND AND RESEARCH OBJECTIVE

1.1 Introduction

1.1.1 Background

Guardrails are designed to protect vehicle occupants from roadway hazards by containing and redirecting the vehicle. However, occupants are still susceptible to injuries when the vehicle strikes guardrail barriers. In the United States in 2005, there were 1,189 fatal crashes and 35,000 injurious crashes into guardrails (NHTSA, 2005). Car and light truck occupants comprised 64% of all fatalities resulting from a guardrail collision from 2000 to 2005 (Gabler and Gabauer, 2007). The distribution of passenger vehicle-guardrail crash fatalities by crash mode showed that frontal impacts accounted for 45 percent of all passenger vehicle-guardrail crash fatalities. Passenger vehicles include cars, light trucks, and vans.

Guardrail systems are installed in an effort to reduce the number of fatalities and serious injuries that result from run-off-road crashes. Guardrail prevents vehicles from leaving the roadway and striking a hazard by containing and redirecting the vehicle back onto the roadway. W-beam guardrail (weak-post and strong-post) has been used for decades because it is an effective guardrail system that can be used in a variety of roadside situations. W-beam guardrail can shield fixed objects and steep slopes, can be used around curves to prevent vehicles from leaving the roadway, and can be used at bridge approaches where there is relatively little room for lateral deflection. Evidence from 32 studies (Elvik, 1995) that have quantified the effects of guardrail shows that guardrail along the edge of the road reduces the number of crashes and their severity. More specifically, guardrail reduced the crash rate by approximately 30 percent. Given that a crash occurred, guardrail reduced the number of fatality and injury crashes by

approximately 45 percent and 50 percent, respectively. These findings apply both to new installations and to replacements of old installations. Another study (Michie, 1994) investigated the performance of guardrail with respect to reported impacts (approximately 10 percent of the total impacts) and unreported impacts (approximately 90 percent of the total impacts). Assuming no injuries or fatalities occur in the unreported impacts, only 6 percent of all guardrail impacts involve an injury or fatality. It as concluded that properly installed and maintained longitudinal barriers may be successfully performing in 97 to 98% of all design range length-of-need impacts, with only 2 to 3% of the impacts causing occupant injuries or fatalities.

Although guardrail systems have usually prevented serious crashes, they can still pose a threat to occupant roadside safety. Sources of occupant injury and fatality include guardrail hardware failure, improper guardrail height, guardrail end treatments, and excessive decelerations of the occupants. Guardrail barriers, especially those with damage from previous crashes, are not likely to be able to contain and redirect the vehicle if any hardware failure happens, i.e. guardrail rupture at a splice connection. The improper guardrail height will result in rollover of the vehicles with a high center of gravity, such as pickup trucks, or the slipping of motorcycles under the guardrail. The end treatments of guardrail barriers are especially hazardous when poorly designed or obsolete ends could penetrate the vehicle and result in occupant injury.

According to the National Cooperative Highway Research Program (NCHRP) Report 350 (Ross et al., 1993), Level 2 tests require that longitudinal barriers be subjected to a full scale vehicle crash test of a 2000-kg pickup truck impacting at a speed of 70 km/h and an angle of 25 degrees and a full scale vehicle crash test of a 820-kg passenger car impacting at a speed of 70 km/h and an angle of 20 degrees. Level 3 tests require that longitudinal barriers be subjected to a

full scale vehicle crash test of a 2000-kg pickup truck impacting at a speed of 100 km/h and an angle of 25 degrees and a full scale vehicle crash test of a 820-kg passenger car impacting at a speed of 100 km/h and an angle of 20 degrees. The current evaluation criteria for impact performance of guardrail barriers are presented in Table 1.

Table 1. **Barrier Performance Requirements**

Criterion	Required Performance
Structural Adequacy	1. Barrier contains and redirects the vehicle
	2. No vehicle penetration, underride, or override
Occupant Risk	3. Vehicle should remain upright during and after the collision; moderate pitch and roll are acceptable
	4. Lateral and longitudinal occupant impact velocity < 12 m/s (as computed by the flail space model)
	5. Lateral and longitudinal occupant ridedown acceleration < 20 G (as computed by the flail space model)
Vehicle Trajectory	6. Vehicle intrusion into adjacent traffic lanes is limited or does not occur
	7. Vehicle exit angle should preferably be less than 60 percent of the impact angle

1.1.2 Flail-Space Injury Risk Model

The flail space model is currently the primary criteria to evaluate occupant injury risk during roadside crashes. Occupant injury risk is assessed by calculating the velocity at which the unrestrained occupant impacts the vehicle interior and the acceleration that the occupant experiences by contacting the vehicle interior (Ross et al., 1993). The assumptions made in the flail-space model were: 1) Occupant was located at the center of mass of the vehicle. 2) Yaw motions of the vehicle were ignored, and the lateral movement of the occupant is independent of the motion in the longitudinal direction. 3) Motion of the vehicle and the occupant is in the x-y plane. 4) Occupant was allowed 0.3 m of motion in the lateral direction before impact with the vehicle side structure, and occupant was allowed 0.6 m of motion in the longitudinal direction before impact with the vehicle dashboard.

The flail-space injury risk model assumed that occupant was allowed to travel in the vehicle compartment 0.6 m in the longitudinal direction and 0.3 m in the lateral direction. The time (t*) when occupant contacted the vehicle interior was determined by the double integration of acceleration.

$$X, Y = \int_0^{t^*} \int_0^{t^*} a_{x,y} dt^2 \qquad \textbf{[Equation 1]}$$

where $a_{x,y}$ is the vehicle acceleration in the longitudinal or lateral directions, X = 0.6 m and Y = 0.3 m. Acceleration in the longitudinal direction is integrated twice with respect to time to find the value of time, t_x*, at which the double integration equals 0.6 m. Acceleration in the lateral direction is integrated twice with respect to time to find the value of time, t_y*, at which the double integration equals 0.3 m. Time t* is the smaller of t_x* and t_y*. The equation for the occupant impact velocity (OIV) is:

$$V_{l_{x,y}} = \int_0^{t^*} a_{x,y} dt \qquad \textbf{[Equation 1]}$$

where $V_{lx,y}$ is the velocity at which the occupant impacts the vehicle interior in the longitudinal or lateral directions.

For the occupant ridedown acceleration (ORA), an arbitrary duration of 10 ms was selected as a time base to calculate average accelerations for occupant risk assessment. The ORA was obtained by finding the highest 10 ms average vehicle accelerations after time t* in the longitudinal and lateral directions.

The calculated occupant impact velocity and occupant ridedown acceleration were compared to the recommended values (Ross et al., 1993). Two limits are given for each injury risk parameter, as listed in Table 2. It is desirable that computed values be below the “preferred” limits, and it is recommended that the computed values be below the “maximum” values. It should be noted that the recommended limits were absolute values.

Table 2. Occupant Injury Risk Limits

Occupant Impact Velocity Limits (m/s)			Occupant Ridedown Acceleration Limits (G's)		
Component	Preferred	Maximum	Component	Preferred	Maximum
Longitudinal	9	12	Longitudinal and Lateral	15	20

However, the assumptions of the flail space model limited its ability to evaluate occupant injury risk in great detail. Since in the flail space model occupant risk is assessed by the response of a hypothetical, unrestrained front seat occupant whose motion relative to occupant compartment is dependent on vehicular accelerations, it is not possible to know the occupant kinematics and injury potential in the vehicles, especially in the new vehicles with occupant restraints, e.g. airbag.

1.1.3 Barrier Types

A survey of the US and Canadian transportation agencies (Gabauer and Gabler, 2009) was conducted by Virginia Tech to gather existing policies and guidelines governing inspection and repair of longitudinal barriers. The survey was used to identify the barrier systems and the types of damage and deterioration within a particular agency's jurisdiction.

Figure 1 shows the distribution of barrier types based on the total length of barrier reported by the responding agencies. Note that the three agencies reporting only total barrier length have been excluded from this plot. The strong post w-beam barrier was the most frequent barrier type, accounting for roughly 60 percent of total barrier length by the responding state agencies. Excluding the two agencies that reported no use of strong post w-beam (South Carolina and British Columbia), the average use of strong post w-beam barrier was approximately 80 percent. Concrete, strong post thrie beam, weak post w-beam and cable barriers were ranked second through fifth, respectively, based on the responding agencies providing detailed barrier information. Strong post w-beam, concrete, and weak post w-beam

barrier systems are shown in Figure 2 (A Guide to Standardized Highway Barrier Hardware, 2009).

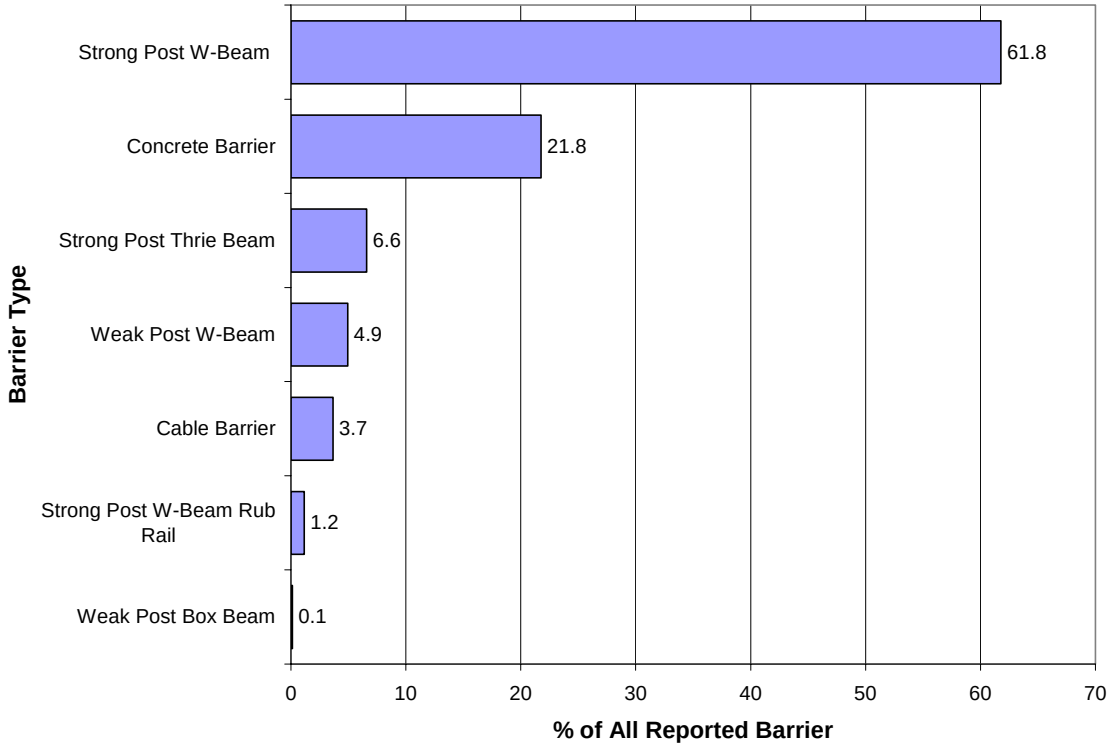

Figure 1. Summary of Barrier Types Reported

(a) **(b)** **(c)**

Figure 2. Barrier Types: (a) Strong Post W-Beam Barrier (b) Concrete Barrier (c) Weak Post W-Beam Barrier

The focus of this research is limited to w-beam barriers, which are by far the most common barriers in use in the United Stated. Strong post w-beam guardrail system is the most commonly used guardrail in the United States. Weak post w-beam guardrail system is mostly used in the northeast states, and it is used extensively in Virginia. It should be noted that cable barrier, thrie beam barrier, and concrete barrier systems are not in the scope of this research.

1.1.4 The Weak Post W-Beam Guardrail Barrier

Two acceptable weak post w-beam guardrail barriers are commonly used, Test Level 2 barrier and Test Level 3 barrier. Test level 3 barriers have safety features that are acceptable for a wide range of high-speed highways, Test level 2 qualified features are deemed acceptable for most local roads and many work zones. For Test Level 3, barriers are tested at a speed of 100 km/h, whereas Test Level 2 barriers are tested at a speed of 70 km/h.

The Test Level 2 weak-post w-beam guardrail is composed of w-beam rails supported on weak posts with welded soil plates. The weak post steel conforms to American Association of State Highway and Transportation Officials (AASHTO) M 183 standard; and the weak post section conforms to the geometry and tolerances of AASHTO M 160 for a S3x5.7 S-section (A Guide to Standardized Highway Barrier Hardware, 2009). The w-beam guardrail is connected to weak posts by bolts and nuts with a diameter of 8 mm and square guardrail washers. Weak-post W-beam guardrails are commonly used where dynamic deflections of at least 87 inches (2200 mm) are acceptable. The spacing between posts is 3810 mm and the rail height is 770 mm. Post was attached to the rail at splices. The bolts in the weak post w-beam guardrail system are designed to fail during an impact to allow the rail to separate easily from the posts. After the rail is separated from the post, the W-beam section redirects the vehicle, acting like a cable that is anchored at the ends.

The Test Level 3 weak-post w-beam guardrail is composed of the same w-beam rails and weak posts with welded soil plates. The main differences between Test Level 3 weak post barrier and Test Level 2 weak post barrier include:

- The top rail height was increased by 50 mm to 820 mm.
- Rail splices were located mid-span between posts rather than at a post.

- A 300-mm w-beam backup plate (12 Gage) was added at each post location.
- Minor changes included the use of two square washers on the traffic side of the post connection bolts and a single round washer and double nut connection on the opposite side of these bolts.

1.1.5 Guardrail Damage

It is required by the transportation agencies that all new guardrail barrier systems should perform acceptably to protect vehicle occupants from striking roadside hazards. However, barrier systems are damaged by a wide range of factors. Such damage could compromise barriers' impact performance and hence the occupant safety. With limited maintenance budgets, state highway agencies often have large backlogs of needed safety-feature repairs. These agencies cannot afford to repair damage that does not alter a barrier's safety performance, but significant barrier damage must be repaired to provide adequate protection for the motoring public.

According to the literature as well as field visits performed by Virginia Tech, guardrail barrier damage can be classified into one of the four following categories based on damaged components: rail element, posts, blockouts, and connections. This damaged component classification scheme is a simple, yet comprehensive way of classifying damage.

For the rail element, the posts, and blockouts, damage can be further classified into deflection damage, tears/breaks and/or missing, and deterioration damage. Examples of damage to the rail element include minor dents, lug nut damage, rail distortions, rail flattening, any type of tear, non-manufacturer holes, cable damage, any type of corrosion as well as loss of tension/cable sag in cable barriers. Examples of damage to posts and blockouts would be post dents, twisted blockouts, rising posts due to frost heave, slope-related barrier lean, split wood blockouts, broken wood posts, rotted wood posts, erosion of soil around posts, and corrosion of

steel posts. The connection damage types most critical to the performance of the barrier appear to be splice damage and missing/loose splice bolts.

1.1.6 Finite Element Models of Guardrail Systems

Finite element analysis has been used in roadside safety research for decades. The advantage of utilizing finite element method in roadside safety research is that it is less expensive than performing full-scale testing when a wide range of parameters must be evaluated. Thus, finite element models become an effective tool in the design and evaluation of barrier systems.

Four finite element models of full scale w-beam guardrail longitudinal barrier systems were found in the literature (NCAC Finite Element Model Archive, 2009): the NCAC w-beam guardrail model, guardrail in mow-strip developed at Texas Transportation Institute (TTI), guardrail behind curb developed at Worcester Polytechnic Institute (WPI), and wood post w-beam model developed at WPI. We plan to use longitudinal barrier models developed at Virginia Tech for both undamaged and damaged barrier simulations. The models will be a hybrid of the NCAC strong post w-beam model and those developed by Virginia Tech. No weak post w-beam guardrail Test Level 2 model was found in the National Crash Analysis Center (NCAC) finite element model archive. Therefore, development of a weak post w-beam guardrail system is needed to evaluate crash performance of the guardrail system and to understand occupant injury risk in vehicle roadside crashes. The developed models will also be used to examine the impact performance of guardrail systems with minor damage. For this study, only the Length of Need, which is the part of a longitudinal barrier or terminal designed to contain and redirect an errant vehicle, was considered in finite element modeling.

1.2 Research Objectives

This thesis is expected to yield several contributions to the field of roadside safety. The objectives from this proposal are designed for the purpose of modeling crash performance of w-beam guardrail barriers in roadside crashes using the finite element method. The finite element models of guardrail barriers are expected to be used to predict crash performance of guardrail systems with minor damage and to investigate the occupant injury potential in roadside crashes. In order to develop robust guardrail models, there are several research objectives that will need to be accomplished.

1. Develop a finite element model of a weak post w-beam guardrail barrier.
2. Validate the strong post and weak post w-beam guardrail finite element models through pendulum testing.
3. Evaluate the crash performance of weak post w-beam guardrail systems with minor damage using finite element method.

The ultimate goal of this research will be the development of finite element models of w-beam guardrail barriers for the evaluation of crash performance of barrier systems and the prediction of occupant injury in accidents involving roadside safety hardware.

2. DEVELOPMENT OF A FINITE ELEMENT MODEL OF WEAK POST W-BEAM GUARDRAIL BARRIERS

2.1 Introduction

W-beam guardrail systems have been used for decades in the United States to reduce the number of fatalities and injuries that result from roadside crashes. W-beam guardrail systems prevent vehicles from leaving the roadway and striking a hazard by containing and redirecting the vehicle. Strong post w-beam guardrail system is the most commonly used guardrail in the United States, while weak post w-beam guardrail system is mostly used in the northeast states (Ray and McGinnis, 1997). The characteristics of weak post w-beam guardrail system in collisions are different from those of strong post guardrail barrier. Larger dynamic and permanent deflections of weak post guardrail were seen in crash tests and real world crashes. Consequently, occupant injury potential that involve roadside accidents with weak post guardrail barriers showed differences from strong post systems. A study conducted by the New York Department of Transportation found that vehicle crashes involving weak post w-beam guardrail system were less severe than strong post w-beam guardrail crashes (Vanzweeden and Bryden, 1997).

The objective of this study is to develop and validate finite element models of the weak post w-beam (G2) guardrail system. Several finite element models of the strong post w-beam guardrail system have been developed. Two types of weak post w-beam guardrail barriers are accepted by Federal Highway Administration (FHWA): Test level 2 weak post w-beam guardrail barrier and Test level 3 weak post w-beam guardrail barrier. The configuration of the Test Level 3 system is different from that of Test Level 2 guardrail system. The differences include: 1) the

w-beam guardrail was mounted 820-mm above the ground as opposed to 770 mm for the TL-2 system, 2) the splices are at mid-span, 3) the W-beam backup plates were mounted at each post, and 4) the post was attached to the rail at non-splice location. Hendricks and Wekezer (1996) developed a reduced G2 guardrail model, but this simulation did not model the splice connection or post-soil interaction.

According to the National Cooperative Highway Research Program (NCHRP) Report 350, Level 2 tests require that longitudinal barriers be subjected to a full scale vehicle crash test of a 2000-kg pickup truck impacting at a speed of 70 km/h and an angle of 25 degrees and a full scale vehicle crash test of a 820-kg passenger car impacting at a speed of 70 km/h and an angle of 20 degrees. Level 3 tests require that longitudinal barriers be subjected to a full scale vehicle crash test of a 2000-kg pickup truck impacting at a speed of 100 km/h and an angle of 25 degrees and a full scale vehicle crash test of a 820-kg passenger car impacting at a speed of 100 km/h and an angle of 20 degrees.

The standard weak post guardrail system in a NCHRP Report 350 test generally consists of at least 9 weak posts and w-beam guardrails for a total length of 30 m excluding terminals. The spacing between posts is 3810 mm and the rail height is 770 mm for Test Level 2 barriers and 820 mm for Test Level 3. Post was attached to the rail at splices for Test Level 2 barriers and at the mid span between posts for Test Level 3. No weak post w-beam guardrail models were found in the NCAC finite element model archive (NCAC Finite Element Model Archive, 2009). The comparisons between the two systems are listed in Table 3.

Table 3. Comparisons between Test Level 2 and Test Level 3 Weak Post W-Beam Systems

	TL2 Weak Post	TL3 Weak Post
Rail Height	770 mm	820 mm
Splice Location	Post	Mid-Span
Backup Plate	None	Yes
Post-Rail Connection	1 Square Washer and 1 Nut	2 Square Washers and 2 Nuts

Development of weak post w-beam guardrail systems is helpful in understanding occupant injury risk in vehicle roadside crashes. In addition, minor damage that results from a low speed collision or sideswipe is commonly seen in the guardrail barrier. The effect of this damage on the performance of the barrier system in subsequent crashes is not well understood. Therefore, the weak post w-beam guardrail models will also help the investigation of injury potential of occupants in vehicle roadside accidents that involve damaged guardrail.

2.2 Methodology

2.2.1 Objective

The objective of this study is to develop and validate finite element models of the weak post w-beam guardrail system.

2.2.2 Finite Element Modeling of the Test Level 2 Weak-Post W-Beam Guardrail System

A detailed finite element model of the Test Level 2 weak-post w-beam guardrail system was developed. The components of the full scale weak post guardrail system are shown in Figure 3. All barrier components were modeled using Hypermesh 8.0. The crash tests were simulated using the LS-DYNA finite element code, and post-processed in LS-PREPOST. The mesh of the w-beam guardrail, soil, and splice bolts and nuts was taken from the NCAC strong post w-beam guardrail model (NCAC Finite Element Model Archive, 2009). The weak post, rail-post bolt and

nut, guardrail washer, soil plate, and end terminals were modeled and assembled with the guardrail system.

The test installation in the model is similar to a NCHRP Report 350 Test Level 2 full scale crash test. The top of the rail in the system was located 770 mm above the ground. The mounting height of the center slot of the guardrail was 610 mm from the ground. The soil plate with the dimension of 600 mm in length, 200 mm in width, and 6 mm in thickness was mounted on the post and located 124 mm below the ground. Simplification was made such that the nodes at the end terminals were only constrained in three translational directions.

All posts, rails, and soil plates were modeled using Belytschlo-Tsay shell formulation with five integration points through the thickness (Wright and Ray, 1996). *MAT_PIECEWISE_ LINEAR_PLASTICITY was used for the posts, rails, and soil plates. The material properties were obtained from literature and coupon tests on guardrail steel (Wright and Ray, 1996). The material behavior of this material model is isotropic elasto-plastic (LSTC, 2007). The same material property was assigned to the end terminals.

The rail-post bolt and nut was modeled and used to connect the w-beam to the post. The rail-post bolts and nuts and washers were modeled using quadrilateral shell elements. The material selected for the rail-post bolt and nut was rigid material. The modeling method of rail-post bolts and nuts was the same as in the NCAC strong post model (NCAC Finite Element Model Archive, 2009). A circular-shaped beam element was created between the bolt and the nut to represent the force and stiffness of the bolt. The material model *MAT_SPOTWELD was selected for the beam elements. The failure axial force resultant for the beam elements was set to 16 kN (Ray et al., 2001).

The soil was modeled using solid elements as a cylindrical block 2.7 m in diameter and 2.0 m in length as shown in Figure 3. A foam and soil material was used for the soil. This material model is a simple model for soil and foam. The material properties of the soil were taken from the NCAC strong post guardrail barrier model. The material properties of this model were obtained from test data of a Bogie vehicle impacting posts embedded in similar soil (Marzougui et al., 2007). *CONTACT_AUTOMATIC_SURFACE_TO_SURFACE was defined between the outer surfaces of the post and inner surfaces of the soil block to simulate the contact between the post and the soil. Friction coefficients between the post and the soil were also taken from the NCAC strong post guardrail model.

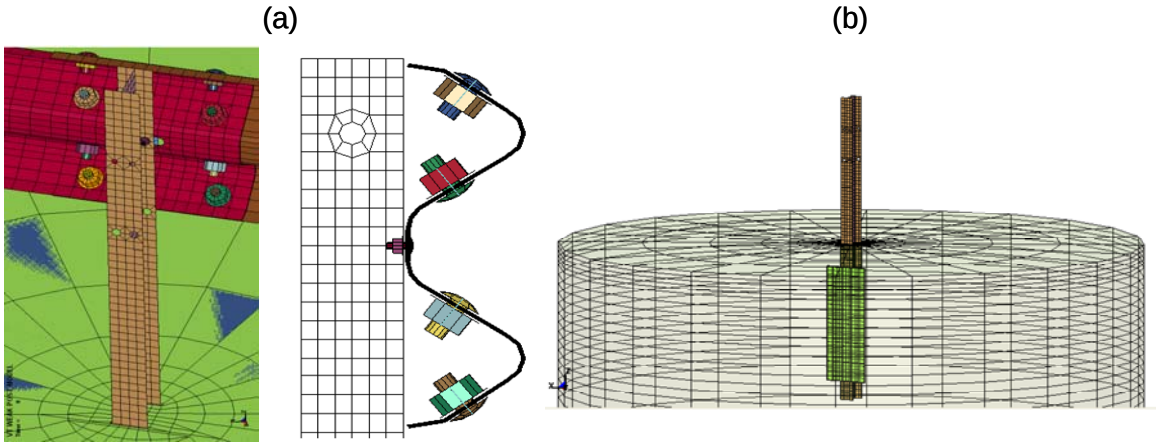

Figure 3. Finite Element Model of Test Level 2 Barrier Components: (a) Finite Element Model of W-Beams Connected to Weak Posts. (b) Finite Element Model of Weak Posts with Soil Plates and Soil Buckets

2.2.3 Validation of the Test Level 2 Weak Post Guardrail Barrier Model

Two full scale vehicle crash tests were selected to provide validation data for the Test Level 2 weak post w-beam guardrail barrier model, Test No. 471470-22 (Mak et al.,1998) and GR-8 (Bronstad et al., 1987). As a NCHRP Report 350 Test Level 2 roadside barrier, the weak post w-beam guardrail barrier is required to perform acceptably with a 2000-kg pickup truck

impacting at a speed of 70 km/h and an angle of 25 degrees and an 820-kg passenger car impacting at a speed of 70 km/h and an angle of 20 degrees.

Test No. 471470-22 (Ross et al., 1993) was conducted at the Texas Transportation Institute. The test setup was based on the NCHRP Report 350 Test Level 2 configuration. The spacing between posts was 3810 mm and the rail height was 770 mm. Each post was attached to the rail at splices. In the test, 17 posts with 3810 mm spacing between posts were used to support the guardrail barrier system. The total test installation was 76.2 m in length with a 7.62 m turned-down terminal at each of the two ends. The top of the rail in this system was located 762 mm above the ground.

A 1985 Chevrolet Custom 20 pickup truck, which had a test weight of 2076 kg, was used for the crash test. The vehicle impacted the guardrail system at midspan between posts 4 and 5 at a speed of 71.0 km/h and an angle of 26.1 degrees. The test vehicle separated from the guardrail at approximately 1.08 s after impact with an estimated exit speed and angle of 25.7 km/h and 9.5 degrees. The guardrail had a maximum dynamic deflection of 1.4 m at 0.372 s after impact. The maximum permanent deflection of the guardrail was 1.3 m. The longitudinal occupant impact velocity was 4.6 m/s at 0.3 s; the highest 10 ms average ridedown acceleration was -4.8 g's between 0.384 and 0.394 s. In the lateral direction, the occupant impact velocity was 3.3 m/s at 0.228 s; the highest 10 ms average ridedown acceleration was 3.1 g's between 0.386 and 0.396 s.

A detailed finite element model of a 1994 Chevrolet C2500 pickup truck developed at the NCAC was used in the simulation. This FE model has a total of 58,313 elements. The Chevrolet C2500 pickup truck model was very similar to the test vehicle in terms of weight, wheelbase and bump height. The simulation setup is shown in Figure 4. *CONTACT_AUTOMATIC_ SURFACE_TO_SURFACE was defined between the vehicle and the guardrail system. The

vehicle model was assigned an initial velocity of 71.0 km/h at an angle of 26.1 degrees to impact the midspan between posts 4 and 5 of the barrier system.

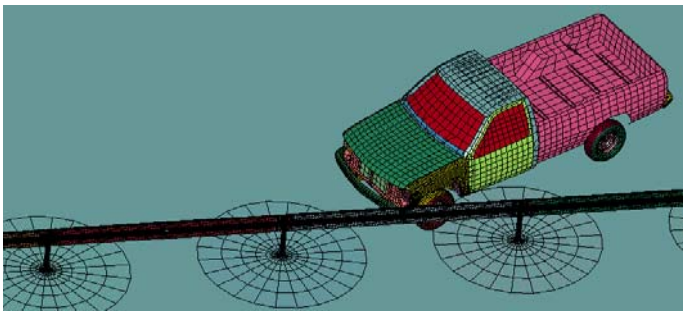

Figure 4. Simulation Setup of the Test Level 2 Weak Post W-Beam Guardrail Impact Test

Test No. GR-8 (Bronstad et al., 1987) was conducted at Southwest Research Institute. The test setup was similar to that of NCHRP Report 350 Test Level 2 tests. A 1979 Honda Civic, which had a test weight of 889 kg, was used for the crash test. The vehicle impacted the weak post w-beam guardrail system at a speed of 94.1 km/h and an angle of 19.3 degrees. The test vehicle separated from the guardrail at approximately 0.52 s after impact with an estimated exit speed and angle of 69.4 km/h and 1.0 degrees. The guardrail had a maximum dynamic deflection of 0.805 m at approximately 0.25 s after impact. The maximum permanent deflection of the guardrail was 0.406 m. No crash test with an 820-kg passenger car impacting at a speed of 70 km/h and an angle of 20 degrees could be found in the literature.

A reduced finite element model of a 1997 Geo Metro passenger car developed at the NCAC was used in the simulation. This FE model has a total of 16,100 elements. Note that no finite element model of a Honda Civic was available in the NCAC Finite Element Model Database (NCAC Finite Element Model Archive, 2009). The FE model of the Geo Metro was the closest FE model available in the NCAC Finite Element Model Database to represent an 820 kg passenger car. The Geo Metro model had similar weight compared to the test vehicle. Also, Geo Metro is a commonly used small car model utilized in the full scale vehicle crash tests. The

simulation setup is shown in Figure 5. *CONTACT_AUTOMATIC_ SURFACE_TO_SURFACE was defined between the vehicle and the guardrail system. The vehicle model was assigned an initial velocity of 94.1 km/h at an angle of 19.3 degrees to impact the barrier system.

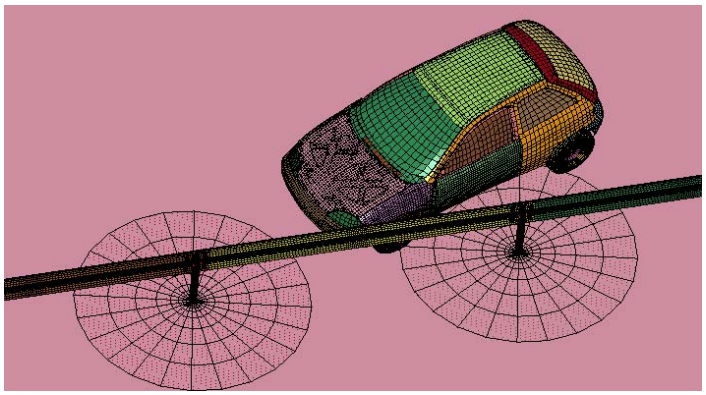

Figure 5. Simulation Setup of the Test Level 2 Weak Post W-Beam Guardrail Impact Test

2.2.4 Finite Element Modeling of the Test Level 3 Weak-Post W-Beam Guardrail System

Test level 3 weak post w-beam barriers have safety features that are acceptable for a wide range of high-speed highways. Test Level 3 weak post barriers are crash tested at a speed of 100 km/h. The Test Level 3 weak-post w-beam guardrail is composed of the same (Designator No. RWM02a) w-beam rails and weak posts with welded soil plates. The main differences between Test Level 3 weak post barrier and Test Level 2 weak post barrier include: The top rail height was increased by 50 mm to 820 mm. Rail splices were located mid-span between posts rather than at a post. A 300-mm w-beam backup plate (12 Gage) was added at each post location. These changed were made to the finite element model of Test Level 2 weak post w-beam model using Hypermesh. The components of the full scale weak post guardrail system are shown in Figure 6.

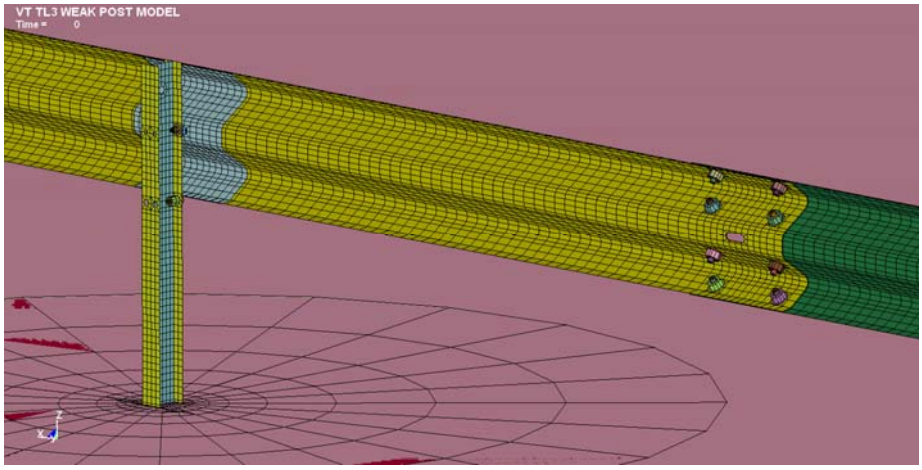

Figure 6. Finite Element Model of Test Level 3 Weak Post W-Beam Barrier Components

2.2.5 Validation of the Test Level 3 Weak Post Guardrail Barrier Model

Test No. 473750-3 was selected to provide validation data for the Test Level 3 weak post w-beam guardrail barrier model. As a NCHRP Report 350 Test Level 3 roadside barrier, the weak post w-beam guardrail barrier is required to perform acceptably with a 2000-kg pickup truck impacting at a speed of 100 km/h and an angle of 25 degrees.

Test No. 473750-3 (Buth et al., 2000) was conducted at the Texas Transportation Institute. The test setup was based on the NCHRP Report 350 Test Level 3 configuration. A 99 m long test installation of Test Level 3 weak post w-beam guardrail was constructed. The installation included 68.6 m of length of need and 15.2 m of turned down terminal on each end. The guardrail system consisted of 1.6 m long posts with soil plates, spaced 3810 mm apart, and 3.8 m long 12 gauge w-beam guardrail. The height of the guardrail was 820 mm. The w-beam rail was connected to the weak posts with 8 mm diameter bolts and nuts, a round washer in the back, and two square washers in the front. Splice connections were located at mid-span between posts. Twelve gauge w-beam backup plates were installed between each weak post and the w-beam guardrail.

A 1995 Chevrolet 2500 pickup truck was used for the crash test. The gross static weight of the vehicle was 2000 kg. The height to the upper edge of the front bumper of the vehicle was 655 mm. The pickup impacted the barrier between posts 6 and 7 at a speed of 102.4 km/h and an angle of 26.5 degrees. The vehicle became parallel with the barrier at 0.371 s and was traveling at a speed of 77.8 km/h. The vehicle lost contact with the rail at 1.418 s and was traveling 59.3 km/h. The exit angle of the vehicle was approximately 2 degrees. In the longitudinal direction, the occupant impact velocity was 3.9 m/s at 0.2 s, and the maximum 0.05 s average acceleration was -3.4 g's between 0.221 s and 0.271 s. In the lateral direction, the occupant impact velocity was 4.2 m/s at 0.2 s, and the maximum 0.05 s average acceleration was 4.0 g's between 0.226 s and 0.276 s.

A detailed finite element model of a 1994 Chevrolet C2500 pickup truck developed at the NCAC was used in the simulation. This FE model has a total of 58,313 elements. The simulation setup is shown in Figure 7. *CONTACT_AUTOMATIC_SURFACE_TO_SURFACE was defined between the vehicle and the guardrail system. The vehicle model was assigned an initial velocity of 102.4 km/h at an angle of 26.5 degrees to impact the midspan between posts 6 and 7 of the barrier system.

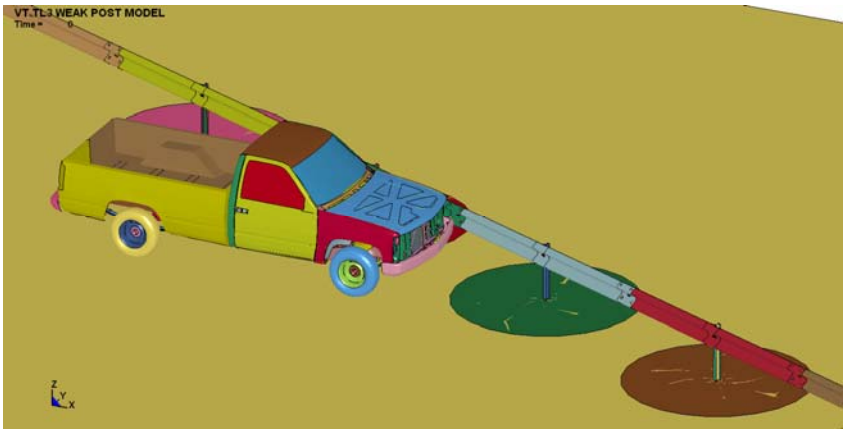

Figure 7. Simulation Setup of the Test Level 3 Weak Post W-Beam Guardrail Impact Test

2.2.6 Validation Method

The finite element model validation process involved a comparison of crash test results with the results of finite element model simulations of the crash tests including the exit speed and angle of the vehicle, roll, pitch, and yaw angles of the vehicle, guardrail deflections, occupant impact velocities, and occupant ridedown accelerations.

2.3 Analysis of Results

2.3.1 Results of Test Level 2 Weak Post Guardrail Barrier Impacted by Pickup Truck

The comparisons of guardrail deflections, vehicle exit velocity and angle, occupant impact velocity, and occupant ridedown acceleration are listed in Table 4. Data from the accelerometer located at the center of gravity of the vehicle were extracted for evaluation of occupant risk. The occupant impact velocity in the longitudinal direction was 5.7 m/s at 0.284 s; the highest 0.05 s average ridedown acceleration in the longitudinal direction was -1.6 g's. In the lateral direction, the occupant impact velocity was 3.2 m/s at 0.238 s; the highest 0.05 average ridedown acceleration was 1.5 g's.

Table 4. Comparisons of Test No. 471470-22 and Simulation of Detailed C2500 with Test Level 2 Weak Post Guardrail Model

	Test No. 471470-22	Detailed C2500
Impact Conditions		
Vehicle Impact Speed (km/h)	71.0	71.0
Vehicle Impact Angle(deg)	26.1	26.1
Test Article Deflection (m)		
Max. Dynamic	1.4	1.46
Max. Permanent	1.3	0.95
Exit Conditions		
Vehicle Exit Speed (km/h)	25.7	23.4
Vehicle Exit Angle (deg)	9.5	4.9
Occupant Risk Values		
Longitudinal OIV (m/s)	4.6	5.7
Lateral OIV (m/s)	3.3	3.2
Longitudinal ORA (G's)	-4.8	-1.6
Lateral ORA (G's)	3.1	1.5
Max. 50-ms Average (G's)		
Longitudinal	-3.1	-3.5
Lateral	2.6	3.1
Vertical	-1.6	-1.5
Vehicle Behavior		
Max. Roll Angle (deg)	9	3
Max. Pitch Angle (deg)	-3	-1
Max. Yaw Angle (deg)	37	30
Vehicle Specifications		
Weight (kg)	2076	2013
Wheelbase (mm)	3350	3382
Bumper Height (Upper Edge) (mm)	680	635

Sequential photographs for Test No. 471470-22 (Mak et al., 1998) and corresponding overhead view snapshots taken from the simulation were compared in Figure 8. It was observed that the overall vehicle kinematics in the test and the simulation were similar. Small variations were found in the time at which different impact events occurred and the corresponding velocity of the vehicle. In the test, the vehicle was traveling parallel to the guardrail barrier at 0.533s, while the vehicle model was traveling parallel to the installation at 0.51 s in the simulation. The vehicle model separated from the guardrail at approximately 0.92 s after impact with an

estimated exit speed of 23.4 km/h at an angle of 4.9 degrees. The guardrail had a maximum dynamic deflection of 1.46 m at 0.280 s after impact. Accelerometer data at center of gravity and 50-ms average accelerations are plotted in Figure 9 to Figure 11. The acceleration data were filtered at 60 Hz according to NCHRP Report 350 (Ross et al., 1993). It was observed that the overall kinematics of the test vehicle and the detailed C2500 pickup model were similar. The vehicle behaviors in the test and the simulations were compared and shown in Figure 12 to Figure 14.

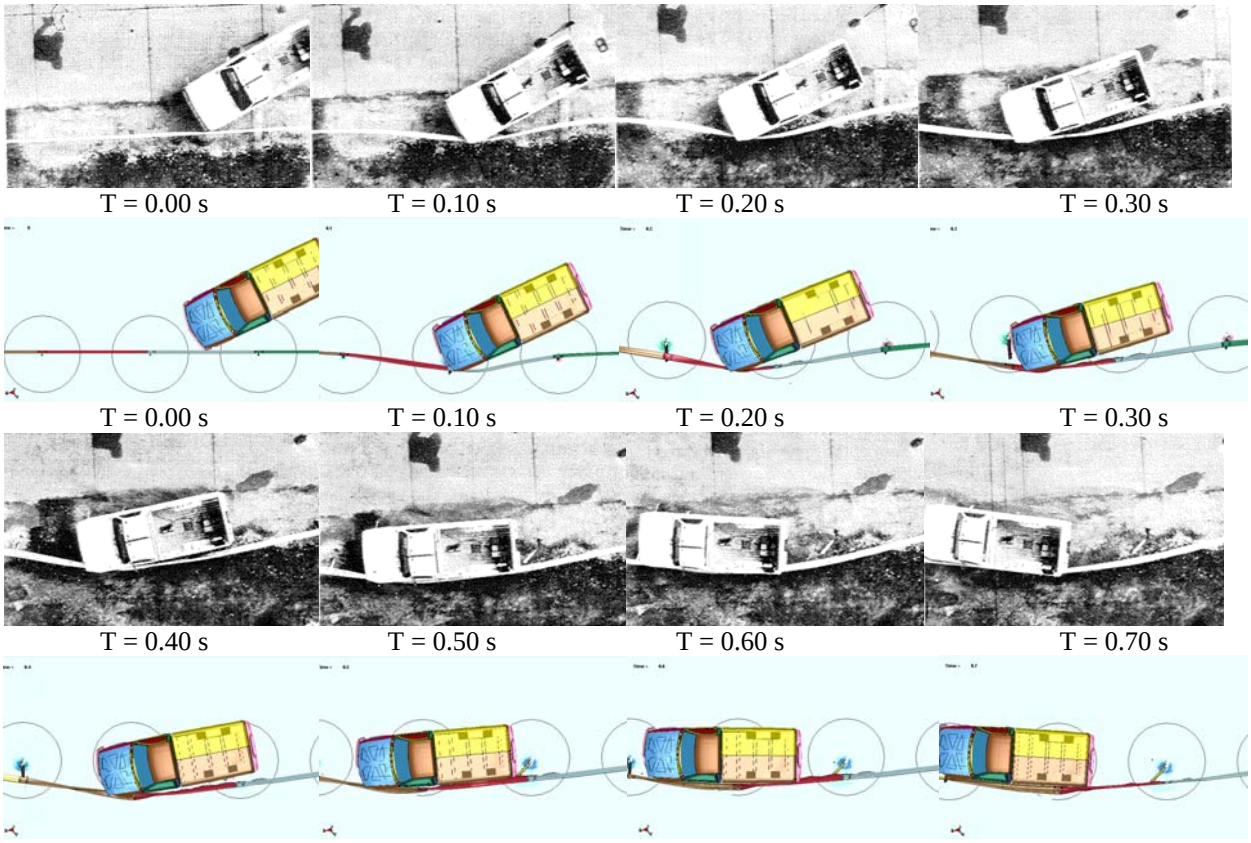

Figure 8. Comparisons of Sequential Photographs from Test No. 471470-22 and Detailed C2500 Model

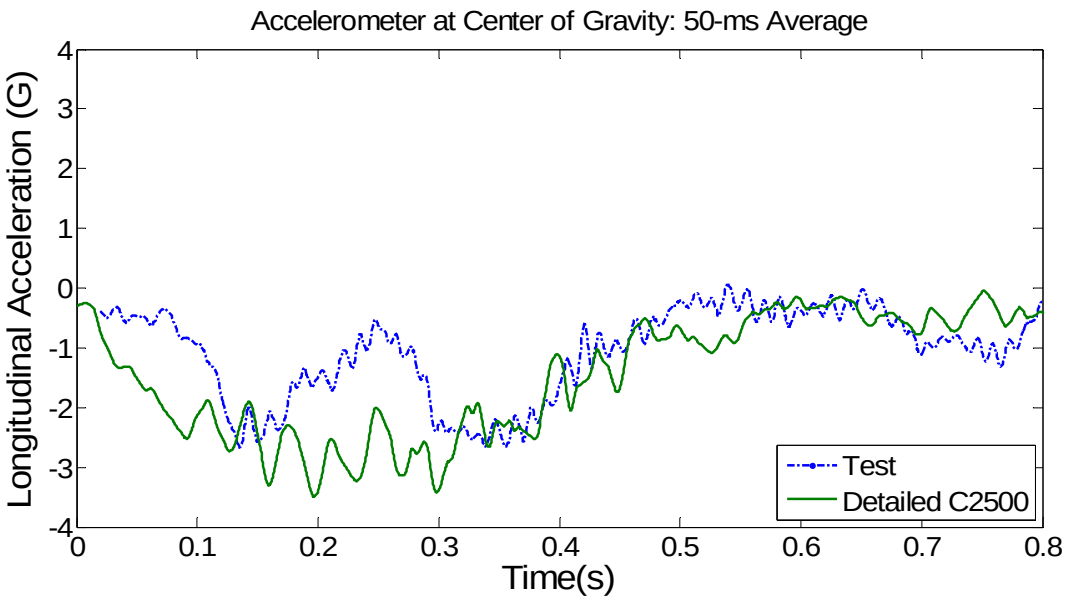

Figure 9. Comparisons of 50-ms Average Longitudinal Acceleration at Center of Gravity between Detailed NCAC C2500 Pickup Model and Test 471470-22

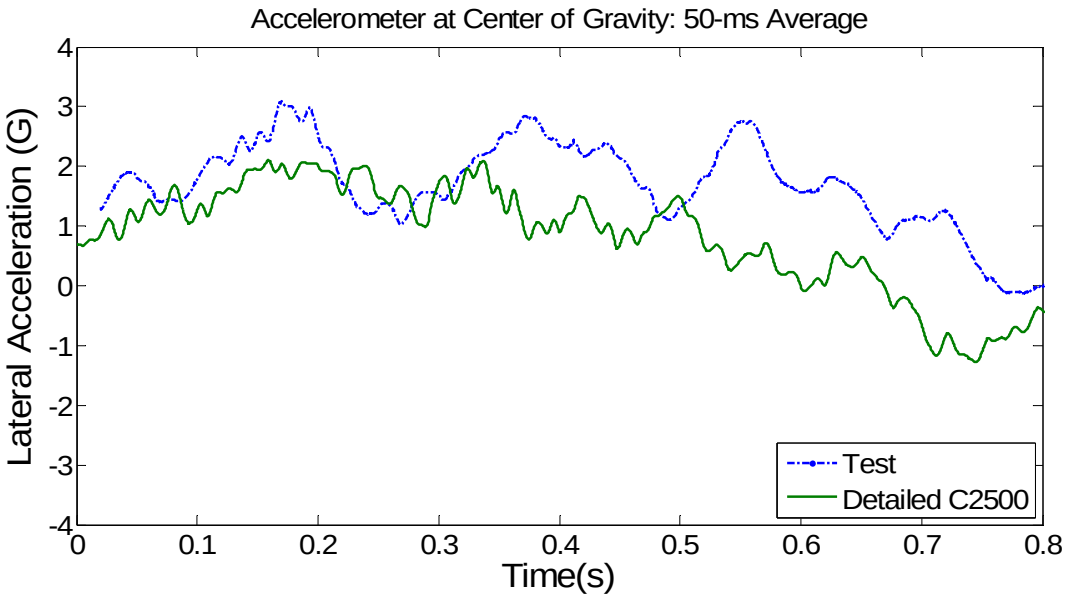

Figure 10. Comparisons of 50-ms Average Lateral Acceleration at Center of Gravity between Detailed NCAC C2500 Pickup Model and Test 471470-22

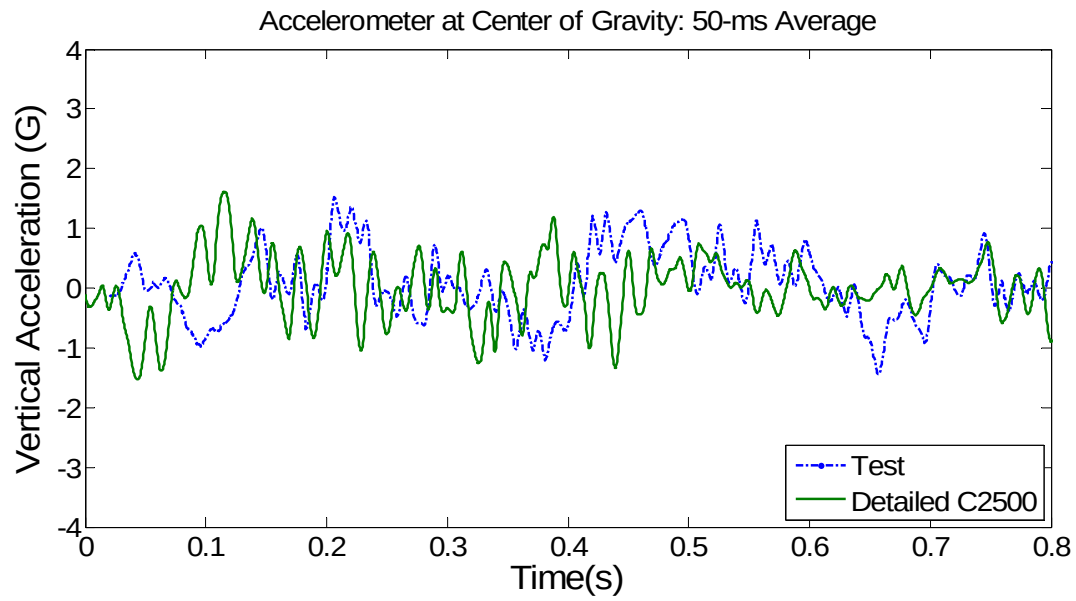

Figure 11. Comparisons of 50-ms Average Vertical Acceleration at Center of Gravity between Detailed NCAC C2500 Pickup Model and Test 471470-22

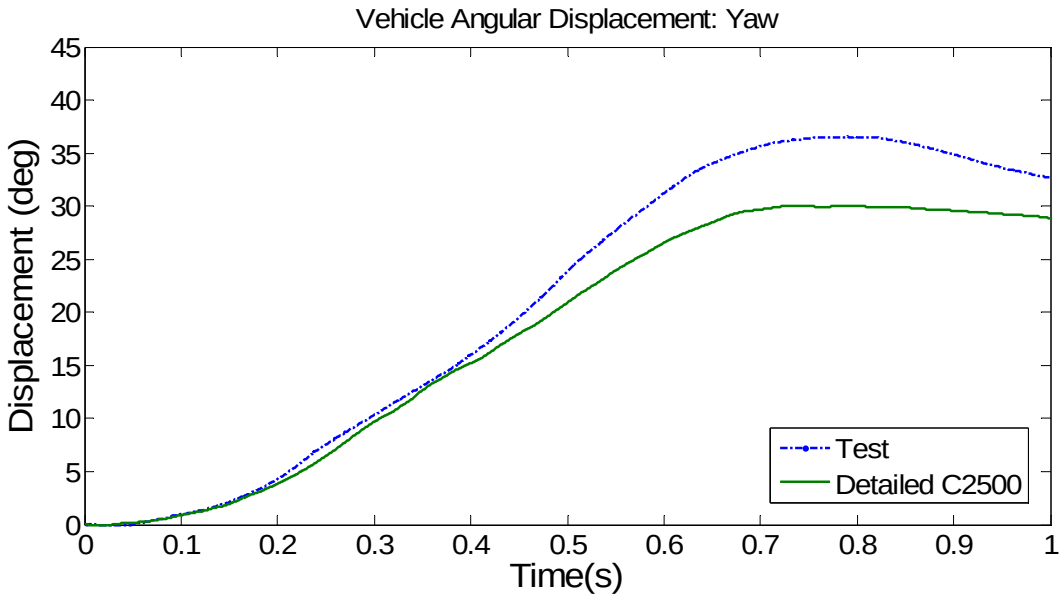

Figure 12. Comparisons of Vehicle Angular Displacements Yaw between NCAC Pickup Models and Test 471470-22

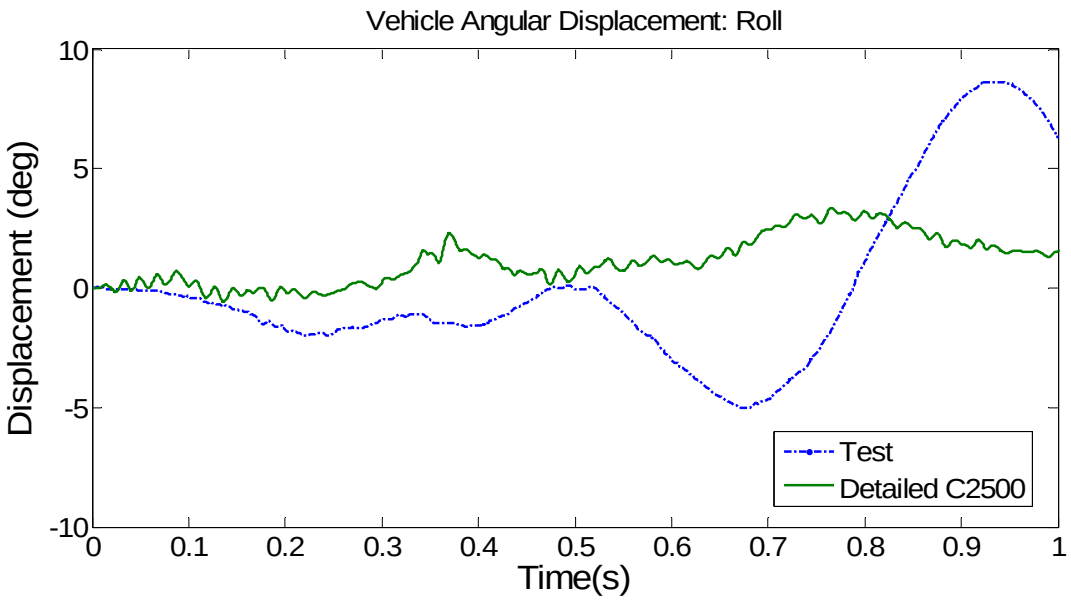

Figure 13. Comparisons of Vehicle Angular Displacements Roll between NCAC Pickup Models and Test 471470-22

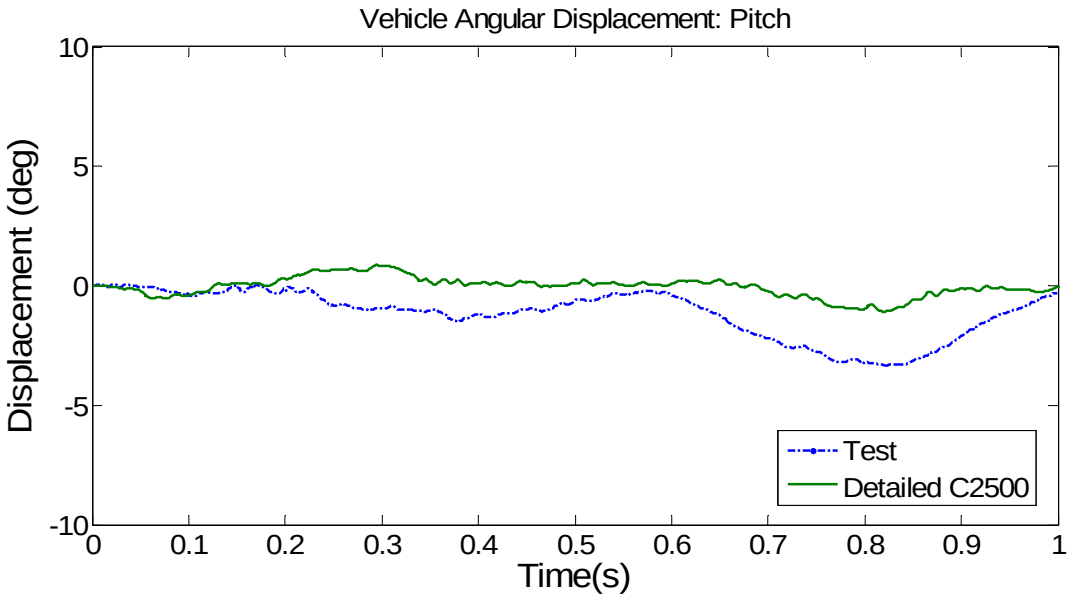

Figure 14. Comparisons of Vehicle Angular Displacements Pitch between NCAC Pickup Models and Test 471470-22

2.3.2 Results of Test Level 2 Weak Post Guardrail Barrier Impacted by Geo Metro

The comparisons of guardrail deflections, vehicle exit velocity and angle are listed in Table 5. Data from the accelerometer located at the center of gravity of the vehicle were used to calculate vehicle exit conditions.

Sequential photographs for Test No. GR-8 (Bronstad et al., 1987) and corresponding overhead view snapshots taken from the simulation were compared in Figure 15. It was observed that the overall vehicle kinematics in the test and the simulation were similar. Difference was found in the exit angle of the vehicle. In the test, the vehicle was separating from the barrier with an estimated exit speed of 69.4 km/h and an angle of approximately 1 degree, while the vehicle model had an estimated exit speed of 69.3 km/h and an angle of 10 degree in the simulation. The guardrail had a maximum dynamic deflection of 0.81 m at 0.25 s after impact. It was observed that the overall kinematics of the test vehicle and the reduced Geo Metro model were similar.

Table 5. Comparisons of Test No. GR-8 and Simulation of Geo Metro Model with Test Level 2 Weak Post Guardrail Model

	Test GR-8	Geo Metro
Impact Conditions		
Vehicle Impact Speed (km/h)	94.1	94.1
Vehicle Impact Angle(deg)	19.3	19.3
Test Article Deflection (m)		
Max. Dynamic	0.81	0.74
Max. Permanent	0.41	0.47
Exit Conditions		
Vehicle Exit Speed (km/h)	69.4	69.3
Vehicle Exit Angle (deg)	1	10
Vehicle Specifications		
Weight (kg)	889	810

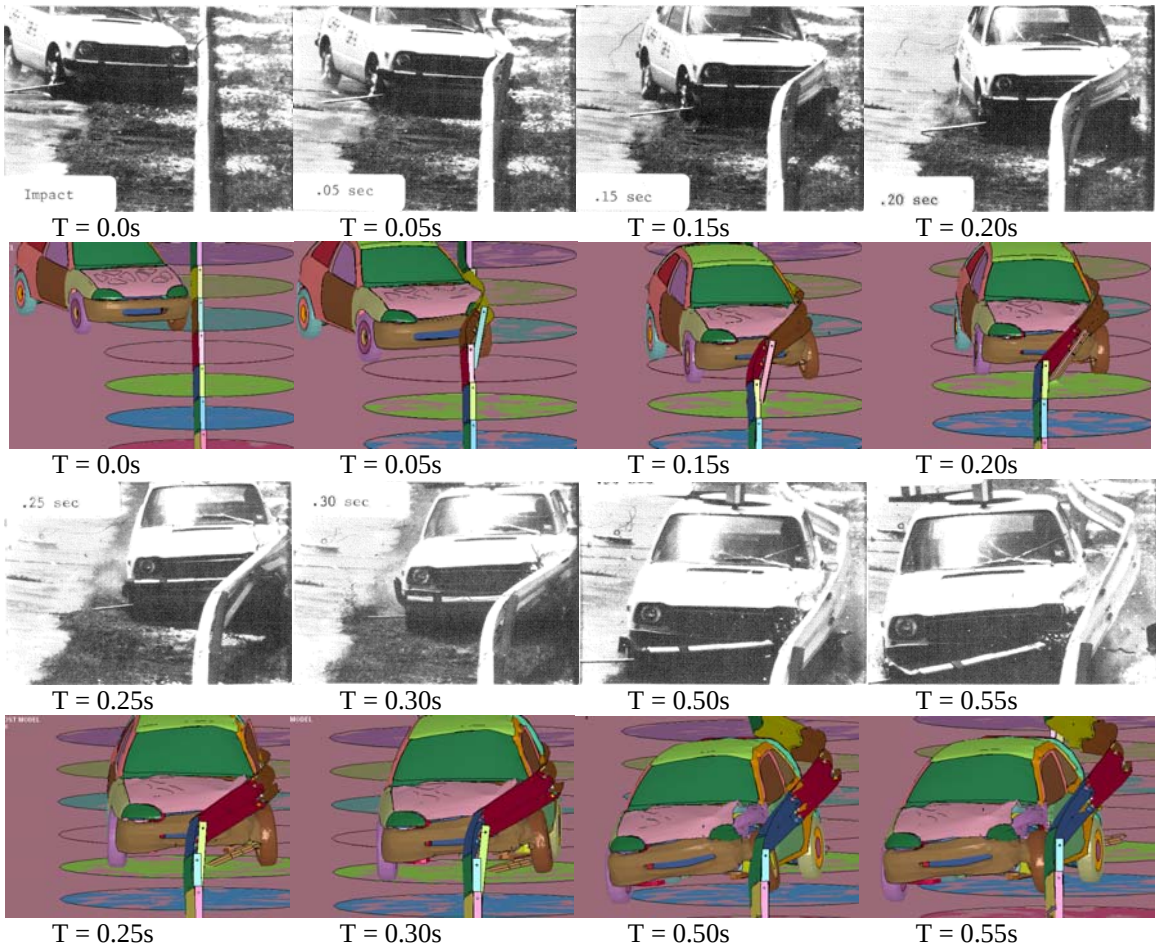

Figure 15. Comparisons of Sequential Photographs from Test GR-8 and Geo Metro Model

2.3.3 Results of Test Level 3 Weak Post Guardrail Barrier Impacted by Pickup Truck

The comparisons of guardrail deflections, vehicle exit velocity and angle, occupant impact velocity, and occupant ridedown acceleration are listed in Table 6. Data from the accelerometer located at the center of gravity of the vehicle were extracted for evaluation of occupant risk. The occupant impact velocity in the longitudinal direction was 7.8 m/s at 0.407 s; the highest 0.05 s average ridedown acceleration in the longitudinal direction was -5.9 g's. In the lateral direction, the occupant impact velocity was 6.8 m/s at 0.395 s; the highest 0.05 average ridedown acceleration was 5.8 g's.

Table 6. Comparisons of Test No. 473750-3 and Simulation of Detailed C2500 with Test Level 3 Weak Post Guardrail Model

	Test No. 473750-3	Detailed C2500
Impact Conditions		
Vehicle Impact Speed (km/h)	102.4	102.4
Vehicle Impact Angle(deg)	26.5	26.5
Test Article Deflection (m)		
Max. Dynamic	2.12	2.41
Max. Permanent	1.64	1.37
Exit Conditions		
Vehicle Exit Speed (km/h)	59.3	26.6
Vehicle Exit Angle (deg)	2	5
Occupant Risk Values		
Longitudinal OIV (m/s)	3.9	7.8
Lateral OIV (m/s)	4.2	6.8
Longitudinal ORA (G's)	-5.9	-8.6
Lateral ORA (G's)	6.4	5.4
Max. 50-ms Average (G's)		
Longitudinal	-3.4	-5.9
Lateral	4.0	5.8
Vertical	-1.9	-4.5
Vehicle Behavior		
Max. Roll Angle (deg)	-12	-2
Max. Pitch Angle (deg)	-5	-1
Max. Yaw Angle (deg)	36	28
Vehicle Specifications		
Weight (kg)	2000	2013
Wheelbase (mm)	3350	3382
Bumper Height (Upper Edge) (mm)	655	635

Sequential photographs for Test No. 473750-3 (Buth et al., 2000) and corresponding overhead view snapshots taken from the simulation were compared in Figure 16. It was observed that the overall vehicle kinematics in the test and the simulation were similar. Variations were found in the time at which different impact events occurred and the corresponding velocity of the vehicle. In the test, the vehicle was traveling parallel to the guardrail barrier at 0.4s, while the vehicle model was traveling parallel to the installation at 0.6 s in the simulation. The vehicle model separated from the guardrail with an estimated exit speed of 26.6 km/h at an angle of 5

degrees. The guardrail had a maximum dynamic deflection of 2.41 m at 0.280 s after impact. It was observed that the overall kinematics of the test vehicle and the detailed C2500 pickup model were similar. Rail tensions of the Test 473750-3 and the simulation of the Test Level 3 weak post guardrail barrier were plotted in Figure 17. The comparison showed that the simulation overestimated the forces along the cross section of the guardrail barrier.

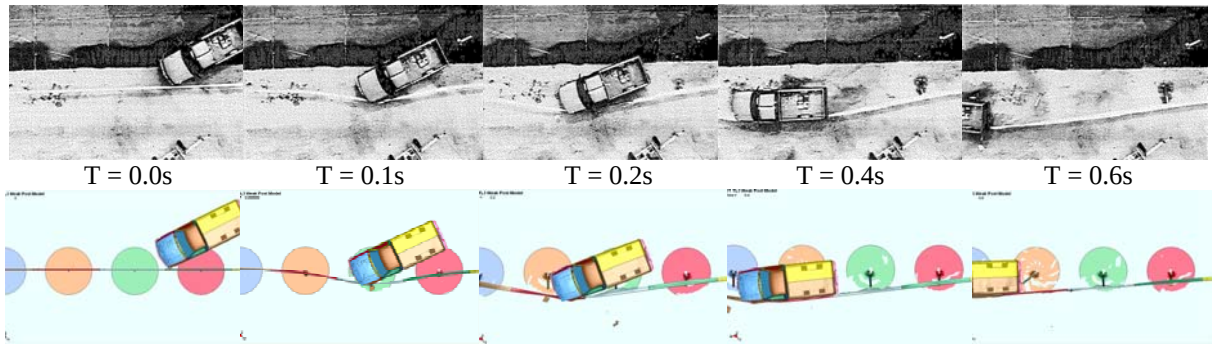

Figure 16. Comparisons of Sequential Photographs from Test No. 473750-3 and Detailed C2500 Model

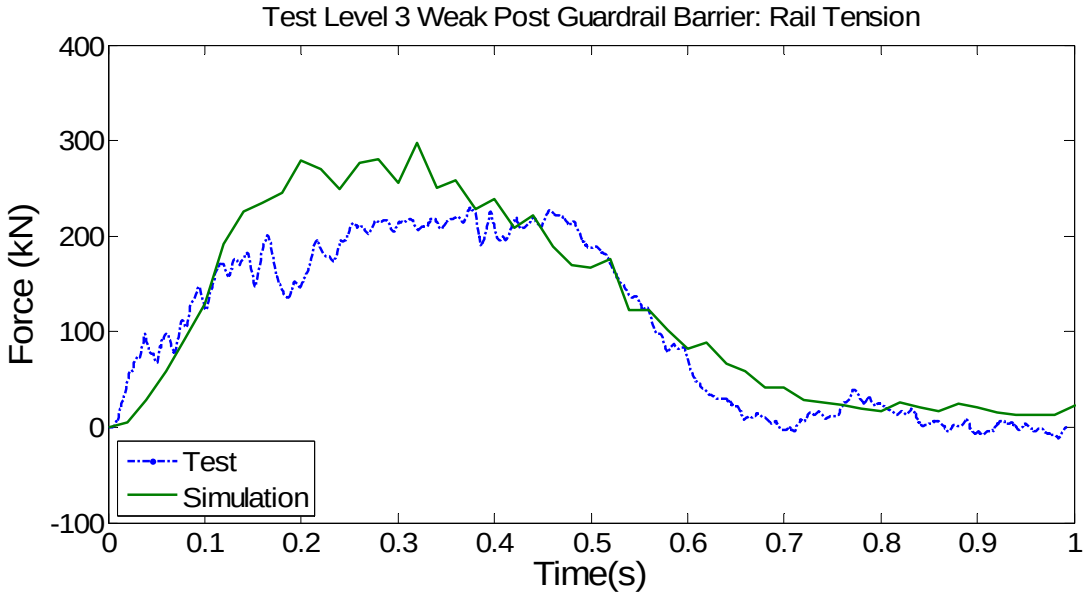

Figure 17. Comparisons of Rail Tension between Test No. 473750-3 and Simulation of Test Level 3 Weak Post Guardrail Barrier

2.4 Discussion

2.4.1 Test Level 2 Weak Post Guardrail Barrier Model

Simulations of Test Level 2 weak post w-beam guardrail impacts were compared to Test No. 471470-22 and Test No. GR-8. It was observed that the maximum dynamic deflections of the guardrail obtained from the simulations were very comparable to those in the tests. The recorded vehicle exit velocities in the simulation were also very similar to test vehicle exit speeds. Occupant impact velocity and ridedown acceleration were calculated from simulation results of the pickup truck impact. The longitudinal OIV values in the test as well as in the simulation were under the preferred and recommended limit. The lateral OIV values obtained from the simulation and the test were very comparable to each other. Both values were below the preferred and maximum limits. Analysis of the ORA showed that the absolute values of the longitudinal and lateral ORA from the numerical model were similar to the test data. All ORA values were considerably lower than the preferred and recommended limits.

2.4.2 Test Level 3 Weak Post Guardrail Barrier Model

The numerical model of Test Level 3 weak post w-beam guardrail impact was compared to Test No. 473750-3. It was observed that the maximum dynamic deflection of the guardrail obtained from the simulations was very comparable to those in the tests. Difference was found in the vehicle exit speed between the test and simulation. The recorded vehicle exit velocity in the simulation was lower than test vehicle exit speed by 55%. The differences in friction conditions between the vehicle and the guardrail barrier as well as the soil condition could account for this discrepancy. The difference in frictional coefficient between two barrier systems was determined by the change in relative velocity. In LS-DYNA (LSTC, 2007), the overall frictional coefficient between contact was a function of dynamic frictional coefficient, static frictional coefficient, and

relative velocity. To closely duplicate Test No. 473750-3, more detailed information about the soil and friction conditions need to be investigated. Occupant impact velocity and ridedown acceleration were calculated from simulation results. The longitudinal OIV value in the simulation was close to the preferred OIV limit. The lateral OIV values obtained from the simulation also overestimated test data. Both values were below the preferred and maximum limits. Analysis of the ORA showed that the absolute values of the longitudinal and lateral ORA from the numerical model were similar to the test data. All ORA values were considerably lower than the preferred and recommended limits.

2.5 Conclusions

Finite element models of both the Test Level 2 and the Test Level 3 weak post w-beam guardrail systems were developed. NCHRP Report Test Level 2 and 3 impacts with pickup trucks and passenger cars were simulated using LS-DYNA. The occupant injury risk during the impact was investigated by computing occupant impact velocity and occupant ridedown acceleration.

The simulation results of Test Level 2 impacts were validated against Test No. 471470-22 and Test No. GR-8. Kinematics of the vehicle and guardrail in the simulations were very similar to the tests. The analysis showed that the vehicle was contained and redirected by the weak post w-beam guardrail barrier. The OIV and ORA calculated from simulation results were in good agreement with test data. It was concluded that the Test Level 2 weak post guardrail model could be used for the investigation of crash performance of barriers with minor damage.

The simulation results of Test Level 3 impact were validated against Test No. 473750-3. Kinematics of the vehicle and guardrail in the simulations were similar to the test. The analysis showed that the pickup was contained and redirected by the weak post w-beam guardrail barrier.

Differences were found in the vehicle exit speed, OIV, and ORA between simulation and test results. It was concluded that further improvement was needed for the Test Level 3 weak post guardrail model. More specifically, the friction conditions between the vehicle and the guardrail barrier and the soil condition needed to be improved.

3. VALIDATION OF THE W-BEAM GUARDRAIL FINITE ELEMENT MODEL THROUGH PENDULUM TESTING

3.1 Introduction

A crucial step in using the finite element model of a guardrail system for crash performance is to validate the predictive power of the model against the results of a full scale crash test (Marzougui et al., 2007). A model of the vehicle-guardrail crash test is first constructed by combining models of the guardrail and impacting vehicle used in test together with initial conditions which represent the impact conditions, i.e. tests speed, angle, and impact point. The validation process involves a comparison of crash test results with the results of a finite element model simulation of the crash test including the exit speed and angle of the vehicle, roll, pitch, and yaw angles of the vehicle, guardrail deflections, occupant impact velocities, and occupant ridedown accelerations. While this is an important measure of the accuracy of the FE model at this single test configuration, uncertainty remains over the ability of the model to predict barrier performance at alternate impact speeds, impact angles, collision partners or with slight changes in geometry. Ideally, FE models would be validated across a range of impact configurations. However, because full systems crash tests are expensive, it can be challenging to identify additional suitable experimental tests against which validation comparisons can be made.

One source of additional validation data is pendulum impact tests. Virginia Tech in collaboration with FHWA has conducted a large series of pendulum tests for NCHRP Project 22-23 (Gabauer and Gabler, 2009). A major goal of NCHRP Project 22-23 is to determine the crash performance and repair recommendations for guardrail systems which have suffered minor

damage after installation such as might occur from low severity car sideswipes or snowplow damage. While the crash performance of new guardrail systems has been thoroughly investigated in crash testing, little is known about the performance of guardrail systems which have sustained minor damage. NCHRP Project 22-23 is examining the crashworthiness of these systems through a two-pronged approach of experimental testing and computational modeling of strong-post w-beam guardrail systems with minor damage. The computational modeling effort is using a modified version of the National Crash Analysis Center (NCAC) full scale strong post w-beam guardrail finite element (FE) model (Whitworth et al., 2003).

In the pendulum experimental tests, minor damage such as missing blockouts or small indentions was artificially introduced into a guardrail section. The primary objective of the pendulum tests was to provide a direct measure of how well guardrail with small defects. A second objective was to provide experimental data against which to validate a full scale strong-post finite element model. Like the physical guardrail system, the performance of finite element models of guardrail systems with minor damage is unknown. Needed is a determination of the ability of the finite element models to predict the influence of small defects on the crashworthiness of a guardrail system.

The study described in this chapter was designed to determine whether current finite element models are sufficiently robust to model guardrails that are similar to, but not identical to, the baseline system. This paper presents the accuracy of the finite element model with two of the common damage types being investigated under NCHRP 22-23, i.e. missing blockouts and twisted blockouts. Both the pendulum tests and corresponding simulations were conducted across at two impact speeds to determine whether the finite element model performance was accurate across a range of crash severities. The rationale is that if the finite element models can

accurately predict the impact performance of a guardrail section extracted from a full guardrail model, this is a favorable indicator of the predictive power of the full finite element model of the guardrail system with minor damage. Although the discussion which follows focuses on the NCAC model, this methodology and validation data set can be readily applied to any of the commonly used guardrail models (Sicking et al., 2002; Plaxico et al., 2000).

The objective of this study was to validate the components of the NCAC full scale strong post and weak post w-beam guardrail system FE models. Our objective is to validate the finite element model of undamaged rail as well as rail with two types of damage. The validation of the NCAC full scale strong post w-beam guardrail system FE model is also useful to the weak post FE model. Many of the components including rails, splices, bolts, are common among w-beam guardrail barriers. In addition, one of the pendulum tests is a rail only test, which is directly applicable to the weak post FE model.

3.2 Methodology

3.2.1 Description of the Pendulum Testing

Pendulum tests were conducted at the Federal Outdoor Impact Laboratory (FOIL) to provide experimental data from which to validate the full scale strong-post and weak-post finite element models. The undamaged strong post guardrail barrier test (Test 01-02) was selected and described in this section to illustrate the common procedure of conducting pendulum tests in this tests series.

In each test, the pendulum impacted the center of the w-beam section. Impact speeds ranged from 15 mph (6.7 m/s) to 20 mph (8.9 m/s). As a pendulum is not capable of reproducing an oblique impact characteristic of NCHRP Report 350 longitudinal barrier test procedures, these tests were designed to mimic the lateral forces experienced in a NCHRP 350 redirectional test.

The 20 mph (8.9 m/s) impact speed was intended to approximate the lateral forces if a 2000 kg test vehicle were to impact at 60 mph (26.8 m/s) and 20 degrees. This is illustrated below in Figure 18. It should be noted that these conditions represent a lateral impact speed approximately 75 percent that of an NCHRP 350 test 3-21 impact (60 mph and 25 degrees). The constraining factor is the maximum speed that the FOIL pendulum can attain is 20 mph (8.9 m/s).

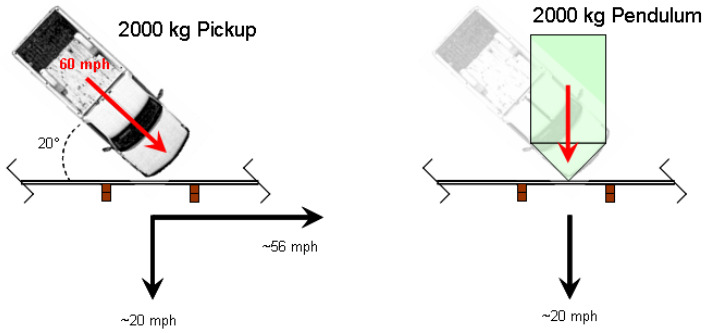

Figure 18. NCHRP 350 and Pendulum Impact Scenarios

The objective of the undamaged strong post guardrail barrier test was to investigate the performance of an undamaged two-post section of strong post w-beam guardrail barrier supported at each end with the 3-cable anchorage system. A schematic of the overall test setup is shown in Figure 19. Two lengths of w-beam were joined together with a standard splice to form a rail section 198 inches in length, which was 2 inches short of the proposed length of 200 inches (5.08 m). The spliced rail element was then suspended between the rigid posts on either side of the pendulum using custom 3 foot long (0.9 m) swaged cables (shown in Figure 20). With the exception of the total cable length, the custom anchor cables are identical to the standard breakaway cable terminal (BCT) type anchor cable. Each end of the w-beam was anchored using three of these cables connected to the rail using three standard BCT-type cable anchor brackets (entire assembly shown in Figure 20). A two-post section of strong post guardrail barrier was constructed and attached to the rigid posts on either side of the pendulum using the three cable anchor device.

The soil used in the test conformed to AASHTO M-147-65 and was compacted to a minimum compaction level of 95 percent. A mechanical tamper was used to compact the soil surrounding each posts in 6 inch (0.15 m) lifts. A nuclear density gauge (Troxler Model 3440) was used to determine the compaction and soil properties of each soil lift for the post. For each lift, the preferred compaction level was 95 percent. As the anchor points on the rigid posts are higher than the standard w-beam rail height, a soil box was used to raise the ground level around the posts by 7 inches (0.18 m) (shown in Figure 21). The soil box was constructed of four 2 by 10 inch pine boards and supported on each side by steel rebar to provide the soil restraining force such that proper compaction could be attained. The final height of the top of the weak post and the top of the w-beam rail with respect to the soil level was 30.0 inches (0.76 m).

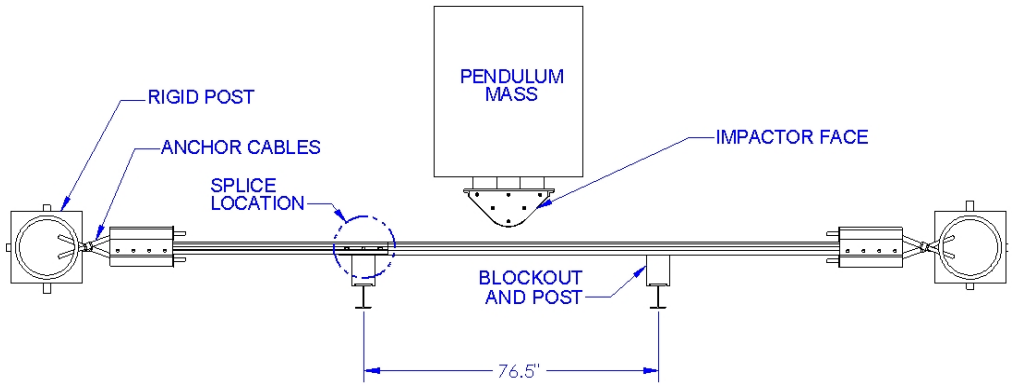

Figure 19. Overall Test Setup of Strong Post Pendulum Test (Top View)

Figure 20. Custom Swaged Anchor Cable (left) and W-Beam Rail End Anchorage Assembly (right)

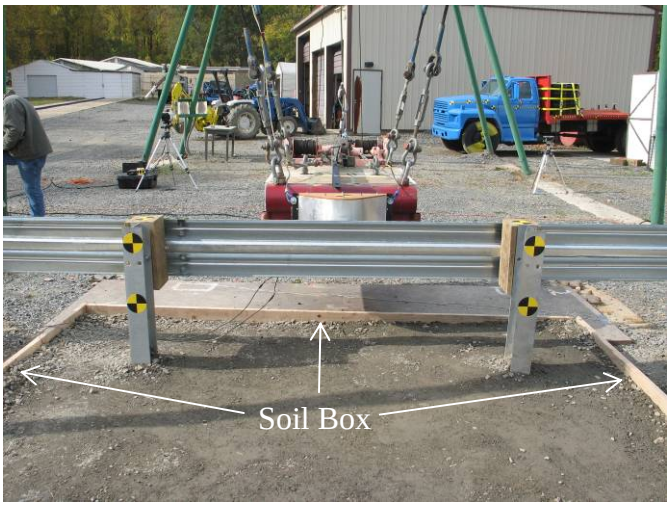

Figure 21. Soil Box used to Raise Ground Level

Instrumentation for all tests included two accelerometers located at the rear of the pendulum mass, as shown in Figure 22. Note that both of these accelerometers are in-line with the pendulum center of gravity and are aligned in the pendulum direction of travel. Four high speed cameras were used for this test: (1) a top view of the middle of the w-beam section, (2) perpendicular front view of the left anchorage, (3) perpendicular front view of the right anchorage, and (4) perpendicular rear view of the entire w-beam section. The views of the anchorages were used to observe damage to the cable and brackets and the global behavior was captured by the overhead and rear cameras. One additional real time camera was used to capture a perspective view of the test in real time.

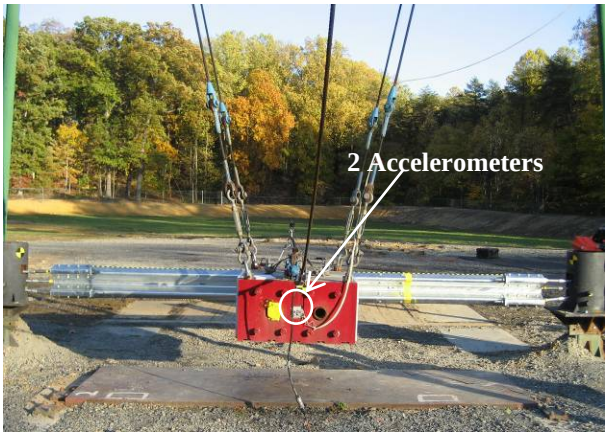

Figure 22. Instrumentation for Pendulum Test

The test section was impacted by a 2061.5 kg pendulum (including the mass of the new impactor face). An image of the new impactor face is shown in Figure 23. The radius of chamfer at the impactor center is 6 inches. This radius was selected based on measurements of several full-size pickup front bumper corners, including a 2006 Chevrolet 1500 pickup. With a height of 16.5 inches (0.42 m), the new impactor face is capable of engaging the full w-beam cross section.

Figure 23. Triangular Impactor Face Mounted to the 2000-kg FOIL Pendulum

3.2.2 Results of the Undamaged Strong Post Guardrail Barrier Test (Test 01-02)

The undamaged barrier successfully contained the pendulum mass impacting at 20.46 mph (9.15 m/s). Based on the pendulum accelerometer data, the maximum dynamic deflection of the rail was 30.15 inches (0.77 m) and occurred 136 ms after initial impact. Based on an analysis of the overhead high speed video data, the maximum static deflection was 18.9 inches (0.48 m). At the splice location, there was approximately 0.75 inches (0.02 m) of relative movement between the two w-beam rail sections (see left image in Figure 24). At the pendulum impact location, the w-beam section was flattened to a cross section height of 18.5 inches (0.47 m) (the original w-beam cross section height is 12.25 inches (0.31 m)). Although the impact was sufficient to disrupt the bond between the galvanization and underlying steel (see right image in Figure 24), there were no visible cracks in the steel at the impact location.

Figure 24. Splice Damage (left) and Impact Location Damage (right)

Figure 25 shows the damage to the posts as a result of the impact. A large amount of torsion was evident in both posts. At the non-splice location, the post bolt pulled through the w-beam rail. The post-rail connection was intact at the splice location. However, the torsion forces generated a crack at the junction between the web and flange of the post (in the circular region highlighted in the right image of Figure 25). Figure 26 shows time sequential snapshots of the test obtained from the high speed camera positioned overhead. Figure 27 shows the filtered average of the two accelerometers located at the rear of the pendulum mass.

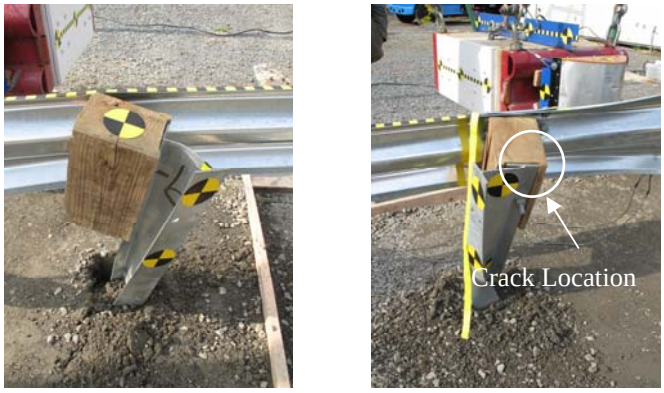

Figure 25. Post Damage at Non-Splice Location (left) and Splice Location (right)

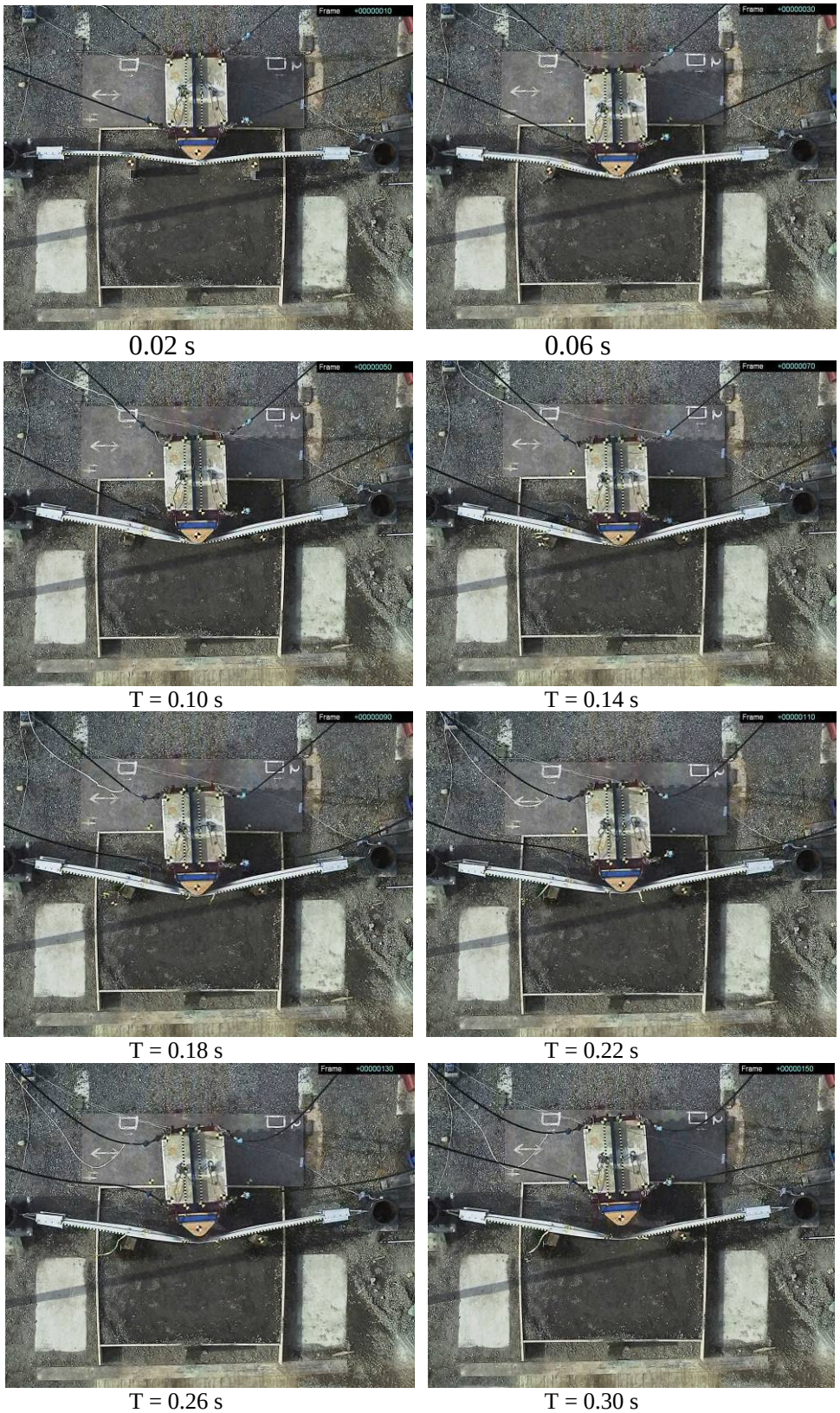

Figure 26. Sequential Photographs for Undamaged Section (Test 01-2): Overhead View

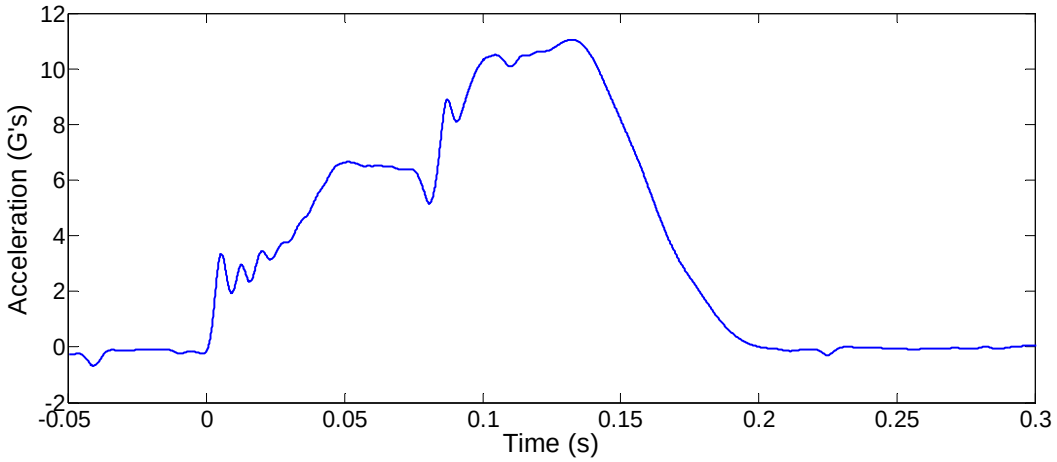

Figure 27. Filtered (60 Hz) Pendulum Acceleration Data for Test 01-2

Two finite element models were developed to represent components of the strong post, weak post guardrail system, and the pendulum. Several damage modes were introduced and simulated using the LS-DYNA finite element code, and post-processed in LS-PREPOST. The pendulum tests that were used in this study are summarized in Table 7. These tests will help better validate the FE models across a range of speeds, and make sure that the models are robust to simulate damaged guardrail systems.

Table 7. Description of the Strong Post and Weak Post Pendulum Tests

Designation	Configuration	Damage Type	Impact Speed (mph)	Crash Performance
Test 01-1	Rail Only	Undamaged	15.91	Containment
Test 01-2	Strong Post W-Beam (three 36” cables)	Undamaged	20.46	Containment
Test 01-4	Strong Post W-Beam (three 36” cables)	Missing Blockout	20.45	Containment, Large Tear Developed at Splice Location
Test 02-2	Strong Post W-Beam(three 36” cables)	Twisted Blockout	19.33	Containment
Test 08-3	Weak Post TL2 W-beam (two 40” cables)	Undamaged	14.9	Containment
Test 08-4	Weak Post TL3 W-beam (two 40” cables)	Undamaged	14.2	Containment

Note that design improvements were made to the two weak post tests. (1) The number of cables was changed from three to two cables. The rationale in switching to a two-cable grip was that the longitudinal force at the rigid end posts would be distributed through two cables rather

than three cables. We anticipated that this would result in more elongation of each cable and larger resulting deflection at the impact point – effectively making a 2-cable system a less stiff system. (2) The length of each cable was increased from the initial 36 inches to 40 inches to prevent failures due to cable kinking. (3) Additional steel plates were used in the back of the guardrail at the anchors to prevent pullout of the rail from the grip bolts during the impact. The thickness of the steel plates was 5 mm.

3.2.3 The Development of the Guardrail Model

The overall test setup for the strong post pendulum tests is shown in Figure 28. A section of strong post guardrail system, which included a 200 inches (5.08 m) long rail section, two standard strong steel posts (w150 x 13.5, 1830 mm in length) with wooden blockouts, and two soil buckets, was taken from the full scale strong post guardrail model. The splice connection was located on the left side of the test section when looking at the back of the w-beam. The w-beam was modeled using shell elements. The splice bolts and nuts modeled explicitly using shell elements were also taken from the full scale strong post guardrail model. The material for the steel rail section was a piecewise linear plastic material model. The material behavior of this material model (Marzougui et al., 2007) is isotropic elasto-plastic. The material properties were obtained from literature and coupon tests on guardrail steel (Wright and Ray, 1996).

Figure 28. Undamaged Strong Post W-Beam Barrier Test Setup

In the experiment setup for strong post pendulum tests, each end of the w-beam rail section was connected to rigid end posts by three custom 3 foot long swaged anchor cables and three standard cable anchor brackets. In the model, the end nodes of the cables were only constrained in translational directions. The end posts were observed to have a small amount of movement during the test, thus they were modeled using shell element with elastic material properties. The cables were modeled using beam elements. The cable anchor brackets were modeled using shell elements. A piecewise linear plastic material model was used for both cables and cable anchor brackets. Nodal rigid bodies were created to represent the bolts and nuts connection used between the cable brackets and the rail section. Shell elements were created to represent the portion of cables inside the anchor brackets in order to improve contact conditions. The assembly of the anchor system is shown in Figure 29.

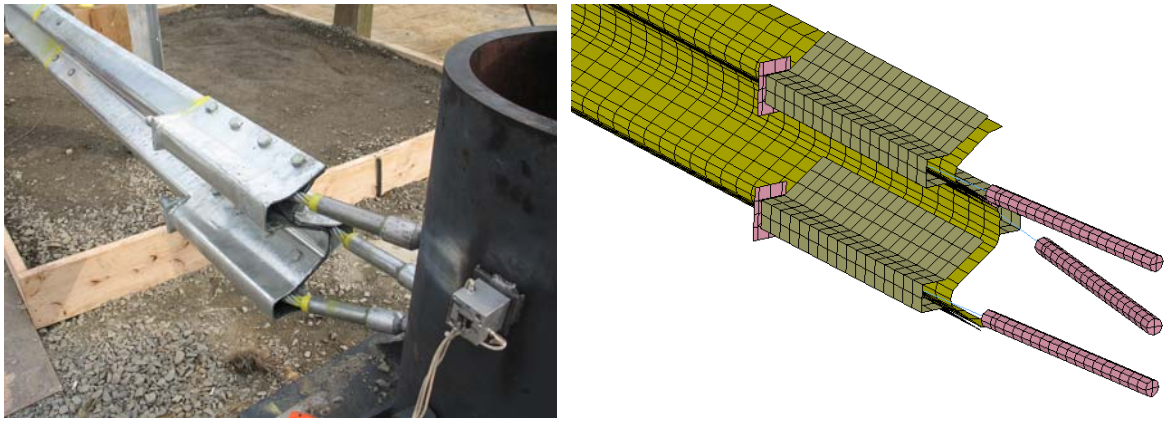

Figure 29. Cables and Anchor Brackets

The strong post and blockout were connected to the w-beam by a post bolt and a nut. The post bolts and nuts were modeled using shell elements, and were joined together by a spring element that represented the properties of the bolt. The distance between posts was 75 inches (1.9 m). The heights of the top of the posts and the top of the w-beam rail with respect to the soil bucket were 28 inches (0.71 m) and 27 inches (0.69 m), respectively.

The soil was modeled using solid elements as a cylindrical block 2.7 m (106 inches) in diameter and 2.0 m (79 inches) in length as shown in Figure 30. The dimension of the soil buckets is consistent with that in the NCAC strong post guardrail barrier model. A foam and soil material was used for the soil. This material model is a simple model for soil and foam. The material properties of the soil were taken from the NCAC strong post guardrail barrier model. The material properties of this model were obtained from test data of a Bogie vehicle impacting posts embedded in similar soil (Marzougui et al., 2007).

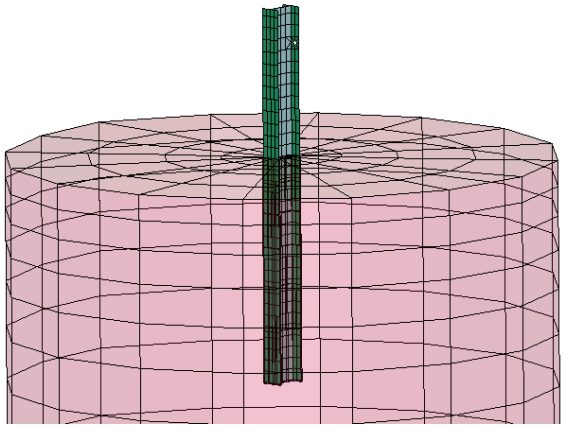

Figure 30. Strong Post and Soil Bucket Connection

3.2.4 The Development of the Pendulum Model

The finite element model of the pendulum consisted of two parts: the pendulum mass and the impactor face. The pendulum mass was modeled using solid elements. Elastic material was used for the solid elements. The impactor face was modeled using shell elements. The dimension of the impactor face was modeled to have a height of 16 inches (0.41 m) in order to engage the full height of the w-beam. Rigid material was assigned to the impactor face. A layer of shell elements was created outside the pendulum mass for the contact between the impact face and pendulum mass. The total mass of the pendulum and impactor face was adjusted to match the actual pendulum and impactor weight of 2061.5 kg. Two accelerometers were created and

positioned at the rear of the pendulum mass. The top of the pendulum was supported by four suspension cables that were modeled using beam elements. A piecewise linear plastic material model was used for the steel cables. The material properties of the cables were taken from the anchor cables of the NCAC strong post guardrail barrier model. The top of the cables were connected to spring and damper elements to add damping effects to the motion of the pendulum. The top four nodes of the spring and damper elements were constrained to allow only rotational movement.

3.2.5 Test 01-1 Rail Only Test

The objective of this test was to ensure that the newly constructed pendulum impactor face was structurally adequate and that the custom length swaged anchor cables were able to provide adequate anchorage of the w-beam.

To simulate this test the soil buckets, post bolts and nuts, and blockouts were deleted from the basic model described above. An initial impact velocity of 15 mph (6.7 m/s) was assigned to the finite element model of the pendulum. The pendulum was positioned such that the impactor nose contacted the midspan of the rail section vertically. Automatic surface to surface contact algorithm was used for the contact between the impactor nose and the rail section. The overall test setup is shown in Figure 31.

Figure 31. Rail Only Test Setup

3.2.6 Test 01-2 Undamaged Strong Post W-Beam Barrier Test

The anchor brackets and cables were the same as those used in the model of rail only test. The model also included two strong posts, blockouts, and soil buckets. For the undamaged strong post w-beam barrier test, an initial impact velocity of 20 mph (8.9 m/s) was assigned to the finite element model of the pendulum. Three 36” (0.91 m) cables were used for each end of the rail section. The pendulum was positioned such that the impactor nose contacted the midspan of the rail section vertically and engaged the whole height of the w-beam.

3.2.7 Test 01-4 Missing Blockout Strong Post W-Beam Barrier Test

A finite element model was created for a two-post section of strong post w-beam barrier with a missing blockout at the splice location. The model was used to investigate the near failure of the splice joint in the pendulum test. The finite element model of the undamaged strong post guardrail system was used as the baseline input. Three 36” (0.91 m) cables were used for each end of the rail section. The routed wooden blockout at the splice location was deleted from the model. Automatic surface to surface contact algorithm was created for the contact between the w-beam and the strong post. The post-rail bolt remained in the model. The distance between the near flange of the post and the back of the w-beam rail was about 8 inches (0.20 m). The rail barrier was impacted by the pendulum at an initial impact speed of 20 mph (8.9 m/s). The rest of the test setup (shown in Figure 32) was the same as that in the undamaged test.

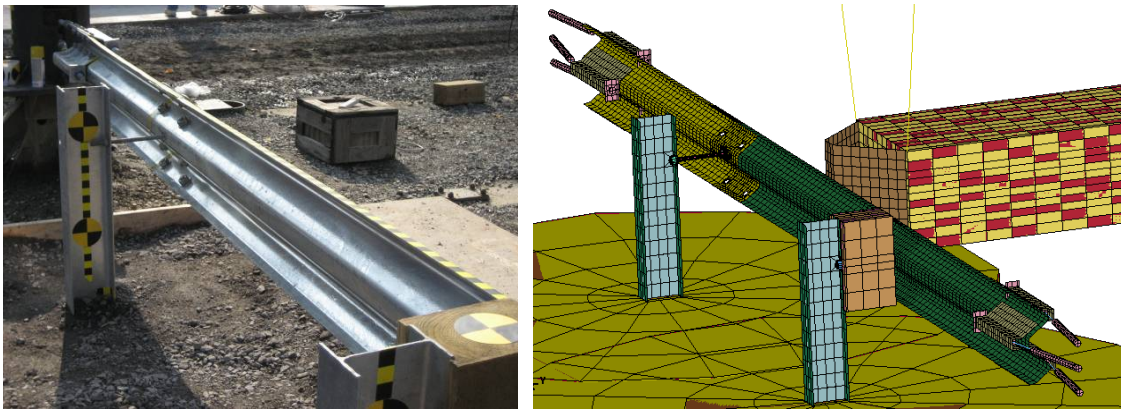

Figure 32. Missing Blockout Strong Post W-Beam Barrier Test Setup

3.2.8 Test 02-2 Twisted Blockout Strong Post W-Beam Barrier Test

A finite element model was created for a two-post section of strong post w-beam barrier with a routed blockout rotated about the post-rail bolt at the splice location. The finite element model of the undamaged strong post guardrail system was used again as the baseline input. Three 36” (0.91 m) cables were used for each end of the rail section. The blockout was rotated 50° clockwise around the post-rail bolt to represent the incorrect installation. An initial impact velocity of 20 mph (8.9 m/s)was applied to the pendulum. The overall test setup is shown in Figure 33.

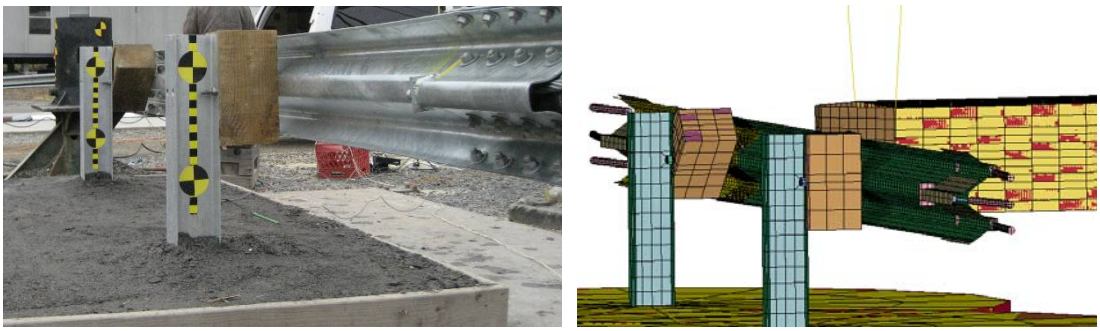

Figure 33. Twisted Blockout Strong Post W-Beam Barrier Test Setup

3.2.9 Test 08-3 Test Level 2 Weak Post W-Beam Barrier Test

A finite element model was created for a one-post section of Test Level 2 weak post w-beam barrier. The finite element model of the undamaged Test Level 2 weak post guardrail

system was used as the baseline input. Two 40” (1.02 m) cables were used for each end of the rail section. The weak post guardrail model and the pendulum model were assembled using Hypermesh. An initial impact velocity of 15 mph (6.7 m/s) was applied to the pendulum. The overall test setup is shown in Figure 34.

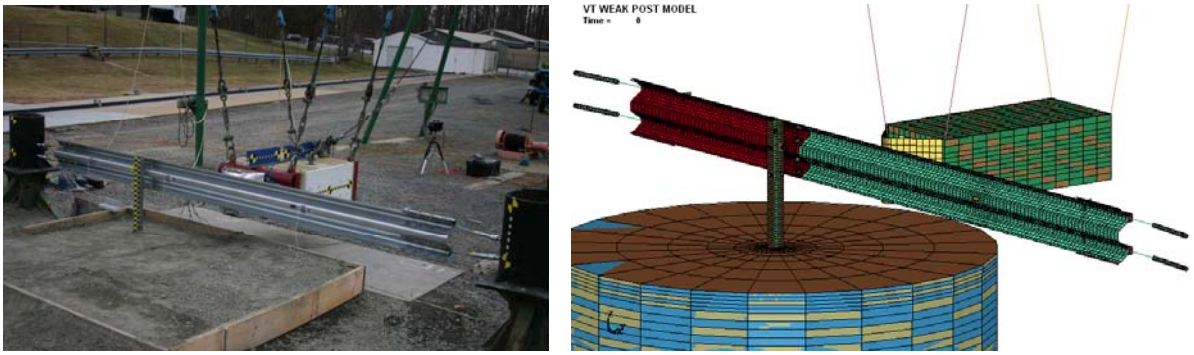

Figure 34. Test Level 2 Weak Post W-Beam Barrier Test Setup

3.2.10 Test 08-4 Test Level 3 Weak Post W-Beam Barrier Test

A finite element model was created for a one-post section of Test Level 3 weak post w-beam barrier. The finite element model of the undamaged Test Level 3 weak post guardrail system was used as the baseline input. Two 40” (1.02 m) cables were used for each end of the rail section. The weak post guardrail model and the pendulum model were assembled using Hypermesh. An initial impact velocity of 15 mph (6.7 m/s) was applied to the pendulum. The overall test setup is shown in Figure 35.

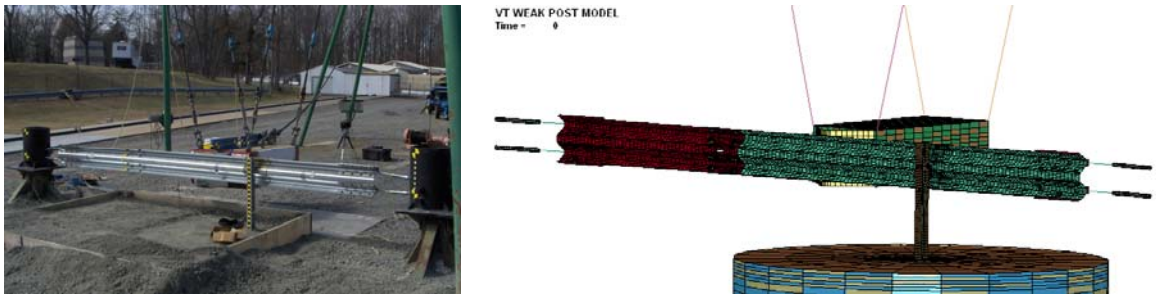

Figure 35. Test Level 3 Weak Post W-Beam Barrier Test Setup

3.2.11 Validation Method

Film analysis was completed to determine rail deflections at the impact point and the strong posts. The rail deflection versus time curve obtained from the overhead view of the test video by tracking the positions of the impact point at each time frame of the video. Due to the movement of the overhead camera during the impact, positions of a marker on the ground were also recorded to calculate the relative displacement of the guardrail. The deflection curve was compared to that in the simulation. The frame rate of the high speed cameras was 500 frames per second.

3.3 Analysis of Results

3.3.1 Test 01-1 Rail Only Test

The simulation results were first compared to the rail only test data. The rail deflection histories at the impact point are shown in Figure 36. The rail only barrier section successfully contained the pendulum mass impacting at 15.91 mph (7.1 m/s). The rail deflections obtained from the simulation and video were comparable to each other. The maximum rail deflection obtained from film analysis was 24.6 inches (0.62 m) at 0.142 s after initial impact, while the maximum rail deflection in the simulation was 24.2 inches (0.61 m) at 0.136 s after impact. A direct measurement of the damaged rail (removed from the test location) indicated a maximum static deflection of 15.75 inches (0.40 m). The rail deflection at the end of the simulation was 16.1 inches (0.41 m). Sequentially images from Test 01-1 and simulation are shown in Figure 37.

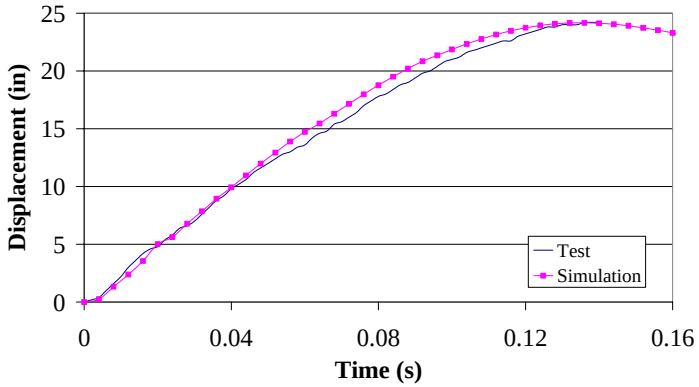

Figure 36. Rail Deflections at the Impact Point (Test 01-1)

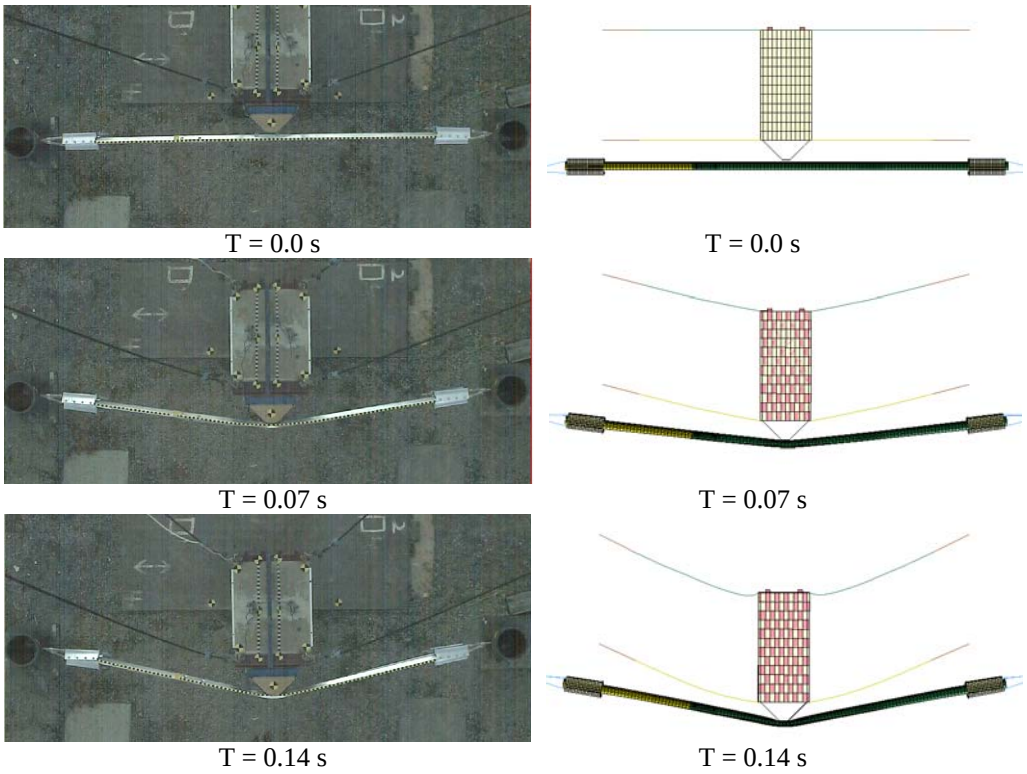

Figure 37. Sequential Images from the Test and Simulation (Test 01-1)

3.3.2 Test 01-2 Undamaged Strong Post W-Beam Barrier Test

The undamaged rail test was simulated using LS-DYNA and the simulation results were compared to the test data. The video from the overhead camera was utilized to analyze the motion of the impact point, anchor cables, and the two strong posts. The rail deflection histories at the impact point, the rail trajectories at the blockout locations, and post trajectories are shown

in Figure 38, Figure 39, and Figure 40 respectively. The displacement of the opposite corners of the strong posts was tracked from the high speed video. The original positions of two strong posts are also plotted in Figure 39. The sequential snapshots were taken from the video and simulation, and are shown in Figure 41. The undamaged barrier successfully contained the pendulum mass impacting at 20.46 mph (9.1 m/s). The maximum dynamic rail deflection obtained from the film and simulation was 26.6 inches (0.68 m) at 0.128 s and 22.2 (0.56 m) inches at 0.13 s after initial impact respectively.

Overall, the pendulum model underestimated the undamaged guardrail test in rail deflections at impact point by 16 % (112 mm). The material properties of soil could account for the difference in rail deflections. The analysis of rail trajectories at blockout locations also showed that the maximum rail deflections in the simulation were less than the values obtained from the video. It was observed from Figure 39 that the trajectories of the left post, where the splice connection was located, were very close to each other in the simulation and test. Significant difference was seen in the trajectories of the right post. Further film analysis revealed that earlier separation of the right blockout from the w-beam in the test than in the simulation led to more lateral movement of the right post. It was also found in the film that the pendulum was not precisely centered between the left and right posts. The pendulum was 3 inches (0.08 m) closer laterally to the right post. This difference was incorporated into the model. Post-test pictures also showed that the severe deformation was observed in the junction between the webbing and flange of the left post. Compared to the left post, the right post had more lateral motion.

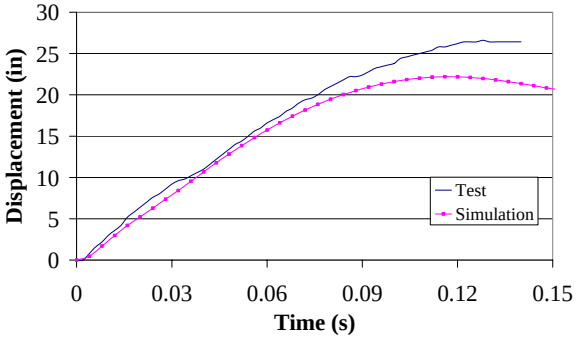

Figure 38. Rail Deflections at the Impact Point (Test 01-2)

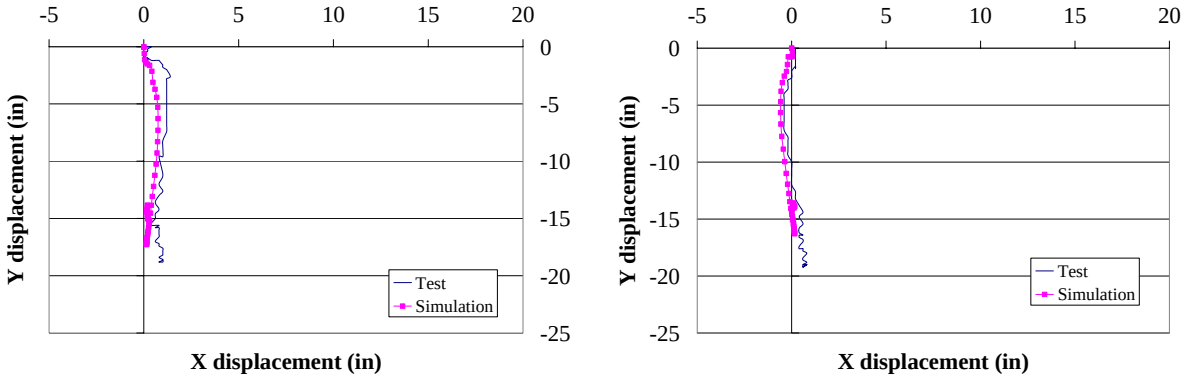

Figure 39. Rail Trajectories at the Blockout Locations (Test 01-2)

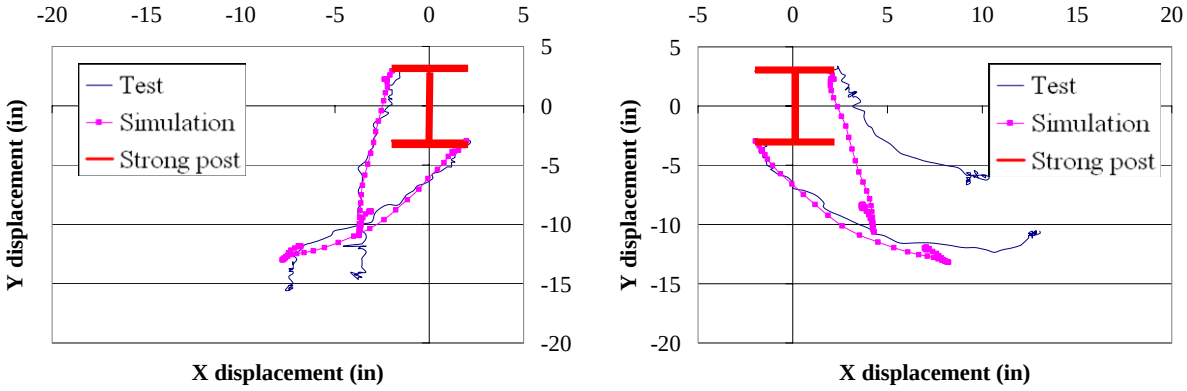

Figure 40. Strong Post Trajectories in the Undamaged Barrier Test (Test 01-2)

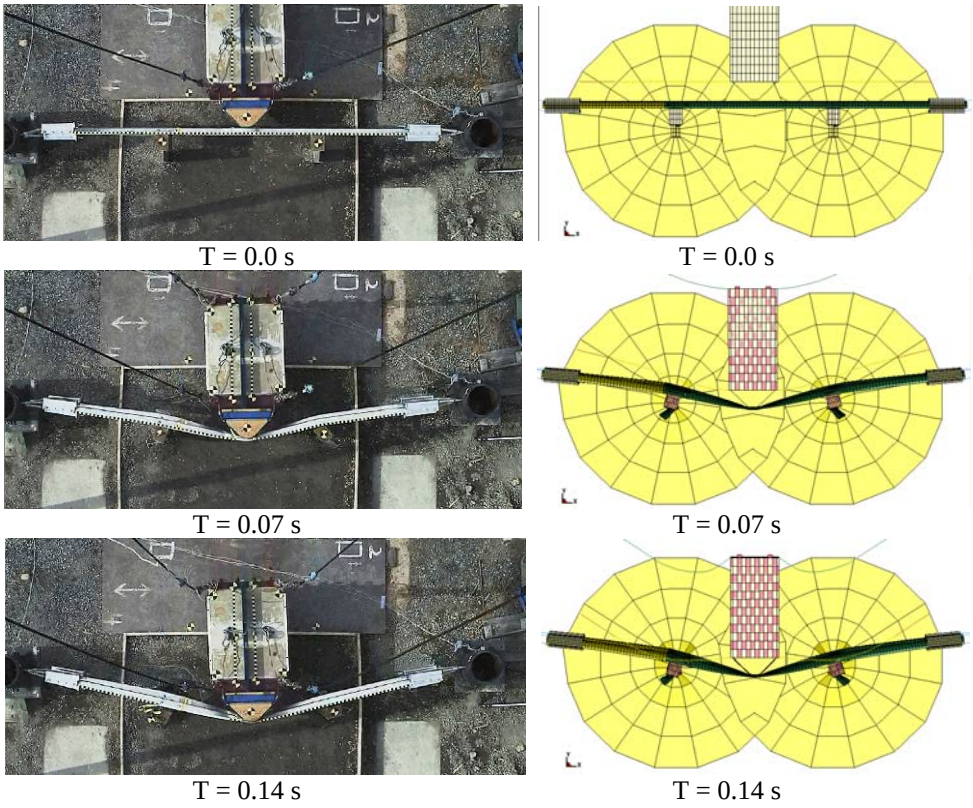

Figure 41. Sequential Snapshots from the Video and Simulation (Test 01-2)

3.3.3 Test 01-4 Missing Blockout Strong Post W-Beam Barrier Test

In this test, the rail barrier was impacted by the pendulum at an initial impact velocity of 20.45 mph (9.1 m/s). In the test, a 9 inch (0.23 m) long vertical tear developed at the splice location during the impact. The missing blockout test was simulated using LS-DYNA to help investigate the cause of near failure at the splice location. The high speed video was utilized to analyze the motion of the impact point and the two strong posts. The displacement of the opposite corners of the strong posts was tracked from the high speed video. The rail deflection histories at the impact point and post trajectories were shown in Figure 42 and Figure 43 respectively. The original positions of two strong posts are also plotted in Figure 43.

Sequentially images from Test 01-1 and simulation are shown in Figure 44. The rail deflections predicted by the model were generally in good agreement with the test data. The

maximum rail deflection in the simulation was 24.4 inches (0.62 m) at 0.13 s after initial impact. The maximum dynamic rail deflection obtain from the overhead video was 25.8 inches (0.66 m) at 0.128 s after initial impact. The analysis of post trajectories showed that the left post had more lateral movement in the simulation than that seen in the test. The right post trajectories of the model and the test were close to each other. Rail tension (Figure 45) versus time data in the missing blockout test was compared to those in the undamaged test to investigate the cause of vertical tear at the splice location. The maximum rail tension force measured at the splice location in the simulation was 413 kN, which was 6.5% higher than that obtained in the undamaged rail barrier test. The maximum rail tension reported in the literature was 500 kN (Gentry and Bank, 1998). This increase in rail tension in the missing blockout test may have contributed to the rail tear at the splice location.

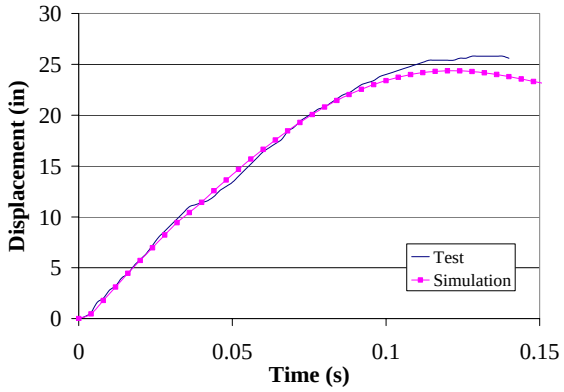

Figure 42. Rail Deflections at the Impact Point (Test 01-4)

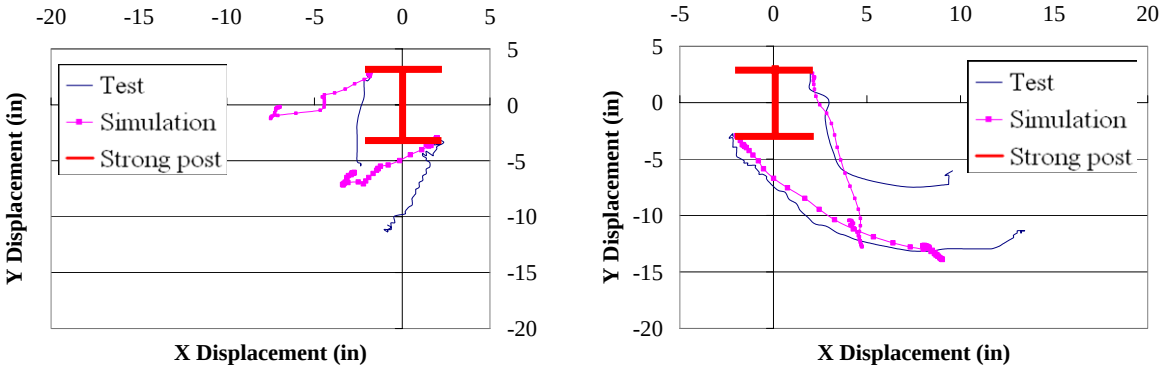

Figure 43. Strong Post Trajectories in the Missing Blockout Test (Test 01-4)

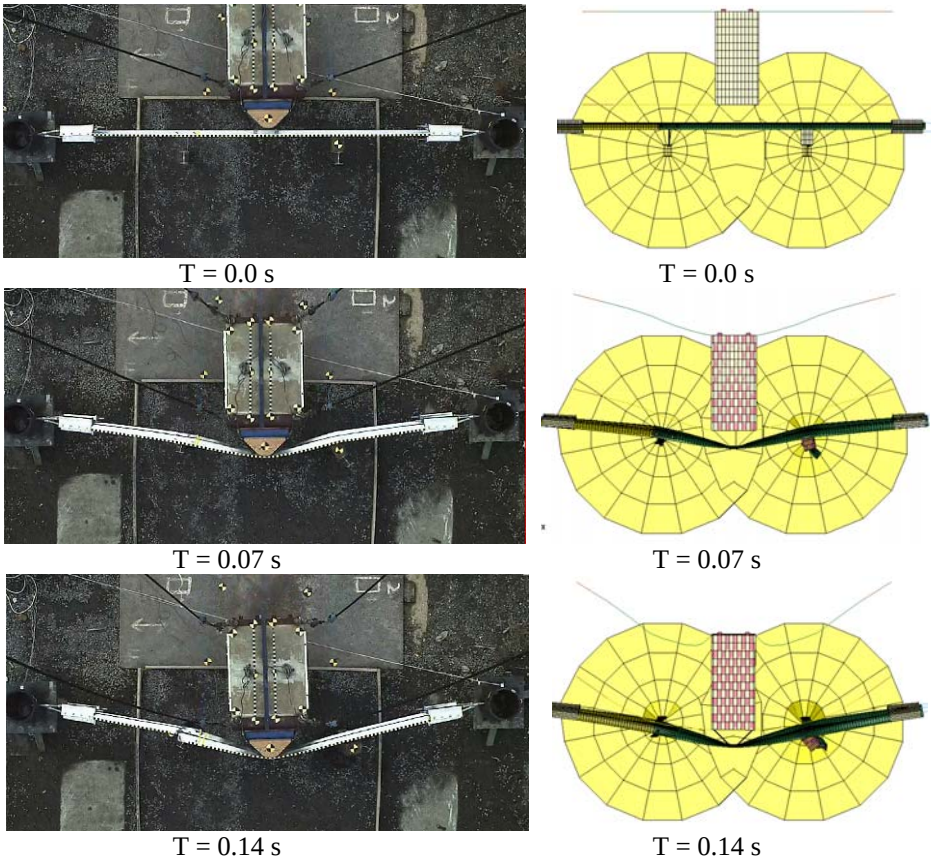

Figure 44. Sequential Snapshots from the Video and Simulation (Test 01-4)

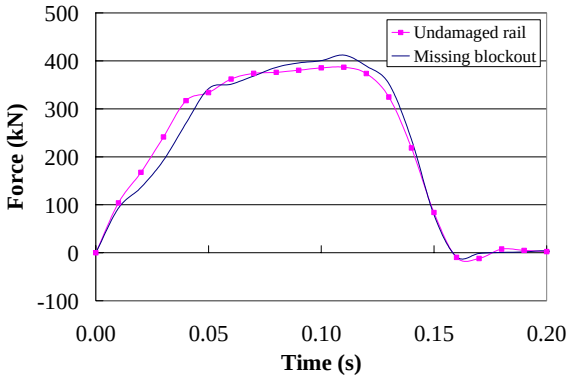

Figure 45. Rail Tension in the Missing Blockout Test (Test 01-4)

3.3.4 Test 02-2 Twisted Blockout Strong Post W-Beam Barrier Test

The twisted blockout test was simulated using LS-DYNA. In the pendulum experiment, the barrier section successfully contained the pendulum with an initial impact velocity of 19.33 mph (8.6 m/s). The high speed video from the overhead camera was utilized to analyze the

motion of the impact point and the two strong posts. The displacement of the opposite corners of the strong posts was tracked from the high speed video. The rail deflection histories at the impact point and post trajectories are shown in Figure 46 and Figure 47 respectively. The original positions of two strong posts are also plotted in Figure 47. The rail deflection predicted by the model was generally in good agreement with the test data. The maximum rail deflection in the simulation was 21.0 inches (0.53 m) at 0.12 s after initial impact. The maximum dynamic rail deflection obtain from the overhead video was 23.6 inches (0.60 m) at 0.118 s after initial impact. The analysis of post trajectories showed that the right post had less lateral movement in the simulation than that seen in the test.

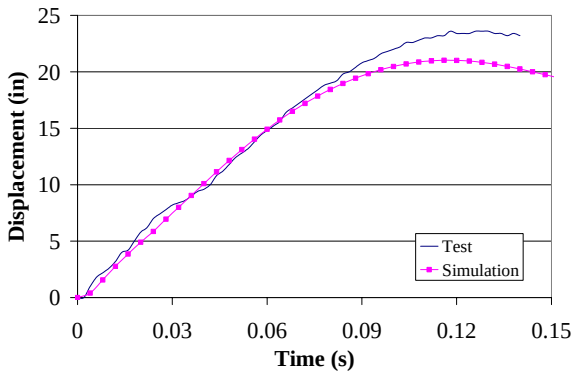

Figure 46. Rail Deflections at the Impact Point (Test 02-2)

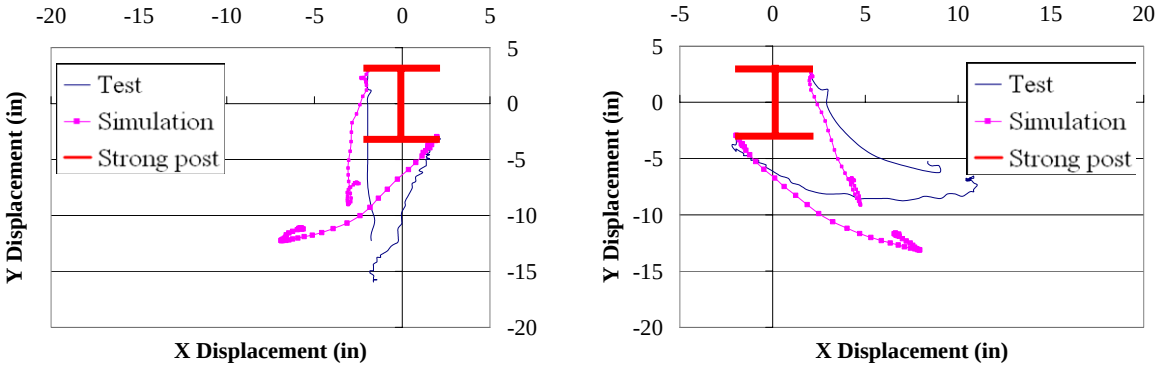

Figure 47. Strong Post Trajectories in the Twisted Blockout Test (Test 02-2)

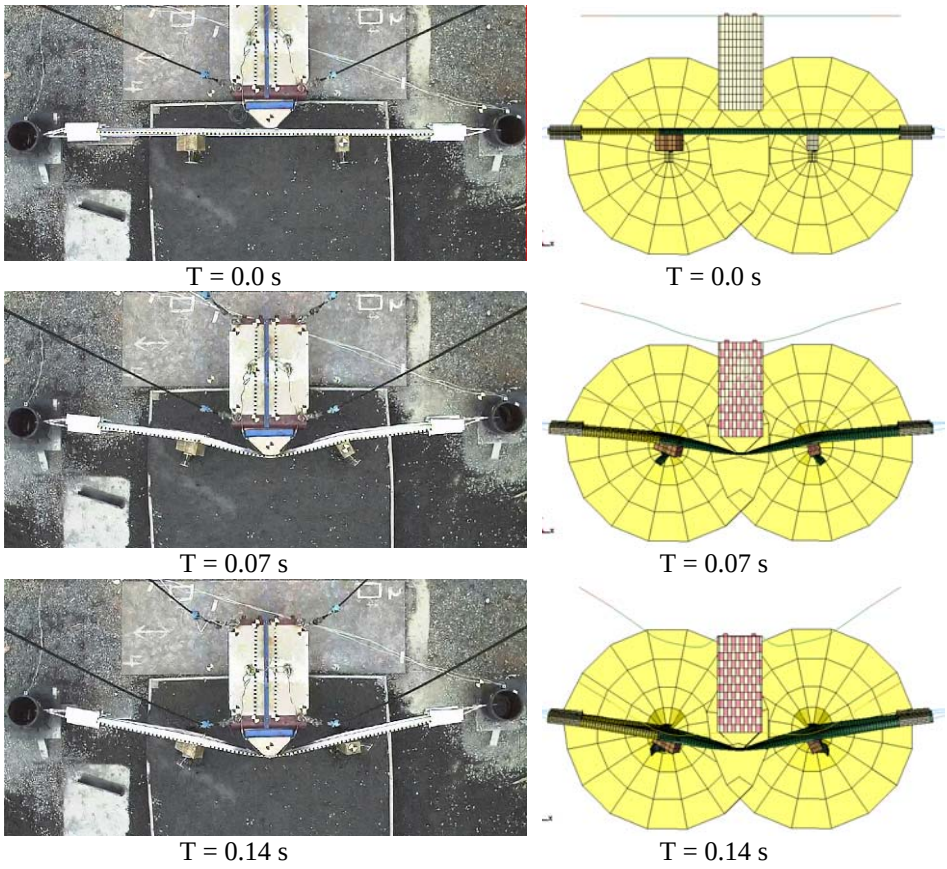

Figure 48. Sequential Snapshots from the Video and Simulation (Test 02-2)

3.3.5 Test 08-3 Test Level 2 Weak Post W-Beam Barrier Test

The Test Level 2 weak post test was simulated using LS-DYNA. In the pendulum experiment, the barrier section successfully contained the pendulum with an initial impact velocity of 14.9 mph (6.7 m/s). It was observed from the test that the weak post separated from the w-beam guardrail due to the impact (Figure 49). The accelerometer in the pendulum was utilized to analyze deflection of the guardrail. Note that overhead camera failed to trigger during the impact. The rail deflection history at the impact point is shown in Figure 50. The rail deflection predicted by the model was generally in good agreement with the test data. The maximum rail deflection in the simulation was 27.6 inches (0.70 m) at 0.14 s after initial impact.

The maximum dynamic rail deflection obtained from the acceleration data was 28.5 inches (0.72 m) at 0.16 s after initial impact.

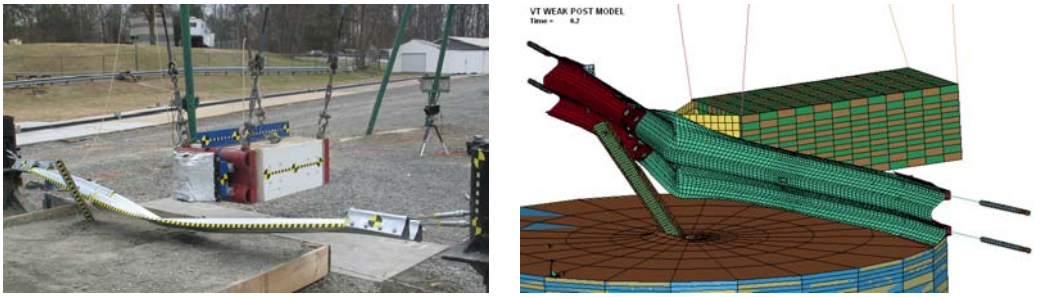

Figure 49. Post Impact Images of Test and Simulation of the Test Level 2 Weak Post Barrier

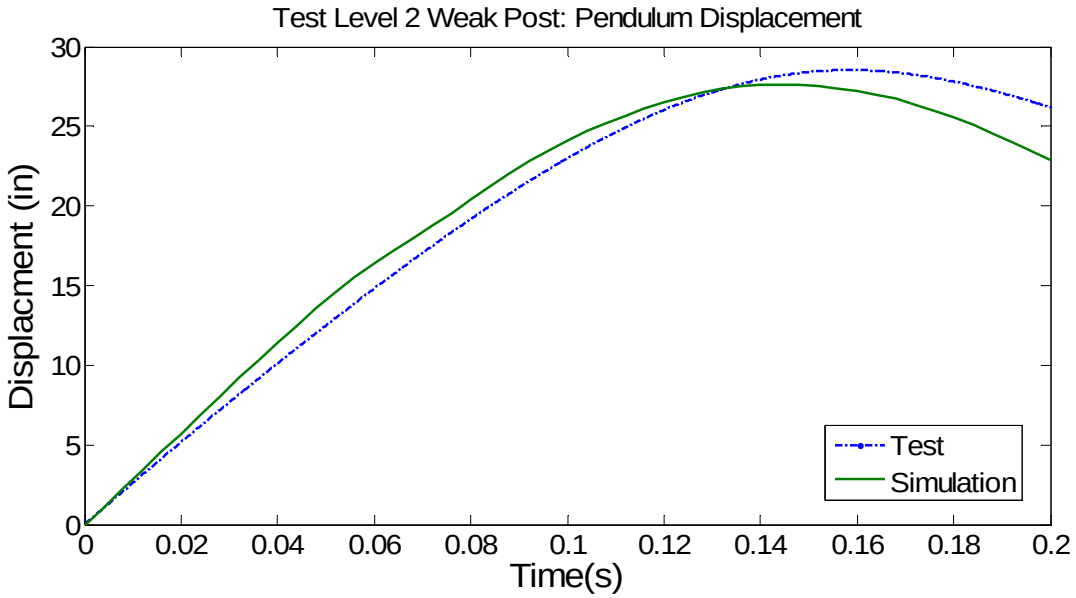

Figure 50. Rail Deflections at the Impact Point (Test 08-3)

3.3.6 Test 08-4 Test Level 3 Weak Post W-Beam Barrier Test

The Test Level 3 weak post test was simulated using LS-DYNA. In the pendulum experiment, the barrier section successfully contained the pendulum with an initial impact velocity of 14.2 mph (6.3 m/s). It was observed from the test that the weak post and backup plate separated from the w-beam guardrail due to the impact (Figure 51). The accelerometer in the pendulum was utilized to analyze deflection of the guardrail. The rail deflection history at the impact point is shown in Figure 52. The rail deflection predicted by the model was generally in

good agreement with the test data. The maximum rail deflection in the simulation was 23.5 inches (0.60 m) at 0.15 s after initial impact. The maximum dynamic rail deflection obtained from the acceleration data was 26.4 inches (0.67 m) at 0.15 s after initial impact. The maximum dynamic rail deflection obtained from the overhead video was 26.0 inches (0.66 m) at 0.15 s after initial impact.

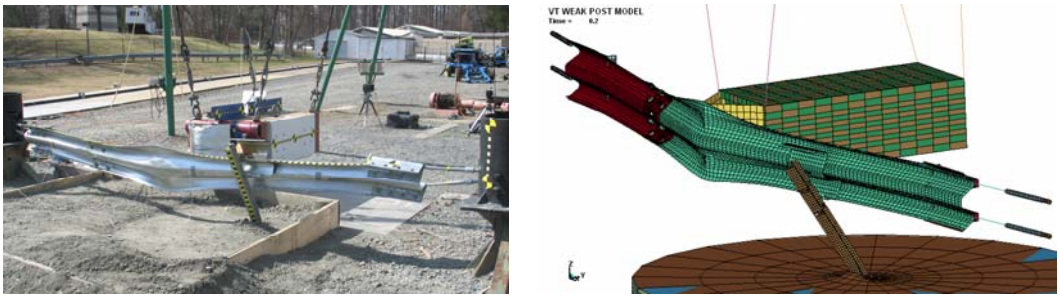

Figure 51. Post Impact Images of Test and Simulation of the Test Level 3 Weak Post Barrier

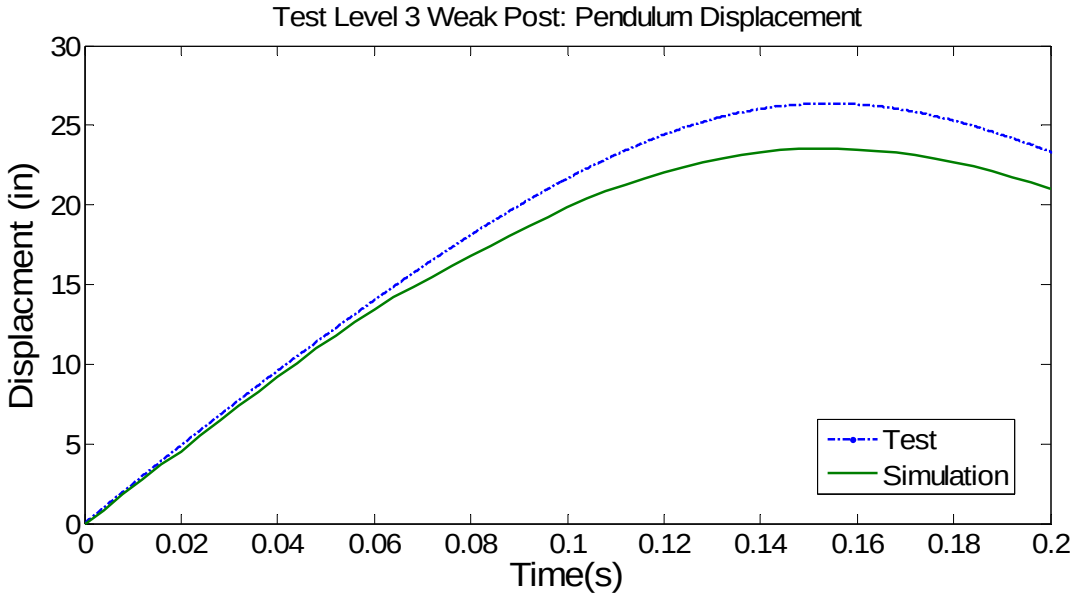

Figure 52. Rail Deflections at the Impact Point (Test 08-4)

3.4 Discussion

Comparisons of experiment and simulation results showed that the deflection of the guardrail test section in the simulations was in good agreement with that in all tests. Generally, simulations underestimated the deflections in the tests by 8 %. This indicates that the full scale

strong and weak post finite element models could correctly predict the deflection and deformation of the guardrail barrier in roadside crashes across multiple speeds. Following are discussions of specific components of the model.

- **Post-Soil Interaction:** Trajectories of the left post in the strong post w-beam simulations were very similar to those in the tests. Much larger variations were seen in the trajectories of the right post between tests and simulations. This difference was a result of limited rotation of the right post in the soil bucket. The results could be improved by refining the mesh of the soil or replacing the current soil material model by other models with better characterized material properties. It is expected that the computational time would increase with the finer mesh.
- **Failure Criteria:** It should be noted that no failure criterion was specified for the guardrail system in the existing NCAC full scale model. This lack of a failure criterion limited the ability of the barrier model to predict any guardrail tearing or rupture. Modeling material failure can be very challenging. The failure mechanism is sensitive to mesh density of the guardrail model. Extensive material testing may be required to obtain an accurate value of failure plastic strain of the rail is needed to describe this failure mode.

This study has shown that pendulum tests are a promising way to study guardrail components with minor damage under controlled testing conditions. Costs of pendulum tests are substantially less than those of full scale crash tests.

One limitation of using pendulum tests to validate the full scale barrier model was the use of rigid end constraints. In the full scale test, the kinetic energy of the vehicle is generally dissipated along several guardrail sections in the barrier system. However, in pendulum tests the

pendulum impacted one section of the guardrail barrier at a single speed and single impact point, which could result in excessive rail tension and consequently the failure of the splice connection.

Also, Energy losses (Coon and Reid, 2005) during a vehicle-barrier impact are due to (1) barrier–vehicle friction; (2) post/soil deformations; (3) guardrail beam deformations, and (4) vehicle energy losses attributed to the vehicle (this is composed of actual vehicle damage and tire–ground friction, with vehicle damage being predominate). In the pendulum setup, the friction between vehicle and barrier was not considered.

Another limitation in the current pendulum test setup was the shape of the pendulum impactor face. In either the full scale vehicle test or the pendulum test, kinetic energy was mostly dissipated through the deformation of the w-beams, post, and the soil. Especially, generally uniform deformation of the guardrail sections was observed along the damage length of the barriers from the post-test pictures of full scale vehicle barrier tests. Due to the shape of the current impactor face, the pendulum can only contact very limited area of the w-beam section. As a result, instead of distributing energy to the whole test section, the pendulum only induced local deformation of the w-beam in the impact area. This could also account for the failure of splice connections observed in some pendulum tests.

3.5 Conclusions

This study has conducted a series of validation tests on the full scale strong and weak post guardrail model. Our approach has been to compare the results of simulations of pendulum impact tests with corresponding test data. The undamaged guardrail section and two damaged guardrail types, the missing blockout and twisted blockout, were tested and simulated. Impact speeds ranged from 15 to 20 mph.

Comparisons of experiment and simulation results demonstrated that the guardrail section taken from the full scale strong and weak post models were good representations of the real test sections in the pendulum tests. The results suggested that the full scale strong and weak post models had good prediction capability in terms of overall guardrail deflection. Some differences were observed in the movement of strong posts between the experiments and simulations. This difference did not impede the ability of the model to accurately predict peak rail deflection. However, this discrepancy could affect the prediction of post or splice failure.

4. FINITE ELEMENT MODELING OF WEAK POST GUARDRAIL SYSTEMS WITH MINOR DAMAGE UNDER NCHRP REPORT 350 TEST LEVEL 2 IMPACTS

4.1 Introduction

The Federal Highway Administration (FHWA) requires that all longitudinal barriers should perform acceptably. Damage to a longitudinal roadside barrier is affected by a variety of activities and factors, and not always characterized by the large rail deformations and sheared posts characteristic of a high severity crash. Minor crashes, snow plowing, mowing operation, and deterioration due to environmental conditions can all contribute to guardrail system damage. Much more common is minor damage such as a shallow dent which is a result of a low speed collision or sideswipe (Figure 53). Such damage may or may not be repaired by maintenance forces and it could compromise the barrier's crash performance. The effect of this minor damage on the performance of the barrier in subsequent impacts is not well understood and there is little barrier repair guidance available for highway personnel tasked with maintaining these systems.

Therefore, the goal of this study is to develop barrier repair guidelines for highway personnel. The guidelines will help determine the degrees of minor damage to guardrail barriers that need maintenance. The research approach in this study will be to evaluate the common damage types with a combination of controlled experiments and finite element modeling.

Figure 53. Minor Rail Deflection to a Strong Post W-Beam Barrier

4.1.1 Approach

Our approach will be to evaluate the more common damage types with a combination of controlled experiments and computational modeling and propose repair guidelines as necessary. The experiments will be used both to directly evaluate barrier performance and to validate the computational models.

4.1.2 Evaluation Criteria

The results of each damaged barrier impact experiment or simulation will be evaluated using criteria heavily based on NCHRP Report 350. For each test, the criteria shown in Table 2 will be used to evaluate crash performance.

Each metal beam barrier simulation will also be qualitatively assessed for barrier pocketing and the interaction between the vehicle suspension elements and the posts. In these cases, the baseline case (for the qualitative comparison) will be the respective vehicle impacting an undamaged barrier. Particular attention will be placed on vehicle stability including roll, pitch and yaw, wheel snagging, and the presence/absence of vaulting.

4.2 Methodology

The objectives were to investigate the limit of damaged weak post guardrail systems under NCHRP Report 350 Test Level 2 impacts and to develop recommendations for repairing weak post guardrail barrier systems with minor damages. Only deflection based minor damage to the weak post w-beam guardrail barrier was considered in this study. According to the National Cooperative Highway Research Program (NCHRP) Report 350, Level 2 tests require that longitudinal barriers be subjected to a full scale vehicle crash test of a 2000-kg pickup truck impacting at a speed of 70 km/h and an angle of 25 degrees and a full scale vehicle crash test of a 820-kg passenger car impacting at a speed of 70 km/h and an angle of 20 degrees. Due to the fact that the vast majority of weak post w-beam in the US is certified to only Test Level 2, the performance of damaged Test Level 3 weak post w-beam guardrail barrier was not included in the current study.

The development and validation of a weak post guardrail system were described in a previous chapter. The details of the model were described in reference (Wang and Gabler, 2008). A detailed finite element model of a 1994 Chevrolet C2500 pickup truck developed by the National Crash Analysis Center (NCAC) (NCAC Finite Element Model Archive, 2009) was used to induce minor damage to the guardrail system.

The proposed damage extents were 3, 6, and 9-inch lateral post/rail deflections. The midspan between two posts in the guardrail system was chosen as the initial impact point, which coincided with that in a NCHRP Report 350 Test Level 2 test. Since weak post w-beam guardrail barrier is a less stiff system compared to the strong post barrier, weak post systems could allow at least 87 inches dynamic deflection. The crash performance of weak post barriers with a more severe initial damage (18-inch post/rail deflection) was also investigated. In addition, simulations

were completed with the impact point at the post to examine the effects of the change in impact points on the performance of guardrail barriers. The proposed full scale vehicle crash test simulations are listed in Table 8.

Table 8. Summary of Proposed Full-Scale Crash Test Simulations

Barrier	Vehicle	Impact Point	Damage Type	Damage Extent
Weak Post W-Beam	2000P	Mid-Span	No Damage	-
			Post/Rail Deflection (no post detachment)	3", lateral
				6", lateral
				9", lateral
				18", lateral
Weak Post W-Beam	2000P	Post	Post/Rail Deflection (no post detachment)	3", lateral
				6", lateral
				9", lateral

4.2.1 Method for Modeling Pre-Existing Damage

The initial impact angle of the vehicle model was 25 degrees. The initial impact velocities were determined so that final static deflections of guardrail systems were 3, 6, 9, and 18 inches. Keyword *INTERFACE_SPRINGBACK_LSDYNA was used in the original simulations to obtain the damaged profiles of the guardrail systems. Simulations were repeated and initial impact speeds were adjusted until the desired the deflections were found.

The damaged weak post guardrail was impacted by the pickup model at the midspan or at the post for the second time. The initial velocity and angle of the vehicle for the second impact was 70 km/h and 25 degrees respectively. Data from the accelerometer located at the vehicle center of gravity were used for evaluation of vehicle performance and occupant injury risk.

A total of seven simulations were completed to generate weak post guardrail systems with minor damage. The maximum post/rail deflections for these impacts were 3, 6, 9, and 18 inches. Due to the height of the vehicle bumper relative to the guardrail top, the lower part of the guardrail section was generally deformed more than the upper part for all three deflection modes.

At the end of all simulations, damage was measured from the point with the most deflection to the back edges of the w-beam cross section before impact. A summary of the initial impact velocities and measured rail/post deflections are presented in Table 9. The contours of the undamaged guardrail and guardrails with 3, 6, 9, and 18-inch deflections are shown in Figure 54.

Table 9. Initial Vehicle Impact Speeds and Induced Guardrail Deflections

Impact Point	Damage Modes	Initial Impact Velocity	Max. Rail Deflection	Max. Post Deflection
Mid-Span	3” Deflection	3.4 mph	3.3”	1.1”
	6” Deflection	7.8 mph	6.0”	2.9”
	9” Deflection	11.2 mph	9.2”	7.4”
	18” Deflection	20.1 mph	19.8”	34.0”
Post	3” Deflection	5.6 mph	2.7”	2.2”
	6” Deflection	8.9 mph	5.7”	4.1”
	9” Deflection	12.3 mph	9.4”	6.6”

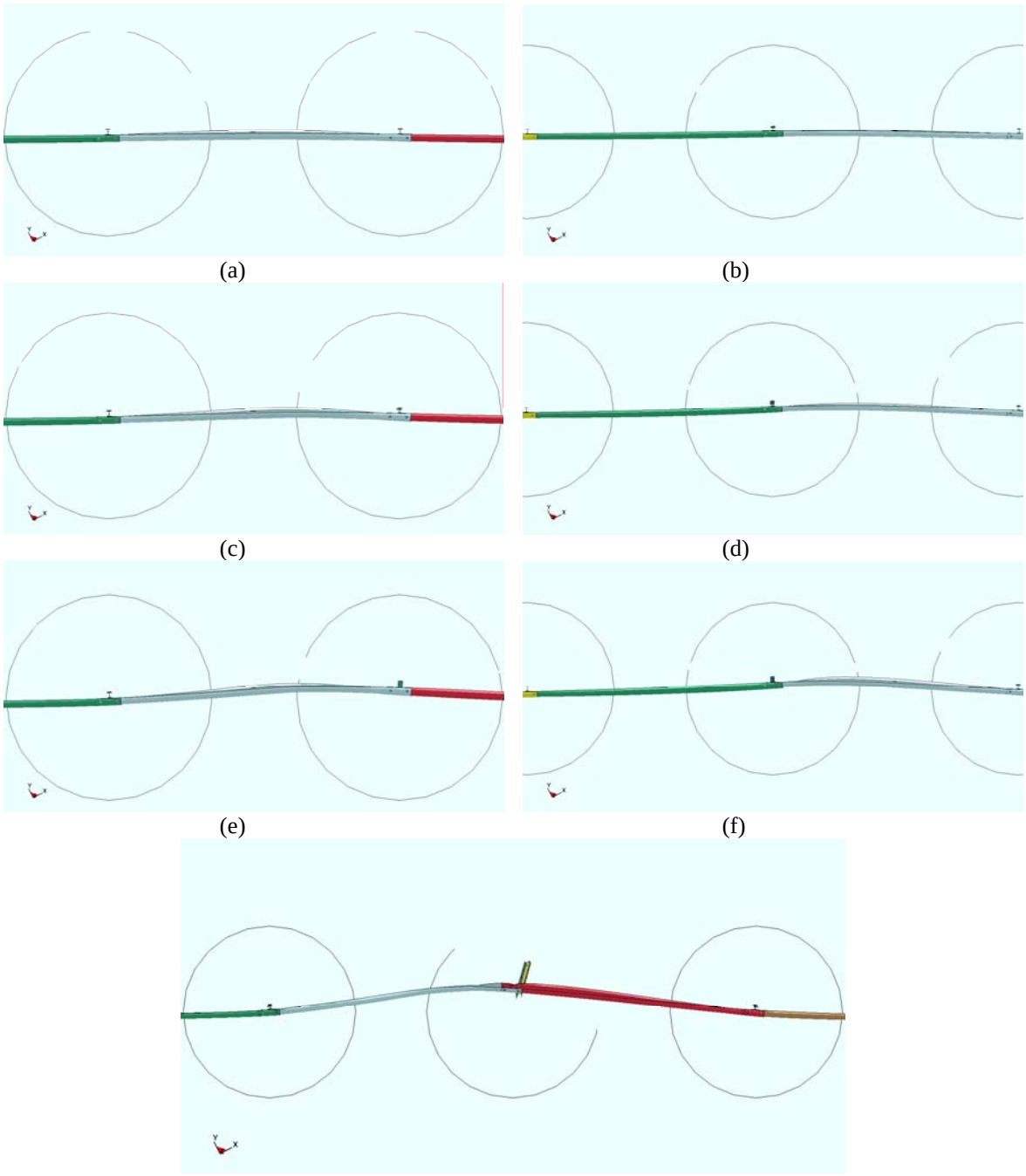

Figure 54. Contours of the Guardrails with Minor Damage: (a) 3-in Deflection at Mid-Span (b) 3-in Deflection at Post (c) 6-in Deflection at Mid-Span (d) 6-in Deflection at Post (e) 9-in Deflection at Mid-Span (f) 9-in Deflection at Post (g) 18-in Deflection at Mid-Span

Because of the support from the posts, the initial velocities of the vehicles used to create pre-existing damage for the simulations with impact point at the post were higher than their counterparts. Maximum post/rail deflections were found downstream of the initial impact point

in all simulations, which was the result of the frontal oblique impact direction. In the simulations with 3, 6, and 9-inch deflections, the weak posts and w-beams remained connected by the post bolts and nuts. However, due to the severity of the initial impact, the post separated from the guardrail in the simulation with 18-inch post/rail deflection. The simulation setup of the Test Level 2 weak post guardrail barriers with 3, 6, 9, and 18-inch deflections are shown from Figure 55 to Figure 58.

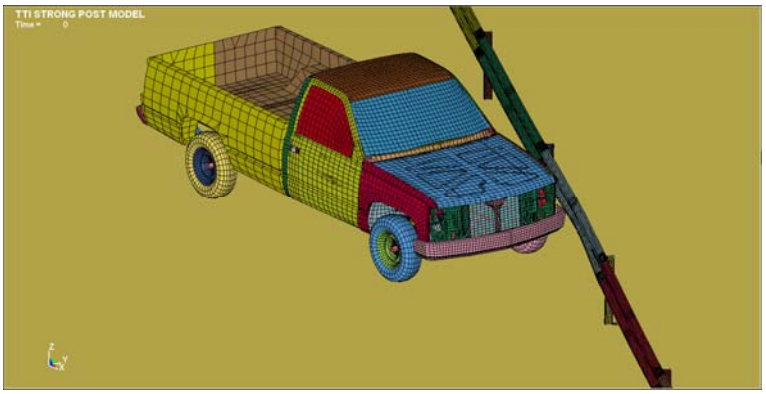

Figure 55. Simulation Setup of the Weak Post Model with 3-Inch Deflection at Mid-Span

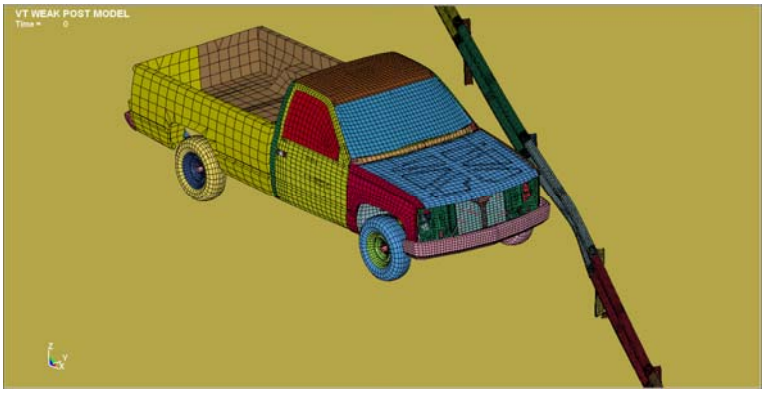

Figure 56. Simulation Setup of the Weak Post Model with 6-Inch Deflection at Mid-Span

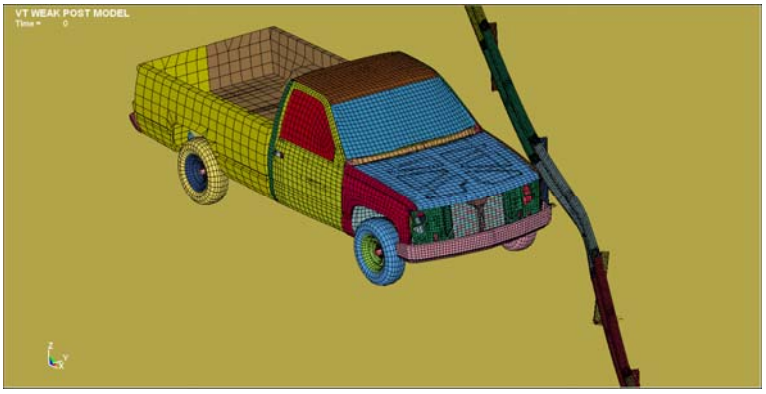

Figure 57. Simulation Setup of the Weak Post Model with 9-Inch Deflection at Mid-Span

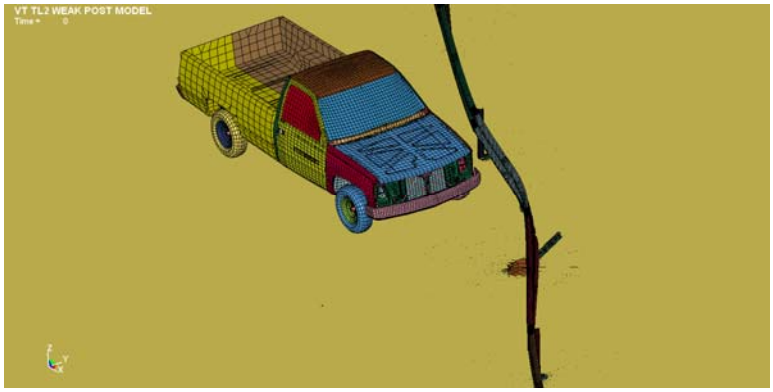

Figure 58. Simulation Setup of the Weak Post Model with 18-Inch Deflection at Mid-Span

4.2.2 Investigation of Sagging of Damaged Guardrail

Simulations results of the initial impact to create weak post barrier with 18-in deflection showed that the post downstream of the impact point separated from the rail. As a result, the damaged guardrail section with a total length of 7.6 m was not supported at the end of the impact.

Therefore, an additional simulation was completed to investigate the effect of gravity on the damaged and unsupported guardrail section. The vehicle model was not included in this simulation. The damaged profile of the guardrail section was obtained from the first impact. The whole weak post w-beam guardrail barrier was only affected by gravity during duration of 2 s. The damage area of the guardrail barrier before and after the simulation was plotted in Figure 59.

Although the rail height in the damaged area was lowered by 94 mm due to gravity, the rail section without the post did not fall to the ground. The profile of the damaged guardrail after sagging was used for the subsequent Test Level 2 impact.

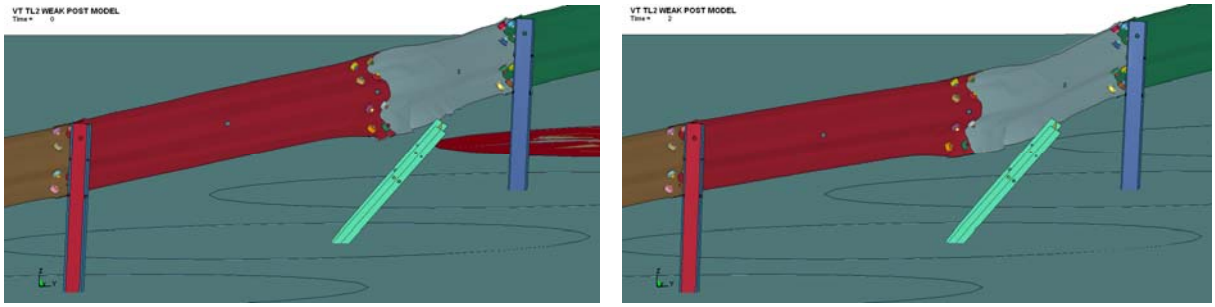

Figure 59. Effect of Gravity on Damaged Guardrail Barriers: Beginning of the Simulation (left) and End of the Simulation (right)

4.3 Results

For the W-beam weak-post roadside barrier system, TTI Test No. 471470-22 (Mak et al., 1998) was selected for result comparison. The test setup was based on the NCHRP Report 350 Test Level 2 configuration. Guardrail deflections, vehicle exit velocity and angle, occupant impact velocity (OIV), and occupant ridedown acceleration (ORA) were computed from the simulations and compared to the undamaged guardrail system as well as test data. A summary of the simulation results of damaged weak post barriers impacted at the midspan is presented in Table 10. A summary of the simulation results of damaged weak post barriers impacted at the post is presented in Table 11.

Table 10. Comparisons of Test Results and Simulations of Damaged Weak Post Barriers under Test Level 2 Impacts at the Mid-Span

	Test No. 471470-22	Undamaged Barrier	3"deflection	6"deflection	9"deflection	18"deflection
Impact Conditions						
Vehicle Impact Speed (km/h)	71.0	71.0	71.0	71.0	71.0	71.0
Vehicle Impact Angle(deg)	26.1	26.1	26.1	26.1	26.1	26.1
Test Article Deflection (m)						
Max. Dynamic	1.4	1.46	1.35	1.52	1.51	1.55
Max. Permanent	1.3	0.95	1.00	0.92	0.81	1.16
Test Article Damage						
Max. Effective Stress (MPa)	N/A	1100	1141	1142	1359	1099
Max. Effective Plastic Strain	N/A	0.311	0.323	0.303	0.403	0.375
Max. Initial Stress (MPa)	N/A	N/A	381	362	416	424
Max. Initial Strain	N/A	N/A	0.035	0.067	0.072	0.087
Max. Rail Tension (kN)	N/A	226	232	264	265	286
Exit Conditions						
Vehicle Exit Speed (km/h)	25.7	23.4	20.8	14.4	24.9	27.1
Vehicle Exit Angle (deg)	9.5	4.9	6.2	5.0	6.3	5.1
Occupant Risk Values						
Longitudinal OIV (m/s)	4.6	5.7	5.6	5.8	5.6	5.5
Lateral OIV (m/s)	3.3	3.2	3.3	3.1	3.1	3.5
Longitudinal ORA (G's)	-4.8	-1.6	-2.6	-2.9	-1.6	-2.5
Lateral ORA (G's)	3.1	1.5	0.1	3.5	0.9	0.4
Max. 50-ms Average (G's)						
Longitudinal	-3.1	-3.5	-3.9	-3.7	-4.0	-3.2
Lateral	2.6	3.1	2.6	2.4	2.8	2.6
Vertical	-1.6	-1.5	-1.5	-1.7	-1.6	-1.3
Vehicle Behavior						
Max. Roll Angle (deg)	9	3	6	4	4	2
Max. Pitch Angle (deg)	-3	-1	-4	-1	-2	-1
Max. Yaw Angle (deg)	37	30	31	29	30	29
Vehicle Specifications						
Weight (kg)	2076	2013	2013	2013	2013	2013
Wheelbase (mm)	3350	3382	3382	3382	3382	3382
Bumper Height (Upper Edge) (mm)	680	635	635	635	635	635

Table 11. Comparisons of Test Results and Simulations of Damaged Weak Post Barriers under Test Level 2 Impacts at the Post

	Test No. 471470-22	Undamaged Barrier	3"deflection	6"deflection	9"deflection
Impact Conditions					
Vehicle Impact Speed (km/h)	71.0	71.0	71.0	71.0	71.0
Vehicle Impact Angle(deg)	26.1	26.1	26.1	26.1	26.1
Test Article Deflection (m)					
Max. Dynamic	1.4	1.46	1.25	1.35	1.28
Max. Permanent	1.3	0.95	0.93	0.81	1.04
Test Article Damage					
Max. Effective Stress (MPa)	N/A	1100	880	1111	1104
Max. Effective Plastic Strain	N/A	0.311	0.205	0.312	0.257
Max. Initial Stress (MPa)	N/A	N/A	324	406	413
Max. Initial Strain	N/A	N/A	0.021	0.051	0.062
Max. Rail Tension (kN)	N/A	226	206	210	247
Exit Conditions					
Vehicle Exit Speed (km/h)	25.7	23.4	23.2	15.5	11.5
Vehicle Exit Angle (deg)	9.5	4.9	5.5	5.8	3.5
Occupant Risk Values					
Longitudinal OIV (m/s)	4.6	5.7	5.6	5.9	5.8
Lateral OIV (m/s)	3.3	3.2	3.4	3.3	3.5
Longitudinal ORA (G's)	-4.8	-1.6	-1.3	-0.5	-4.8
Lateral ORA (G's)	3.1	1.5	4.0	2.2	1.3
Max. 50-ms Average (G's)					
Longitudinal	-3.1	-3.5	-3.6	-3.7	-3.8
Lateral	2.6	3.1	2.9	2.5	2.8
Vertical	-1.6	-1.5	-2.0	-1.7	-1.4
Vehicle Behavior					
Max. Roll Angle (deg)	9	3	4	2	2
Max. Pitch Angle (deg)	-3	-1	-4	-1	-1
Max. Yaw Angle (deg)	37	30	31	30	29
Vehicle Specifications					
Weight (kg)	2076	2013	2013	2013	2013
Wheelbase (mm)	3350	3382	3382	3382	3382
Bumper Height (Upper Edge) (mm)	680	635	635	635	635

The calculated occupant impact velocity and occupant ridedown acceleration were compared to the recommended values (Ross et al., 1993). Two limits are given for each injury risk parameter, as listed in Table 2. It is desirable that computed values be below the "preferred" limits, and it is recommended that the computed values be below the "maximum" values. It should be noted that the recommended limits were absolute values.

4.3.1 Damage to Test Installation

As can be seen in all the simulations, the guardrail installation received considerable damage in the area of contact. The final damage profiles of the weak post barriers with pre-existing deflections after the Test Level 2 impacts were plotted in Figure 60.

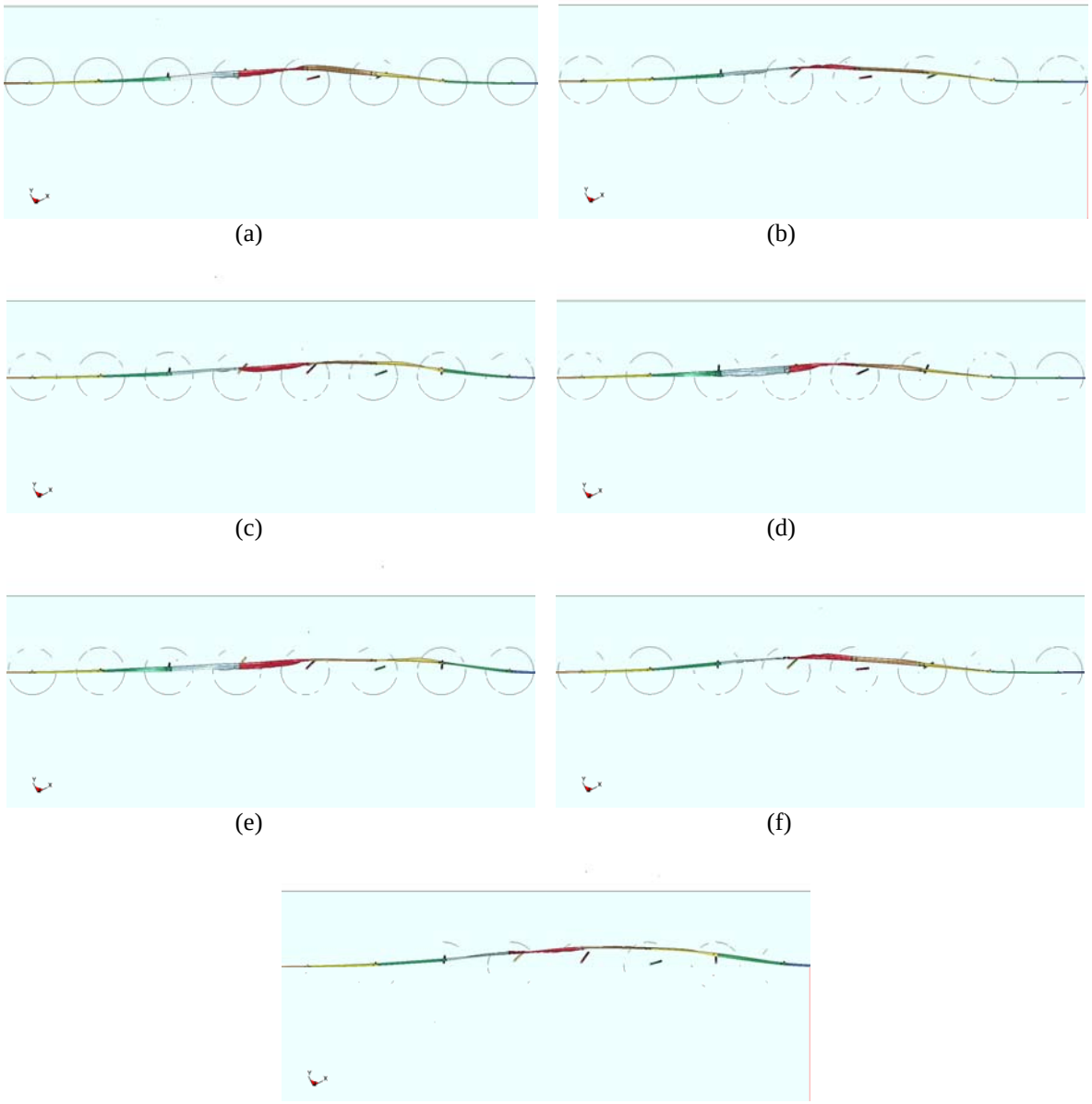

(a) (b) (c) (d) (e) (f) (g)

Figure 60. Final Damage Profiles of Weak Post Barriers after the TL 2 Impacts: (a) 3-in Deflection at Mid-Span (b) 3-in Deflection at Post (c) 6-in Deflection at Mid-Span (d) 6-in Deflection at Post (e) 9-in Deflection at Mid-Span (f) 9-in Deflection at Post (g) 18-in Deflection at Mid-Span

Rail deflections in Table 10 and Table 11 showed that the maximum dynamic and permanent rail deflections did not change significantly as the pre-damage level increased. The analysis of effects of initial impact points on guardrail performance showed that the rail deflections in the simulations with the impact point at the post were in general lower than those with the impact point at the midspan.

In addition, maximum rail tension was measured from the simulations. The rail tension was measured using the built-in function “Section Plane Interface” in LS-PREPOST. Three nodes were picked in the vertical direction of the guardrail to construct a cross-section plane of the rail. The normal force in the section plane, which is in the tensile direction of the guardrail section, was plotted. Multiple section places were created along the guardrail to obtain the maximum tension in the rail. The maximum rail tension was generally found at the first splice location downstream of the impact point. A slight increase in the rail tension was observed as the initial damage level increased. However, all rail tension values were well below the maximum value (500 kN) reported in the literature (Gentry and Bank, 1998).

4.3.2 Occupant Injury Risk

Analysis of occupant injury risk showed that the occupant injury velocities calculated from the damaged guardrail models were comparable to those in the undamaged weak post guardrail model. All the occupant injury velocity occupant ridedown acceleration values were below the preferred and maximum limits.

4.3.3 Vehicle Performance

The impacting vehicle remained stable in all of these simulations. Vehicle exit velocities and exit angles were compared to the results from the undamaged weak post barrier test.

Variations in vehicle exit velocities were observed in the simulations, which was a result of several factors in the current implementation of LS-DYNA finite element code. Firstly, because of the computational cost, the single precision version of the LS-DYNA solver was used for the simulations. Secondly, the element formulations with reduced integration were used in the majority of the parts of guardrail barrier and vehicle models. Finally, element penetration was found in some contact definitions due to the nature of the dynamic impact and the large number of parts involved in the simulation. These factors all could contribute to the increase in sliding interface energy and hourglass energy of the system, and also the uncertainty of the simulation results. To improve the robustness and accuracy of the results, the double precision version of the LS-DYNA solver, fully-integrated element formulations, and more specific contact definitions between the parts identified with penetration issues could be considered in the simulations.

4.4 Discussion

4.4.1 Analysis of Results

The finite element simulations show that weak post w-beam systems with minor rail deflection are able to successfully contain and redirect the vehicle model when impacted under NCHRP 350 Test Level 2 conditions. The maximum dynamic deflection of w-beam with existing damage was generally higher than that in the undamaged weak post guardrail system model.

Analysis of occupant injury risk showed that the occupant injury velocities calculated from the damaged guardrail models were comparable to those in the undamaged weak post guardrail model. All the occupant injury velocity occupant ridedown acceleration values were below the preferred and maximum limits.

4.4.2 Evaluation of Rail Rupture with the Use of Failure Criteria

It was important to mention that the failure strain was not specified for the material model of the guardrail steel in the current simulations. Therefore, rupture, tearing, and fracture of the guardrail barrier could not be evaluated in this study.

It was found in the literature that the guardrail steel was a rate-dependent material and had higher failure strain at higher loading rate (Wright and Ray, 1996). In order to improve the predicting capability of the current model, more information about the guardrail steel need to be obtained through material testing under various high loading rates. Additionally, a finer mesh should be used in the damaged area of the guardrail barrier to better simulate the failure behavior. The failure criteria used in LS-DYNA should be validated against material testing data and correspond to this specific mesh density in the simulation.

4.5 Conclusions

The weak post w-beam guardrail model was used to investigate crash performance of guardrail barriers with minor damage under NCHRP 350 Test Level 2 impact conditions. More importantly, this study was to provide quantitative guidelines for the repair and maintenance of damaged or deteriorated longitudinal barriers. Analysis of results of finite element simulations showed that weak post w-beam systems with minor rail deflection were able to successfully contain and redirect the vehicle model. The maximum dynamic deflection of w-beam with existing damage was generally higher than that in the undamaged weak post guardrail system model. The vehicle remained stable in all of these simulations. No conclusion can be drawn however whether these large deflection would have resulted in rail rupture.

5. SUMMARY OF RESEARCH PROGRAM AND CONTRIBUTION TO THE FIELD

5.1 Research Summary

The goal of this research was to develop finite element models of w-beam guardrail barriers for the evaluation of crash performance of barrier systems and the prediction of occupant injury in accidents involving roadside safety hardware. Upon completion of this goal, several research objectives were attained:

1. Development of finite element models of the weak post w-beam guardrail barriers.
2. Validation of the strong and weak post w-beam finite element models through pendulum testing.
3. Evaluation of the crash performance of weak post w-beam guardrail systems with minor damage using finite element method.

The finite element models of full scale longitudinal guardrail barriers developed under this research were validated against both full scale vehicle crash tests and pendulum testing. The validated models could allow researchers have more confidence in the model predictions. The models were used to evaluate the impact characteristics of the guardrail systems during the vehicle-roadside crashes. The models were also used to investigate the crash performance of the guardrail systems with minor damage as well as the occupant injury risk in roadside accidents. Damage to a longitudinal roadside barrier is affected by a variety of activities and factors. Much more common is minor damage such as a shallow dent which is a result of a low speed collision or sideswipe. The effect of this minor damage on the performance of the barrier in subsequent impacts is not well understood. The fully validated finite element models of guardrail systems

were used to develop barrier repair guidance for highway personnel tasked with maintaining barrier systems.

A summary of the primary findings for each of these research objectives is detailed below.

5.1.1 Develop a Finite Element Model of the Weak Post W-Beam Guardrail Barrier

Finite element models of the Test Level 2 and 3 weak post w-beam guardrail systems were developed. NCHRP Report Test Level 2 and 3 impacts with pickup trucks and passenger cars were simulated using LS-DYNA. The occupant injury risk during the impact was investigated by computing occupant impact velocity and occupant ridedown acceleration.

The simulation results of Test Level 2 impacts were validated against Test No. 471470-22 and Test No. GR-8. Kinematics of the vehicle and guardrail in the simulations were very similar to the tests. The analysis showed that the vehicle was contained and redirected by the weak post w-beam guardrail barrier. The OIV and ORA calculated from simulation results were in good agreement with test data. It was concluded that the Test Level 2 weak post guardrail model could be used for the investigation of crash performance of barriers with minor damage.

The simulation results of Test Level 3 impact were validated against Test No. 473750-3. Kinematics of the vehicle and guardrail in the simulations were similar to the test. The analysis showed that the pickup was contained and redirected by the weak post w-beam guardrail barrier. Differences were found in the vehicle exit speed, OIV, and ORA between simulation and test results. It was concluded that further improvement was needed for the Test Level 3 weak post guardrail model. More specifically, the friction conditions between the vehicle and the guardrail barrier and the soil condition needed to be improved.

5.1.2 Validation of the W-Beam Guardrail Finite Element Model through Pendulum Testing

This study has conducted a series of validation tests on the full scale strong and weak post guardrail model. Our approach has been to compare the results of simulations of pendulum impact tests with corresponding test data. The undamaged guardrail section and two damaged guardrail types, the missing blockout and twisted blockout, were tested and simulated. Impact speeds ranged from 15 to 20 mph.

Comparisons of experiment and simulation results demonstrated that the guardrail section taken from the full scale strong and weak post models were good representations of the real test sections in the pendulum tests. The results suggested that the full scale strong and weak post models had good prediction capability in terms of overall guardrail deflection. Some differences were observed in the movement of strong posts between the experiments and simulations. This difference did not impede the ability of the model to accurately predict peak rail deflection. However, this discrepancy could affect the prediction of post or splice failure, and should be investigated in future studies.

5.1.3 Evaluation of the Crash Performance of Weak Post W-Beam Guardrail Systems with Minor Damage Using Finite Element Method

The weak post w-beam guardrail model was used to investigate crash performance of guardrail barriers with minor damage under NCHRP 350 Test Level 2 impact conditions. More importantly, this study was to provide quantitative guidelines for the repair and maintenance of damaged or deteriorated longitudinal barriers. Analysis of results of finite element simulations showed that weak post w-beam systems with minor rail deflection were able to successfully contain and redirect the vehicle model under the assumption that the rail did not rupture. The maximum dynamic deflection of w-beam with existing damage was generally higher than that in

the undamaged weak post guardrail system model. No conclusion can be drawn however whether these large deflections would have resulted in rail rupture.

REFERENCES

A Guide to Standardized Highway Barrier Hardware. 2009. *Online Barrier Hardware Guide*. Website: http://aashtotf13.tamu.edu/.

Bronstad ME, Michie JD, Mayer JD. 1987. NCHRP Report 289: Performance of Longitudinal Traffic Barriers. *Transportation Research Board*, National Research Council, Washington, D.C.

Buth EC, Menges WL, Schoeneman SK. 2000. *NCHRP Report 350 Test 3-11 On The Modified PennDOT Type 2 Guide Rail-Test 3*, Texas Transportation Institute, Texas A&M University System, College Station, Texas.

Coon BA, Reid JD. 2005. Crash Reconstruction Technique for Longitudinal Barriers. *Journal of Transportation Engineering* 131(1): 54-62.

Elvik R. 1995.The Safety Value of Guardrails and Crash Cushions: A Meta-Analysis of Evidence from Evaluation Studies. *Accident Analysis and Prevention* 27(4): 523-549.

Gabauer DJ, Kusano KD, Gabler HC, Marzougui D, Opiela K, Hargrave M. 2008. Pendulum Testing as a Means of Assessing the Crash Performance of Longitudinal Barrier with Minor Damage. *Journal of Transportation Engineering (submitted)*.

Gabauer DJ, Gabler HC. 2009. Evaluation of Current Repair Criteria for Longitudinal Barrier with Crash Damage, *Journal of Transportation Engineering* 135 (4): 225-234.

Gabler HC, Gabauer DJ. 2007 Opportunities for Reduction of Fatalities in Vehicle-Guardrail Collisions. *51st Annual Proceedings of the Association for the Advancement of Automotive Medicine*, Melbourne, Australia.

Gentry TR, Bank LC. 1998. Finite Element Modeling and Model Verification of Steel W-Beam Guardrails Subject to Pendulum Impact Loading. In *Transportation Research Record: Journal of the Transportation Research Board, No. 1647*, Transportation Research Board of the National Academies, Washington, D.C.

Hendricks BF, Wekezer JW. 1996. Finite Element Modeling of G2 Guardrail, *Transportation Research Record*, No. 1528: Highway and Facility Design. Current Research on Roadside Safety Features. National Academy Press, Washington, D.C., 130-137

LS-DYNA® KEYWORD USER'S MANUAL. 2007. Version 971. Livermore Software Technology Corporation (LSTC)

Mak K, Bligh R, Menges W. 1998. Volume XI: Appendix J – Crash Testing and Evaluation of Existing Guardrail Systems. *Research Study No. RF 471470 Contract No. DTFH61-89-C-00089*, Federal Highway Administration U.S. Department of Transportation Washington, D.C.

Marzougui D, Mohan P, Kan CD, Opiela K. 2007. Evaluation of Rail Height Effects on the Safety Performance of W-Beam Barriers. *6th European LS-DYNA Users' Conference*.

Michie JD, Bronstad ME. 1994. Highway Guardrails: Safety Feature or Roadside Hazard? In Transportation Research Record: *Journal of the Transportation Research Board*, No. 1468, Transportation Research Board, National Research Council, Washington, D.C., 1-9.

National Highway Traffic Administration (NHTSA). 2006. Traffic Safety Facts 2005: A Compilation of Motor Vehicle Crash Data from the Fatality Analysis Reporting System and the General Estimates System. *U.S. Department of Transportation Report*, DOT HS 810 631, 2006a.

NCAC Finite Element Model Archive. 2009. Website: http://www.ncac.gwu.edu/vml/models.html.

Plaxico CA, Ray MH, Hiranmayee K. 2000. Comparison of the Impact Performance of the G4(1W) and G4(2W) Guardrail Systems under NCHRP Report 350 Test 3-11 Conditions. In *Transportation Research Record: Journal of the Transportation Research Board, No. 1720*, Transportation Research Board of the National Academies, Washington, D.C.

Ray MH, Engstrand K, Plaxico CA, McGinnis RG. 2001. Improvements to the Weak-Post W-Beam Guardrail. Proceedings of the 80th Annual Meeting of the Transportation Research Board, Washington, D.C.

Ray MH, Plaxico CA, Engstrand K. 2001. Performance of W-Beam Splices. In *Transportation Research Record: Journal of the Transportation Research Board, No. 1743*, Transportation Research Board of the National Academies, Washington, D.C.

Ray MH, McGinnis RG. 1997. NCHRP Synthesis of Highway Practice 244: Guardrail and Median Barrier Crashworthiness. *Transportation Research Board*, National Research Council, Washington, D.C.

Reid JD, Sicking DL. 1998. Design and Simulation of a Sequential Kinking Guardrail Terminal. *International Journal of Imapct Engineering* 21: 76l-772.

Ross HE, Sicking DL, Zimmer RA, Michie JD. 1993. National Cooperative Highway Research Program Report 350 Recommended Procedures for the Safety Performance Evaluation of Highway Features. *Transportation Research Board.*

Sicking DL, Reid JD, Rohde JR. 2002. Development of the Midwest Guardrail System. In *Transportation Research Record: Journal of the Transportation Research Board, No. 1797*, Transportation Research Board of the National Academies, Washington, D.C.

Standard Specifications for Transportation Materials and Methods of Sampling and Testing, 26th ed. 2006. American Association of State Highway and Transportation Officials. AASHTO, Washington, D.C.

Vanzweeden J, Bryden JE. 1977. In-Service Performance of Highway Barriers. *Research Report 51.* Engineering Research and Development Bureau, New York State Department of Transportation, Albany,

Wang Q, Gabler HC. 2008. Validation of Finite Element Models of Injury Risk in Vehicle-Roadside Barrier Crashes, *Biomedical Sciences Instrumentation:* 298-303.

Whitworth HA, Bendidi R, Marzougui D, Reiss R. 2003. Finite Element Modeling of the Crash Performance of Roadside Barriers. *International Journal of Crashworthiness* 9(1): 35-43.

Wright AE, Ray MH. 1996. Characterizing Guardrail Steel for LS-DYNA3D Simulations. *Transportation Research* Record 1528. Transportation Research Board, Washington, D.C.

APPENDIX A: EVALUATION OF LS-DYNA MATERIAL MODELS OF GUARDRAIL STEEL THOUROUGH QUASI-STATIC TENSILE TESTING

INTRODUCTION

Finite element models have been used in roadside safety research for many years. Accurate finite element models are required in order to simulate vehicles impacting roadside barriers successfully. Among different components of roadside barrier models, the material property of the guardrail is especially important in understanding the response of the hardware during vehicle-roadside crashes.

The objective of this study is to evaluate several existing material models of guardrail steel by comparing the experiment and simulation results of quasi-static coupon tests on AASHTO M 180 Class A Type II guardrail steel.

METHODS

Standard Specification for Guardrail

Standard specification for corrugated sheet steel beams for highway guardrail is described in the document AASHTO M 180 (AASHTO, 2006). For this project, AASHTO M 180 Class A Type II guardrail steel was used.

Thickness

- The base metal nominal thickness for Class A guardrail steel is 2.67 mm (0.105 in.).
- The nominal thickness for the finished AASHTO M 180 Class A Type II guardrail steel is 2.82 mm (0.111 in.).

Coating requirement

- The coating requirement for Type II guardrail steel is Zinc coated, 1100 g/m2 (3.60 oz/ft2) minimum single-spot.

Mechanical properties

- Yield point, minimum, 345 MPa (50000 psi);
- Tensile strength, minimum 483 MPa (70000 psi); and
- Elongation, in 50 mm (2 in.), minimum, 12 percent.

Width

- The beam elements shall be formed from sheets having nominal widths of 483 mm (19 in.).

Testing Setup

American Society for Testing and Materials (ASTM) A 370-05 was followed as the standard testing procedure of guardrail steel. Four specimens were cut from a section of w-beam guardrail in the longitudinal direction. The orientation of the specimen was in accordance with the common loading direction of the w-beam guardrail during vehicle-barrier impacts. The dimensions of specimens after machining are shown in Figure 61. The gauge length of the specimen was 50.8 mm. An extensometer with a gauge length of 50.8 mm (2 inches) was used in the tests. The specimen was loaded in the tensile direction at a speed of 5 mm/min with a hydraulic Instron testing machine. The speed of testing was within the range specified in ASTM A 370-05. The testing setup is shown in Figure 62. Tensile load, crosshead displacement, and strains were recorded for each test. Additionally, for Test 4 three markers were drawn on the specimen at the center of the gauge length. The distance between markers was 0.5 inch. For that specimen, the machine was stopped at an increment of 2 mm, and thickness and width of the specimen at the markers were measured. The thickness and width were used to calculate the change in area during the test.

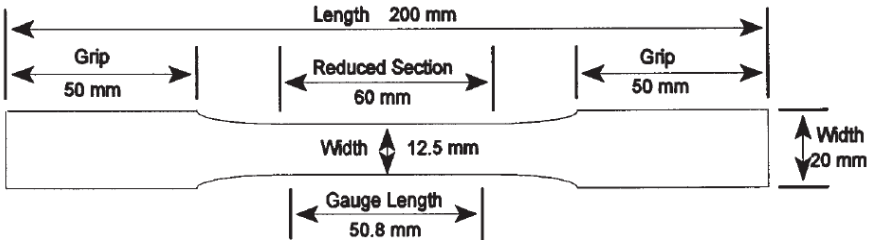

Figure 61. Longitudinal Tensile Specimen

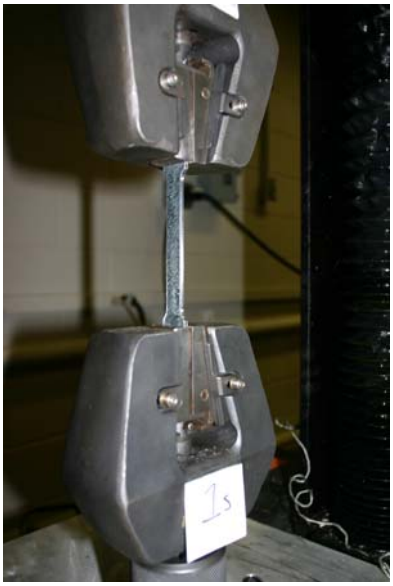

Figure 62. Quasi-Static Tensile Testing Setup

Finite Model Development

The goal of this study is to evaluate three existing material models of guardrail steel by comparing finite element simulation results with quasi-static coupon tests on guardrail steel. A finite element model of the test was developed using Hypermesh 9.0 and simulated in LS-DYNA. The dimensions of the guardrail specimen in the testing were used to create the finite element model. One end of the specimen was constrained at all directions. Prescribed uni-axial velocity of 5 mm/min was applied to the other end of the coupon. The guardrail specimen was modeled using fully integrated shell formulation with 5 integration points through the thickness. The smallest size of the elements was 3 mm. LS-DYNA material model 24 MAT_PIECEWISE_LINEAR_PLASTICITY was used for the model. The implicit solver was activated in LS-DYNA for the simulation of quasi-static testing. The termination time of the

simulation was set to 300 s. The double precision version of the LS-DYNA solver 971.r3 was used for the simulation.

Three studies were found in the literature on characterizing guardrail steel using LS-DYNA MAT 24. Three groups of material parameters for MAT 24 were reported by The FHWA/NHTSA National Crash Analysis Center (NCAC Finite Element Model Archive, 2009), Texas Transportation Institute (TTI) (Reid and Sicking, 1998), and Worcester Polytechnic Institute (WPI) (Wright and Ray, 1996). A summary of these three material models is listed in Table 12 and Figure 63. It should be noted that the failure strain mentioned in the study by WPI was not explained or completely justified by the author. Also, it was observed in Figure 63 that the input data points of strain for NCAC and TTI models were generally below 0.25, whereas strain data for WPI model were more evenly distributed between 0 and 1.

Table 12. Summary of Material Parameters for LS-DYNA MAT 24

	NCAC	TTI	WPI
Density (Ton/mm^3)	7.86E-09	7.86E-09	7.86E-09
Young's Modulus (MPa)	200000	200000	200000
Poisson's Ratio	0.30	0.28	0.33
Yield Stress (MPa)	298	450	415
Strain Rate effects	Yes	No	No
Plastic Strain at Failure	No	No	0.66

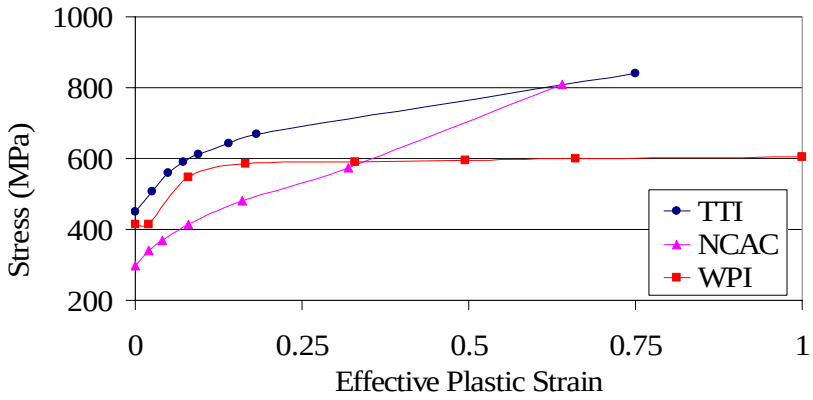

Figure 63. Increments of Guardrail Material Stresses and Strains in the LS-DYNA MAT 24

RESULTS

Results of Tensile Testing of Guardrail Coupons

All four specimens were loaded to failure. The failure locations were random due to the inhomogeneous property of the material. Failed specimens are shown in the Appendix A. The force versus displacement curves were obtained from the tests and shown in Figure 64. Test results showed that the average force at yielding was 14 kN. Based on the area measured in Test 4, the average calculated yield stress was around 400 MPa. The average maximum tensile force obtained from the tests was 18.3 kN. Average maximum engineering strain measured by the extensometer with a gauge length of 2 inches was 0.28. Observations from Test 4 (Figure 65) showed that the local engineering strain calculated between the two markers was 0.5, which suggested that for quasi-static tensile testing the true strain higher than 0.5 should have been obtained at failure location if more measurements were taken. Measurements and calculations for Test 4 are listed in the Appendix B. Also in the Appendix B, since Marker 3 was the closest to the location of failure, the calculation of stress at Marker 3 indicated that for quasi-static tensile testing the true stress at the failure location should be higher than 650 MPa. The number of tests was not enough to show if the effect of strain rate was significant, although Test 4 demonstrated lower maximum force and lower engineering strain at failure.

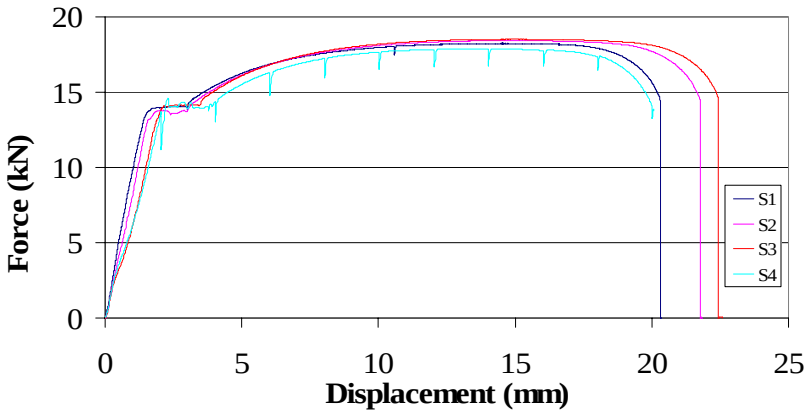

Figure 64. Force vs Displacement Curves Obtained from Quasi-Static Tensile Testing on Guardrail Steel Coupons

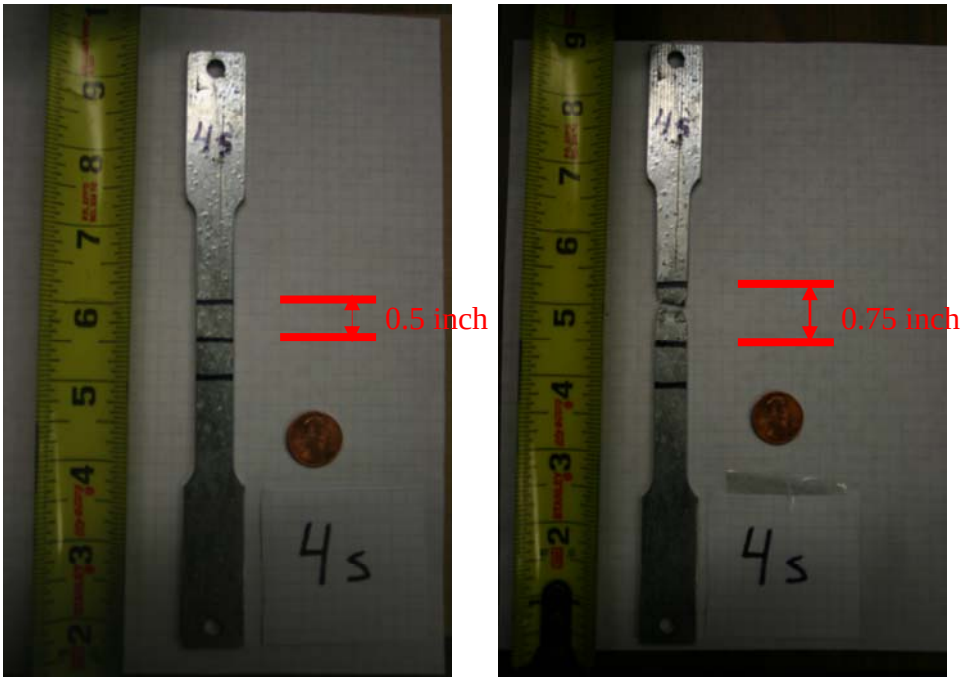

Figure 65. Coupons before and after the Test

Results of Simulations of Guardrail Tensile Testing

The material parameters in the aforementioned three studies (NCAC, TTI, and WPI) were incorporated into the finite element model of the guardrail tensile testing, and three simulations were completed. No failure plastic strain was specified for any of the three simulations. The force versus displacement curves extracted from the simulations were compared to test data and shown in Figure 66. It was observed from the results that all three models reached yield stress

almost immediately after the loading. The force at yielding in the WPI model was in better agreement with the experiment data. Comparisons of maximum forces also showed that the WPI model was closest to the experiment data. Effective stress and effective plastic strain levels at the end of the simulations are shown in Figure 67, Figure 68, and Figure 69 respectively. Effective stress, or Von Mises stress, is equal to 1st principal stress for tensile loading conditions. Different stresses and strains at the end of tensile loading were observed between the models. Compared to the findings from the tensile testing, none of the three models generated similar stress (≥ 650 MPa) and strain (≥ 0.5) levels at the same time. However, visual comparisons showed that the simulation using WPI material parameters had necking in the specimen at the end of loading, which was observed in the tests.

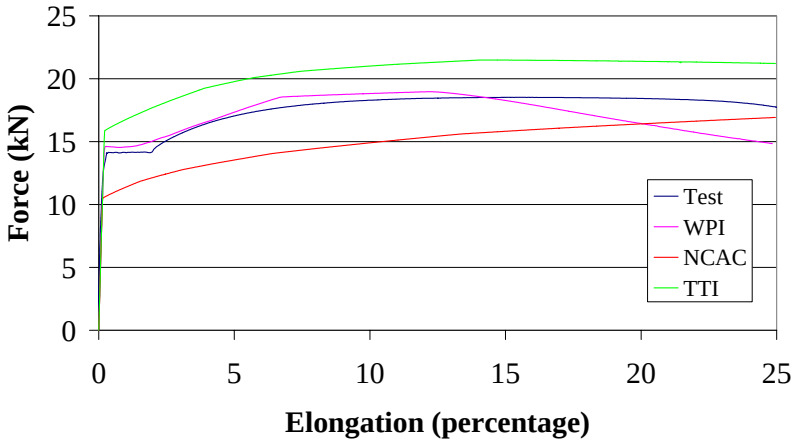

Figure 66. Comparisons of Force vs Elongation Curves from Simulations and Testing

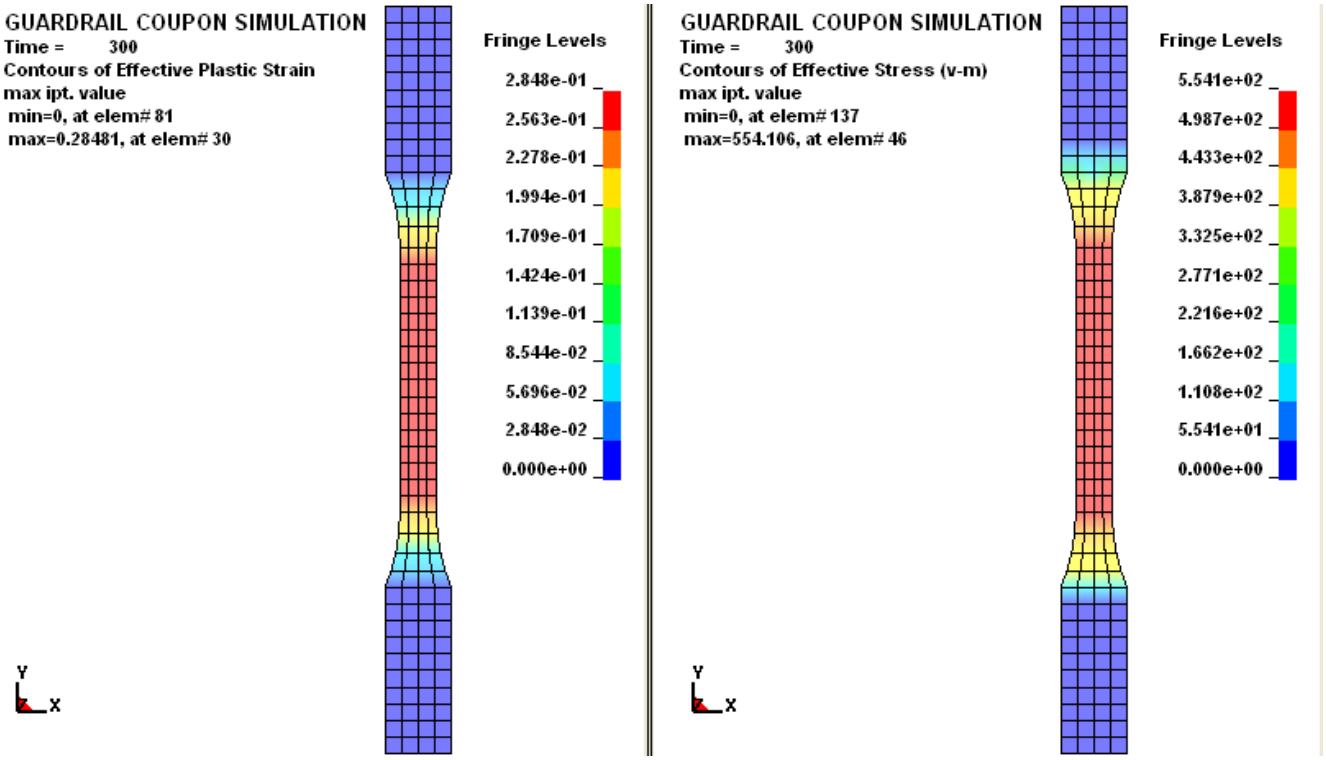

Figure 67. Strain and Stress (MPa) Levels of the Simulation Using NCAC Material Parameters

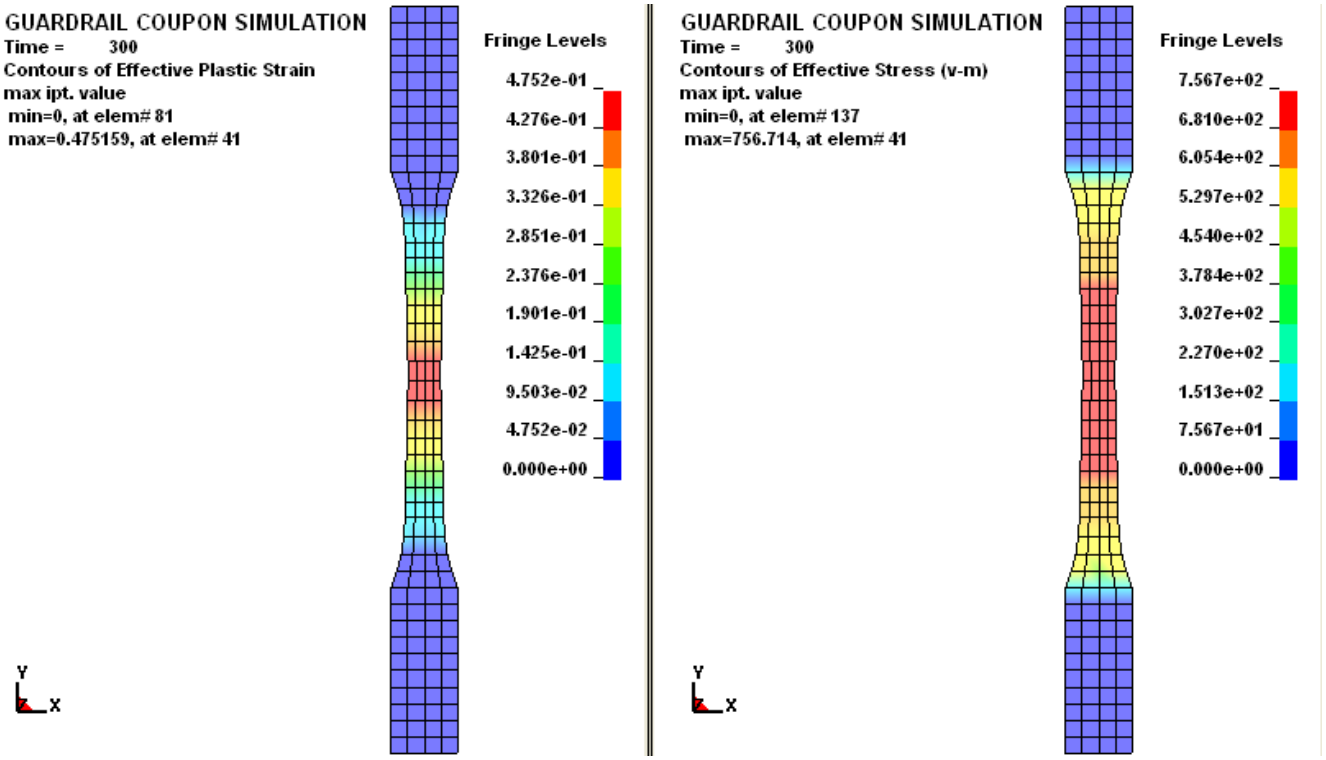

Figure 68. Strain and Stress (MPa) Levels of the Simulation Using TTI Material Parameters

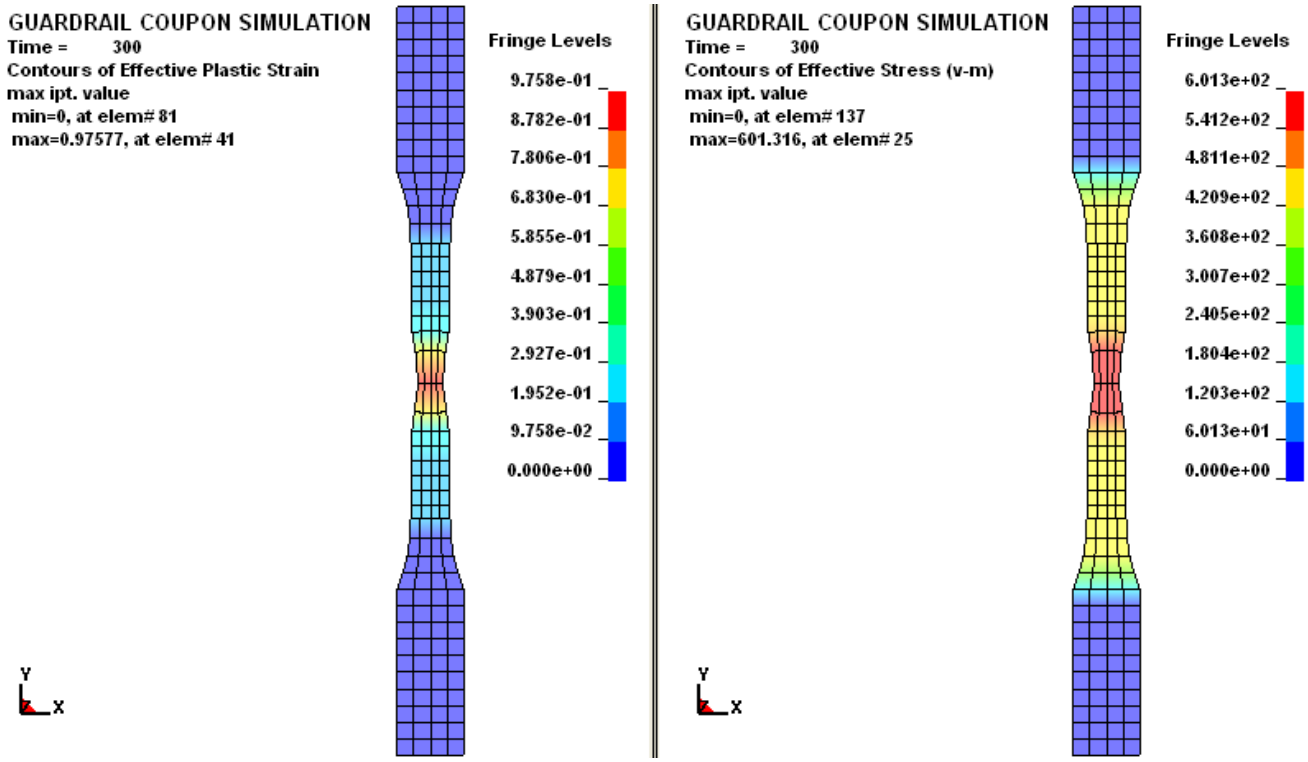

Figure 69. Strain and Stress (MPa) Levels of the Simulation Using WPI Material Parameters

APPENDIX B: COMPARISONS OF PENDULUM TESTS AND FULL SCALE BARRIER TEST USING FINITE ELEMENT SIMULATION

Background

The NCHRP 22-23 Project has conducted pendulum tests to evaluate the effect of minor damage to w-beam guardrail. These component tests are less expensive than a full barrier test, but, to be valuable, must be a good representation of the full barrier tests. Finite element models of pendulum tests were used to help determine whether the pendulum tests were a good representation of the full scale guardrail barrier system.

One concern is whether the rail tension in the pendulum tests is similar to the rail tension in the full barrier tests. If the rail tension is higher in the pendulum tests, this may lead to unrealistic failures. For example, in the missing blockout pendulum test, a vertical tear was developed at the splice. This failure mode is not commonly seen in full scale strong post guardrail barrier tests. The question was raised whether the three-cable anchorage mechanism resulted in excessive rail tension in the pendulum tests. The concern was that the rail section failure was a result of the rigid cable constraints and consequently high tension force along the w-beam rails.

Objective

The objective of this study was to determine the similarity between pendulum tests and full scale guardrail barrier tests.

Methods

In the Wang and Gabler paper (2008), we presented a finite element model of the FOIL pendulum experiments. Two additional finite element models were developed to investigate the problem mentioned above. We investigated the use of two cables to anchor each end of the rail.

The previous model and experiments used three cables on each end. Firstly, each center cable at the ends of the rail section in the undamaged test was removed. The reason was that we hypothesized that tension forces were too high in previous pendulum simulations. The rest of the simulation setup was identical to that of the undamaged barrier model.

Secondly, the finite element model of the pendulum was incorporated into the full scale strong post guardrail barrier model. This model was described in the previous QPR (Wang and Gabler, 2008). The height of the pendulum was the same as that in the previous pendulum tests. The full scale guardrail model was impacted by the pendulum with an initial velocity of 20 mph. The simulation setups for full scale, three-cable, and two-cable pendulum tests are shown in Figure 70, Figure 71 and Figure 72 respectively. Section planes along the rail section were created in LS-PREPOST to examine axial forces in the w-beams.

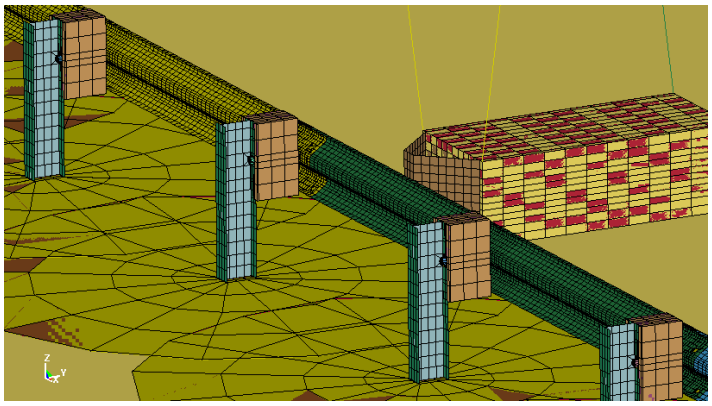

Figure 70. Full Scale Pendulum Simulation Setup

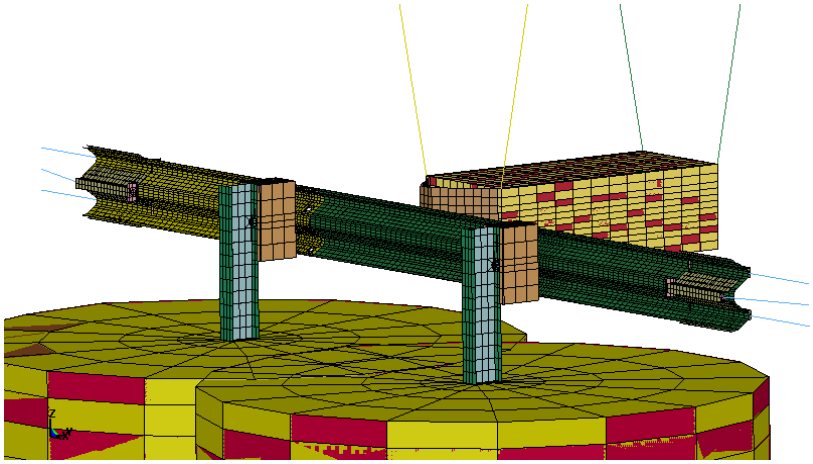

Figure 71. Three-Cable Pendulum Simulation Setup

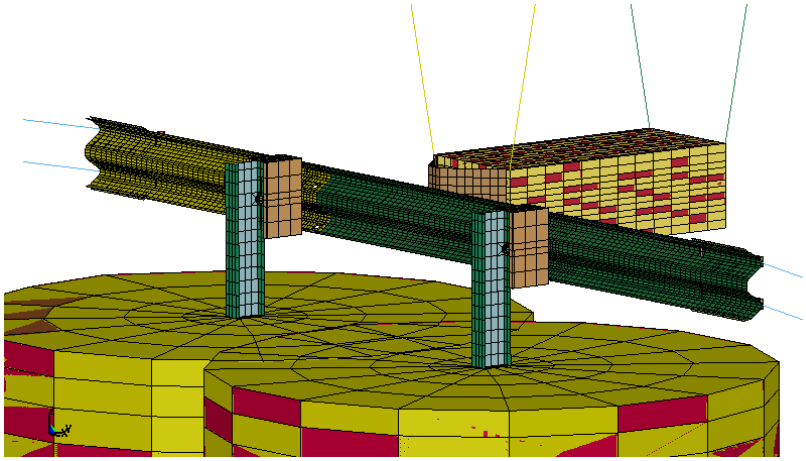

Figure 72. Two-Cable Pendulum Simulation Setup

Finite Element Simulation Results

The force versus time responses from the two aforementioned simulations were plotted in Figure 73 and compared to the rail tension in undamaged barrier test with three cables. It was seen that the rail tension in the three-cable undamaged test was approximately 90 kN higher than that in the other two simulations. The maximum rail tensions in the undamaged test with two cables and in the full scale barrier test were comparable to each other. Another notable difference was that the duration of the force in the full scale guardrail model was longer than that in guardrail component tests. It was observed in the full scale model that the top of the two posts at each end of the two-piece rail section had around 40 mm movement in the direction of pendulum

impact. This flexibility of the rail sections upstream and downstream of the test section could explain the longer duration of the rail tension in the full scale model.

The dynamic rail deflections at the impact point from the three simulations were also compared and shown in Figure 74. The maximum dynamic rail deflection at impact point was 654 mm for the full scale guardrail model. Despite the rigid end constraints in the guardrail section tests, the rail deflections were similar to that observed in the full scale guardrail model. The maximum dynamic rail deflections for three-cable and two-cable pendulum tests were 582 mm and 595 mm respectively.

Furthermore, the rail tension in the full scale strong post guardrail model impacted by the pendulum at 20 mph was compared to that in the full scale strong post guardrail model impacted by a 2000 kg pickup truck traveling at 60 mph and 20 degrees. It was shown in Figure 75 that the rail tension response in full scale pendulum simulation was similar to that in full scale vehicle simulation in terms of magnitude and duration. The spike observed after 0.2 s in the curve in full scale vehicle simulation was due to the rear of the pickup truck contacting the guardrail barrier. Based on these simulation results, it was concluded that the undamaged barrier test with two cables was a better representation of the full scale guardrail model.

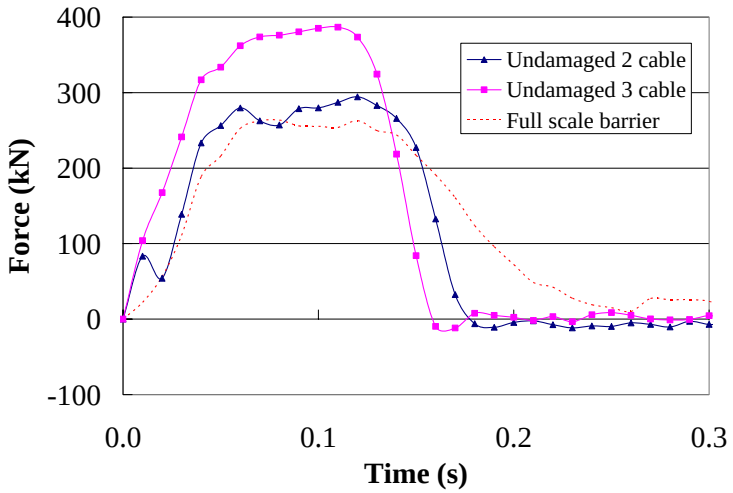

Figure 73. Comparisons of Rail Tension between Undamaged Barrier Test with Two Cables, Undamaged Barrier Test with Three Cables, and Full Scale Pendulum Test

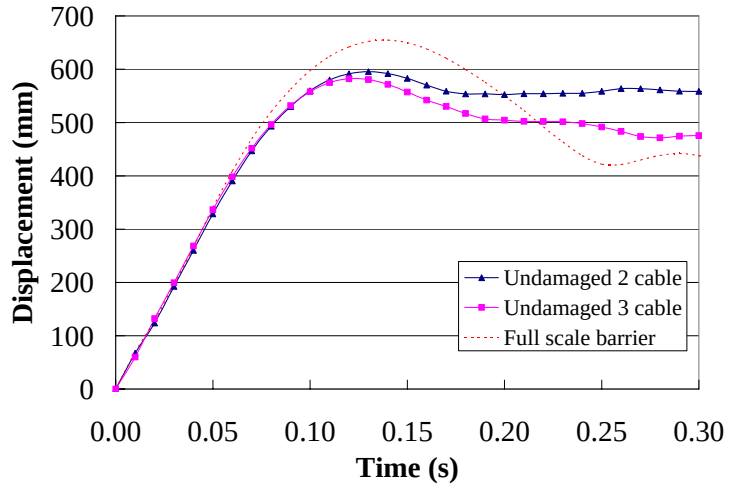

Figure 74. Comparisons of Rail Deflections at Impact Point Undamaged Barrier Test with Two Cables, Undamaged Barrier Test with Three Cables, and Full Scale Pendulum Test

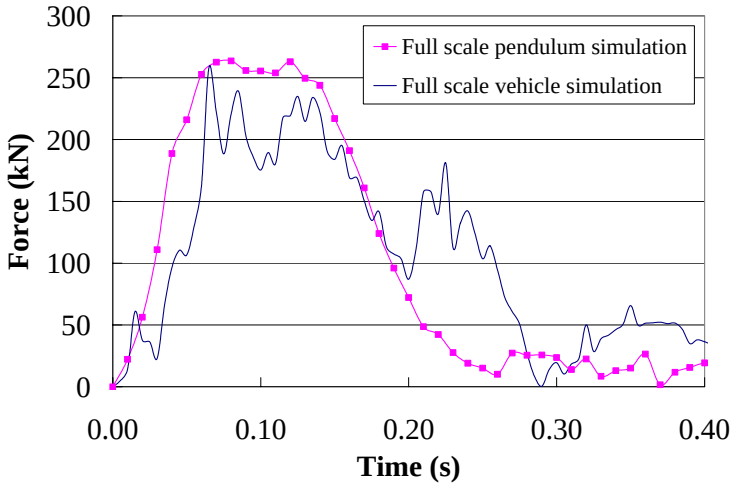

Figure 75. Comparisons of Rail Tension Forces between Full Scale Pendulum Simulation and Full Scale Vehicle Simulation